AEDC-TR-67-236

cy 3

EFFECTS OF RADIATED AERODYNAMIC NOISE ON MODEL BOUNDARY-LAYER TRANSITION IN SUPERSONIC AND HYPERSONIC WIND TUNNELS

S. R. Pate and C. J. Schueler

ARO, Inc.

March 1968

VON KÁRMÁN GAS DYNAMICS FACILITY
ARNOLD ENGINEERING DEVELOPMENT CENTER
AIR FORCE SYSTEMS COMMAND
ARNOLD AIR FORCE STATION, TENNESSEE

NOTICES

When U. S. Government drawings specifications, or other data are used for any purpose other than a definitely related Government procurement operation, the Government thereby incurs no responsibility nor any obligation whatsoever, and the fact that the Government may have formulated, furnished, or in any way supplied the said drawings, specifications, or other data, is not to be regarded by implication or otherwise, or in any manner licensing the holder or any other person or corporation, or conveying any rights or permission to manufacture, use, or sell any patented invention that may in any way be related thereto.

Qualified users may obtain copies of this report from the Defense Documentation Center.

References to named commercial products in this report are not to be considered in any sense as an endorsement of the product by the United States Air Force or the Government.

EFFECTS OF RADIATED AERODYNAMIC NOISE ON MODEL BOUNDARY-LAYER TRANSITION IN SUPERSONIC AND HYPERSONIC WIND TUNNELS

S. R. Pate and C. J. Schueler
ARO, Inc.

FOREWORD

The work reported herein was sponsored by Headquarters, Arnold Engineering Development Center (AEDC), Air Force Systems Command (AFSC) in support of Project 8953, Task 895303, Program Element 6240533F.

The results of the research presented were obtained by ARO, Inc. (a subsidiary of Sverdrup & Parcel and Associates, Inc.), contract operator of AEDC, AFSC, Arnold Air Force Station, Tennessee, under Contract AF 40(600)-1200. This report contains experimental data obtained during the period June 3, 1966 to January 23, 1967 under ARO Project Nos. VT5717 and PS2702, and the manuscript was submitted for publication on October 11, 1967.

This technical report has been reviewed and is approved.

Carl E. Simmons
Captain, USAF
Research Division
Directorate of Plans
and Technology

Edward R. Feicht
Colonel, USAF
Director of Plans
and Technology

ABSTRACT

The influence of radiated aerodynamic noise (generated by the tunnel wall turbulent boundary layer) on model boundary-layer transition in supersonic and hypersonic wind tunnels was investigated. Boundary-layer transition measurements were made at supersonic Mach numbers on sharp-leading-edge hollow-cylinder models in the AEDC-VKF 12-in. Tunnel D, the 40-in. Tunnel A, and the AEDC-PWT 16-ft Supersonic Tunnel. These data showed, conclusively, a significant and continuous increase in transition Reynolds number with increasing tunnel size. Results from a shroud configuration placed concentrically around a hollow-cylinder transition model in the AEDC-VKF Tunnel A demonstrated a significant change in the magnitude and trend in transition Reynolds number with unit Reynolds number, as compared to transition Reynolds numbers without the shroud, when the boundary layer on the shroud inner wall changed from a laminar to turbulent boundary layer. A flat-plate model equipped with a microphone confirmed that a significant increase in the root-mean-square (RMS) radiated pressure fluctuations accompanied the decrease in the transition Reynolds numbers between the AEDC-VKF 40-in. and 12-in. tunnels and the decrease in transition as the shroud inner wall boundary layer changed from laminar to turbulent. From transition data obtained in these investigations, previously published data from the AEDC-VKF Tunnels A and D, and data from six other wind tunnels, a correlation of transition Reynolds numbers was developed. The correlation was based on zero bluntness, flat-plate and hollow-cylinder transition data which covered a Mach number range from 3 to 8 and unit Reynolds number range from 0.05×10^6 to 1.1×10^6 per inch. The correlation was found to be dependent only on the tunnel wall, turbulent boundary-layer, aerodynamic noise parameters (displacement thickness and skin friction) and the tunnel test-section circumference.

CONTENTS

		Page
	ABSTRACT	iii
	NOMENCLATURE	vii
I.	INTRODUCTION	1
II.	EXPERIMENTAL CONDITIONS	
	2.1 Wind Tunnel Facilities	5
	2.2 Basic Transition Models and Apparatus	6
	2.3 AEDC-VKF Tunnel A Shroud Model	8
III.	BASIC TRANSITION RESULTS	10
IV.	SHROUD TRANSITION AND NOISE RESULTS	13
V.	TRANSITION CORRELATION	18
VI.	COMPARISONS OF CORRELATION PREDICTIONS WITH EXPERIMENTAL RESULTS	
	6.1 Influence of Unit Reynolds Number, Mach Number, and Tunnel Size	24
	6.2 Mach Number Effect	29
VII.	CONCLUDING REMARKS	33
	REFERENCES	35

ILLUSTRATIONS

Figure		
1.	AEDC-PWT-16S Transition Model Installation	7
2.	Long Shroud Installation in the AEDC-VKF Tunnel A	9
3.	Comparison of Probe Pressure Transition Traces in the AEDC-VKF Tunnels A and D and AEDC-PWT-16S for M_∞ = 3.0	11
4.	Basic Transition Reynolds Number Data from the AEDC-VKF 12-in. Tunnel D and 40-in. Tunnel A and the AEDC-PWT 16-ft Supersonic Tunnel at M_∞ = 3.0	12
5.	Comparisons of Transition Reynolds Numbers and Root-Mean-Square Radiated Pressure Fluctuations at M_∞ = 3.0	
	a. Boundary-Layer Development inside Long Shroud	15
	b. Transition Reynolds Numbers on the 3.0-in.-diam Hollow-Cylinder Model	15
	c. Root-Mean-Square Radiated Pressure Fluctuations	15

Figure		Page
6.	Comparisons of Transition Reynolds Numbers and Root-Mean-Square Radiated Pressure Fluctuations at M_∞ = 5.0	
	a. Boundary-Layer Development inside Long Shroud	16
	b. Transition Reynolds Numbers on the 3.0-in.-diam Hollow-Cylinder Model	16
	c. Root-Mean-Square Radiated Pressure Fluctuations	16
7.	Influence of Tunnel Size on the Boundary-Layer Transition Reynolds Number Correlation	21
8.	Tunnel Size Parameter	22
9.	Correlation of Transition Reynolds Number	23
10.	Comparison of Measured and Estimated Transition Reynolds Numbers from Several Tunnels for Various Mach Numbers and Unit Reynolds Numbers	
	a. Mach Number and Unit Reynolds Number Effects (b = 0)	25
	b. Tunnel Size and Unit Reynolds Number Effect at M_∞ = 3, b = 0	26
11.	Effect of the Tunnel Size on Transition at M_∞ = 3	27
12.	Variation of Transition Reynolds Number with Increasing Tunnel Mach Number	28
13.	Transition Reynolds Numbers as a Function of Local Mach Number for Sharp Cones and Pitched Flat Plates	
	a. Sharp Cones at M_∞ = 8	30
	b. Pitched Flat Plate at M_∞ = 6.0	31
	c. Pitched Flat Plate at M_∞ = 6 and 8	32

TABLE

I.	Source and Range of Data Used in the Correlation	20

APPENDIXES

I.	Transition Data and Tunnel Wall Boundary-Layer Characteristics from the AEDC-PWT-16S Tunnel	41

Page

II. Transition Reynolds Number Data and Tunnel Wall Boundary-Layer Characteristics from the AEDC-VKF Tunnel A 53

III. Experimental Results from the Long Shroud Configuration Installed in the AEDC-VKF Tunnel A 62

IV. Transition Reynolds Number Results from the AEDC-VKF Tunnel D 76

V. Displacement Thickness Correlation and Turbulent Skin-Friction Coefficients 82

NOMENCLATURE

b	Model leading-edge thickness at a specific location, in.
$\bar{b}$	Average value of model leading-edge thickness, in.
C_F	Mean turbulent skin-friction coefficient
c	Tunnel test-section circumference, in.
c_1	Tunnel test-section circumference of 12- by 12-in. tunnel (c_1 = 48 in.)
ℓ_m	Axial distance from tunnel throat to model leading edge, in.
ℓ_r	Axial distance from tunnel throat to wall boundary-layer rake, in.
M_δ	Local Mach number outside the boundary layer
M_∞	Free-stream Mach number
p	Surface probe pitot pressure, psia
p_o	Tunnel stilling chamber total pressure, psia
p_o'	Total pressure downstream of a normal shock wave, psia
p_s	Model static pressure, psia
p_∞	Free-stream static pressure, psia
$\tilde{p}$	Root-mean-square value of radiated pressure fluctuation, psia

q_∞	Free-stream dynamic pressure, psia
Re_{ℓ_r}	Length Reynolds number
Re_t	Transition Reynolds number (based on local conditions), $Re_t = (Re/in.)_\delta x_t$
$(Re/in.)_\delta$	Local Reynolds number per inch
$(Re/in.)_\infty$	Free-stream Reynolds number per inch
r	Shroud internal radius, in. (r = 5.72 in.)
T_o	Tunnel stilling chamber total temperature, ^oR
U_L	Local velocity outside the long shroud inner wall boundary layer, ft/sec
U_∞	Free-stream velocity, ft/sec
u	Local velocity in boundary layer, ft/sec
x	Axial distance, in.
x_s	Shroud lip shock impingement location
x_t	Axial location of boundary-layer transition, in.
y	Distance normal to the model surface, in.
α	Angle of attack, deg
δ^*	Boundary-layer displacement thickness, in.
$\bar{\delta}^*$	Boundary-layer displacement thickness parameter
θ	Boundary-layer momentum thickness, in.
θ_c	Cone half-angle, deg
θ_{LE}	Leading-edge bevel angle, deg
ρ	Local density in the boundary layer, lbm/ft^3
ρ_L	Local density outside the long shroud inner wall boundary layer, lbm/ft^3
ρ_∞	Free-stream density, lbm/ft^3

SECTION I
INTRODUCTION

The conditions which have an influence on transition from laminar to turbulent flow are of considerable importance because of the far-reaching influence boundary-layer flow has on vehicle performance. Although the subject of boundary-layer transition has received considerable attention during the past fifteen years, there has been a renewal of interest in the subject in the past several years because of its influence on various aspects of re-entry vehicle performance.

Extensive testing programs have been conducted in wind tunnels and account for the bulk of the information on transition at supersonic, hypersonic, and hypervelocity speeds. Aeroballistic ranges have also been used in transition studies, and some flight tests have been conducted to provide transition data; however, they generally account for the smallest percentage of the results.

There have been some successes in theoretically predicting boundary-layer instability; however, little progress has been made toward theoretically predicting the location of transition. Explanations of the behavior of transition results obtained from wind-tunnel measurements, and predictions of the transition location at supersonic and hypersonic speeds have usually been attempted through the use of data correlations with the assumption that the tunnel free-stream disturbances are unimportant at high supersonic and hypersonic speeds.

Experience in subsonic tunnels showed that transition results were critically dependent on the quality of flow and, therefore, were different from one wind tunnel to another. Similar disagreement was found in transition results measured at low supersonic speeds in different wind tunnels and indicated that studies were necessary to ascertain whether the results were affected by tunnel disturbances. In the early fifties, the NACA initiated comparative transition tests with zero heat transfer on a 10-deg cone in many of its supersonic facilities (Ref. 1). These tests, made under comparable conditions in tunnels of various sizes, showed a wide range of transition Reynolds numbers which decreased as the Mach number was increased up to about four. The significant scatter of the transition Reynolds number was believed to be caused by free-stream disturbances of various degrees present in the different wind tunnels.

Kovasznay (Ref. 2) found that the disturbances in wind-tunnel flows may be of three types: (a) vorticity fluctuations

(turbulence), (b) entropy fluctuations (temperature spottiness), and (c) sound waves.

The vorticity and entropy fluctuations are essentially convected along streamlines and are traceable to conditions in the settling chamber. The sound disturbances can travel across streamlines, and they may originate in the stilling chamber and from the boundaries of the test section (Ref. 3).

The vorticity (turbulence) fluctuations were investigated at Mach numbers from 1.7 to 4 by Laufer (Ref. 4) by varying the turbulence level in the stilling chamber from 0.6 to 7 percent. In the low Mach number flow, $M_\infty < 2.5$, the stilling chamber turbulence level was found to have a strong effect on the boundary-layer transition Reynolds number; however, no significant effect was noted for $M_\infty > 2.5$. Similar experiments were conducted at Mach 1.76 by Morkovin (Ref. 5), and no measurable shift in transition resulted when the settling chamber turbulence was raised from 0.7 to 4.6 percent.

Sources of the entropy fluctuations (temperature spottiness) are traceable to the settling chamber and farther upstream. In the test section, the temperature fluctuations are related isentropically to those in the stilling chamber. Effective means such as the use of mixing sections and screens in the supply passage are used to reduce the fluctuations to small levels in supersonic tunnels where their influence on transition is thought to be insignificant.

The third type of unsteady disturbances, the sound fluctuations (Ref. 3) generated by the turbulent boundary layer on the walls of the test section, remain as a possible major factor affecting transition in supersonic and hypersonic wind tunnels ($M_\infty > 2.5$). Sound energy generated along the walls is predominantly radiated in the general direction of the free-stream Mach waves even though individual wave fronts may be inclined at different angles if the sound sources are moving with respect to the free-stream flow and solid boundary (Refs. 3 and 6).

Laufer (Ref. 7) conducted a series of experiments at Mach 1.5 to 5 and showed that the fluctuating field existing in the wind tunnel was a sound field with an intensity which increases rapidly as the Mach number is increased. Schlieren photographs taken of a model in free flight revealed a sound field emanating from the turbulent boundary layer. The orientation of the sound field was found to be different from the Mach-wave direction and corresponded to a sound-source velocity of approximately one-half the free-stream velocity

for Mach numbers 3 to 5. Laufer argued that the fluctuations picked up by a hot wire in the free stream originated from the boundary layers on the tunnel walls. To confirm this, he shielded the hot wire from one of the walls by a flat plate, and he noted that the mean-square voltage fluctuation across the wire decreased by about 20 percent when the wire was behind the plate.

Hot-wire experiments in the boundary layer of a Mach 1.76 nozzle (Ref. 3) disclosed the presence of a high intensity, thin turbulent layer within the much thicker nozzle wall boundary layer. Since turbulence in a low, supersonic boundary layer is produced largely near the wall and then diffused outward, the thin turbulent layer was interpreted as being associated with the higher shear.

Vrebalovich, JPL, in commenting on Morkovin's paper on free-stream disturbances (Ref. 8) indicated that hot-wire measurements made in the test section of the JPL tunnels showed that when the wall boundary-layer was turbulent the free-stream mass flow fluctuations not only increased with Mach number but were higher at the lower unit Reynolds number. From experiments in the JPL 12-in. supersonic tunnel with laminar, transitional, and fully turbulent boundary-layer flow on the tunnel wall, the following results were obtained: (a) free-stream pressure fluctuation levels were smallest when the boundary-layer was laminar and (b) tripping the boundary layer introduced less fluctuations in the free stream than when transition from laminar to turbulent flow occurred naturally between the nozzle throat and test section. These experiments in which the only change was in the nature of the tunnel wall boundary layer showed that a dominant source of free-stream disturbances at the higher Mach numbers was the aerodynamic sound radiated from the wall boundary layers.

Phillips (Ref. 9) proposed a theory to describe the generation of sound by turbulence at high Mach numbers. Laufer (Ref. 6), in commenting on Phillips' theory, noted that it is based on the premise that the sound-generating mechanism consists of a moving, spacially random, virtually wavy wall formed by an eddy pattern that is convected supersonically with respect to the free-stream and is consistent with the principal features of the sound field found in experiments. Using this view, Laufer derived an expression for the pressure fluctuation intensity which is shown to be a function of the mean skin-friction coefficient, the wall boundary-layer thickness, lengths which scale with the boundary-layer thickness, convection speed, angle of the radiated disturbance, and free-stream Mach number. This theory was found to be in partial agreement with experimental data at Mach numbers from 1.5 to 3.5 and considerably below experimental data at Mach 5.

Kistler and Chen (Ref. 10) reported on pressure fluctuation measurements that were made with microphones in a flat plate and in the tunnel sidewall at Mach numbers from 1.33 to 5.00. Laufer (Ref. 11) discussed the radiation field generated by a supersonic turbulent boundary layer at Mach numbers from 1.5 to 5 and compared the hot-wire results with those obtained by Kistler and Chen (Ref. 10) with microphones in the wall of the tunnel. In each of these tests, the wall and free-stream pressure fluctuations were found to scale with the mean wall shear for all Mach numbers. In addition, it was noted that the intensity of the radiated pressure fluctuations was two orders of magnitude less than the pressure fluctuations on the wall. In these experiments, Laufer also showed that the intensity of the radiated pressure fluctuations was proportional to the size of the test section. For example, radiation from one wall was approximately equal to one-fourth the radiation measured from four walls.

In 1952, AGARD established a series of calibration models with somewhat the same general objective as the NACA had in testing a 10-deg cone in several wind tunnels. One of the calibration models was a high fineness ratio, parabolic body (AGARD Calibration Model A) which had been tested extensively by the NACA to compare zero lift drag measurements made in many different wind tunnels. Tests of the same model in the Arnold Engineering Development Center, von Kármán Facility (AEDC-VKF) 12-in. and 40-in. supersonic tunnels (Gas Dynamic Wind Tunnels, Supersonic (D) and (A)) revealed discrepancies in base pressure and drag data that could be explained by differences in transition Reynolds numbers in these tunnels (Ref. 12). These tests were followed by tests of a hollow-cylinder model to obtain transition locations for a range of Mach numbers and unit Reynolds numbers. Schueler (Ref. 13) showed from these tests that transition Reynolds numbers obtained in the AEDC-VKF 40-in. supersonic tunnel are much larger than those from the AEDC-VKF 12-in. supersonic tunnel and discussed the possibility of differences in the aerodynamic noise generated in the tunnel boundary layers as being responsible for the variations in transition Reynolds numbers.

No work, either theoretical or experimental, has shown the manner in which boundary-layer transition is affected by aerodynamic noise; however, progress to date has considerably enhanced the understanding of the factors which influence the intensity of the radiation field generated by tunnel wall boundary layers. The more important factors include Mach number, the type boundary layer, boundary-layer thickness, mean shear, and test-section size.

Using these factors as a guide, previously published transition Reynolds numbers obtained at Mach numbers from 3 to 8 in eight facilities on two-dimensional models were correlated as a function of the tunnel wall turbulent boundary-layer displacement thickness in the test section, the average tunnel wall turbulent skin-friction coefficient, and the test-section circumference. This research included an experimental program designed to determine the effects of radiated aerodynamic noise on transition and to provide basic transition Reynolds number data from the AEDC-VKF 12-in. Tunnel D, 40-in. Tunnel A, and AEDC, Propulsion Wind Tunnel Facility (PWT) 16-ft supersonic tunnel (Propulsion Wind Tunnel, Supersonic (16S)) to test the validity of the correlation proposed.

SECTION II
EXPERIMENTAL CONDITIONS

2.1 WIND TUNNEL FACILITIES

New experimental data included in this report were obtained in AEDC-VKF Tunnels A and D and in AEDC-PWT-16S.

2.1.1 AEDC-PWT 16-by 16-ft Supersonic Tunnel

Tunnel 16S is a closed-circuit, variable-density wind tunnel with an automatically controlled, flexible plate-type nozzle. Current test capabilities include a Mach number range from 1.65 to 3.20 at stagnation pressures from approximately 0.7 to 11 psia. For these tests, the stagnation temperature was held constant at approximately 200°F. The test section is 16 ft square by 40 ft long, and the transition model was located in the first 10 ft of the test section. Additional information on the tunnel may be found in Ref. 14 and in Appendix I.

2.1.2 AEDC-VKF 40- by 40-in. Supersonic Tunnel A

Tunnel A is a continuous, closed-circuit, variable-density wind tunnel with an automatically driven, flexible plate-type nozzle and a 40- by 40-in. test section. The tunnel can be operated at Mach numbers from 1.5 to 6 at maximum stagnation pressures from 29 to 200 psia, respectively, and stagnation temperatures up to 300°F (M_∞ = 6). Minimum operating pressures range from about one-tenth to one-twentieth of the maximum pressures. A description of the tunnel and airflow calibration information may be found in Ref. 15. Additional information on the Tunnel A geometry and tunnel wall boundary-layer characteristics can be found in Appendix II.

2.1.3 AEDC-VKF 12- by 12-in. Supersonic Tunnel D

Tunnel D is an intermittent, variable density wind tunnel with a manually adjusted, flexible plate-type nozzle and a 12- by 12-in. test section. The tunnel can be operated at Mach numbers from 1.5 to 5 at stagnation pressures from about 5 to 60 psia and at average stagnation temperatures of about 70°F. A description of the tunnel and airflow calibration information may be found in Ref. 16. An illustration showing the Tunnel D geometry is presented in Fig. IV-1, Appendix IV.

2.2 BASIC TRANSITION MODELS AND APPARATUS

2.2.1 AEDC-PWT

Figure 1 shows the transition model installed in the test section of the AEDC-PWT-16S tunnel. The model was a 12-in.-diam by 115-in.-long, steel hollow cylinder having an external surface finish of 15 microinches (μin.). The location of transition was determined from pressure data obtained from four equally spaced, external surface pitot probes (0.016- by 0.032-in. tip geometry).

Three interchangeable, leading-edge, nose sections with an internal bevel angle of 6.5 deg and average leading-edge bluntness ($\bar{b}$) of 0.0015, 0.0050, and 0.0090 in. were tested. The maximum bluntness deviation around the leading edge was approximately ± 0.0005 in.

A sliding collar arrangement which was separated from the model surface by eight Teflon® inserts supported the four pitot probes and housed four differential pressure transducers. An actuating apparatus consisting of a coil spring and a hydraulic cylinder for compressing the spring provided the means for automatically positioning the pitot probes along the surface. Probe pressure data were recorded at small intervals of probe travel at discrete model axial locations.

Profiles of the boundary layer on the tunnel straight wall and flexible plate at the model location were measured with two 14-probe rakes to determine the characteristics of the wall turbulent boundary layer.

Details of the model and the experimental boundary-layer characteristics obtained on the tunnel walls can be found in Figs. I-2 and I-3, respectively, in Appendix I.

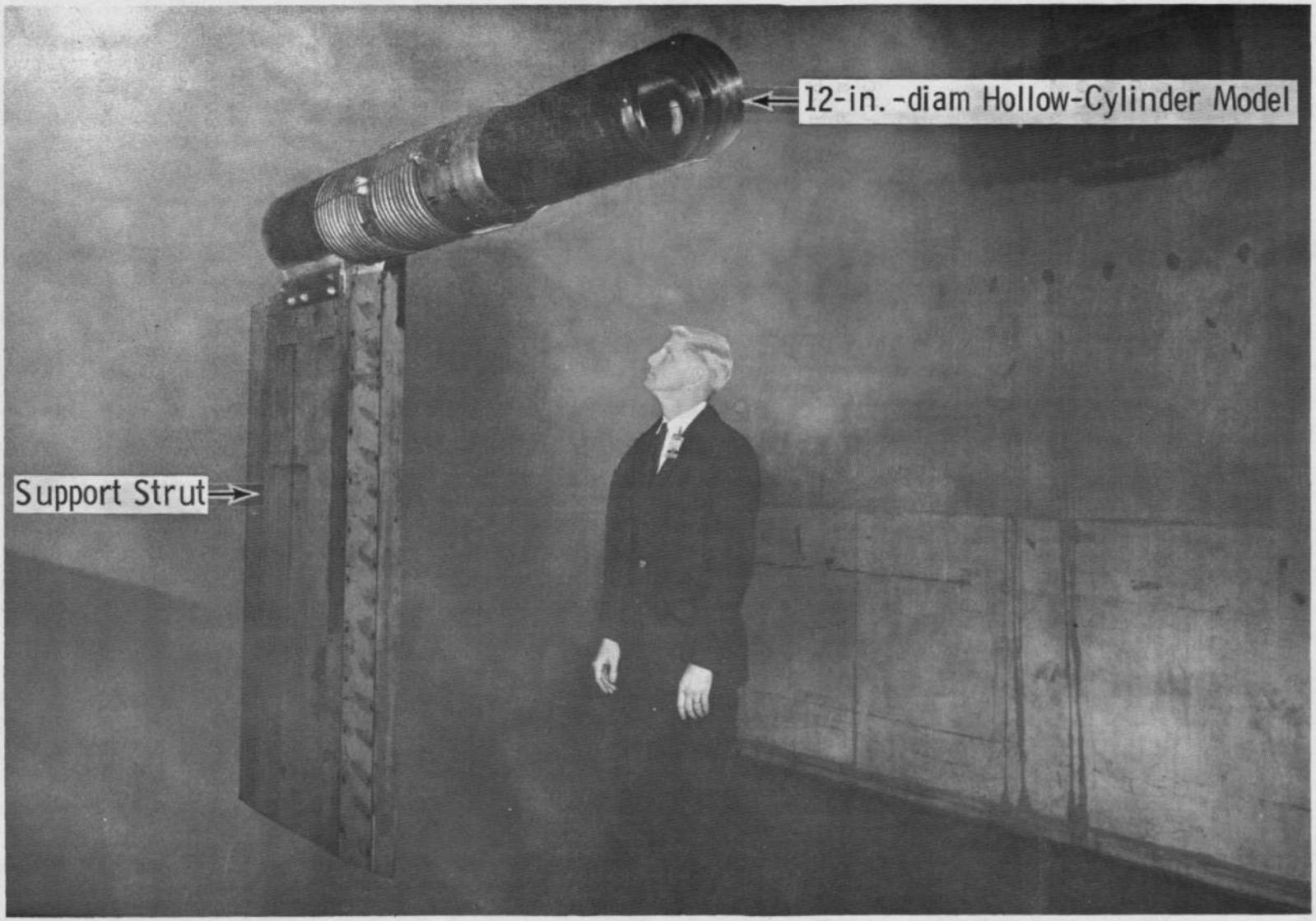

Fig. 1 AEDC-PWT-16S Transition Model Installation

2.2.2 AEDC-VKF

A 3.0-in.-diam by 32-in.-long hollow cylinder having a surface finish of 15 μin. was the transition model used in the AEDC-VKF Tunnels A and D. This is the same model used in the previous investigations of Potter and Whitfield (Ref. 17) and Schueler (Ref. 13). Interchangeable nose sections having leading-edge, internal bevel angles of 6 and 12 deg and leading-edge bluntness ($\bar{b}$) of 0.0013, 0.0021, 0.0030, and 0.0036 in. were tested. The maximum deviation of the nose bluntness was ± 0.0001 in. around the leading-edge circumference. A remotely controlled, electrically driven, surface pitot probe provided a continuous trace of the probe pressure on an X-Y plotter from which the location of transition was determined.

Boundary-layer profiles were measured in the AEDC-VKF Tunnel A on the flexible plate near the model location with a 23-probe pitot rake to determine the characteristics of the wall turbulent boundary layer.

Additional information on the design of the AEDC-VKF 3.0-in.-diam transition model and the experimental values of the AEDC-VKF Tunnel A flexible plate boundary-layer characteristics are presented in Figs. II-2 and II-3, respectively, in Appendix II.

2.3 AEDC-VKF TUNNEL A SHROUD MODEL

The 12-in.-diam shroud and 3.0-in.-diam, hollow-cylinder, transition model installation in the AEDC-VKF Tunnel A are shown in Fig. 2. The steel shroud had an external, leading-edge bevel angle of 10-deg and a leading-edge bluntness value of approximately 0.007 in. with an internal surface finish of 50 μin. The shroud design was such that the weak shock waves emanating from the shroud leading edge did not impinge on the test area of the 3.0-in.-diam transition model, as illustrated in Fig. 2. A 15-probe rake was used to measure the boundary-layer profiles on the inside shroud wall. From these data, the condition of the boundary layer, whether turbulent or laminar, along with other boundary-layer characteristics were determined.

Detailed information pertaining to the shroud design and the experimental test results obtained using the shroud are presented in Appendix III.

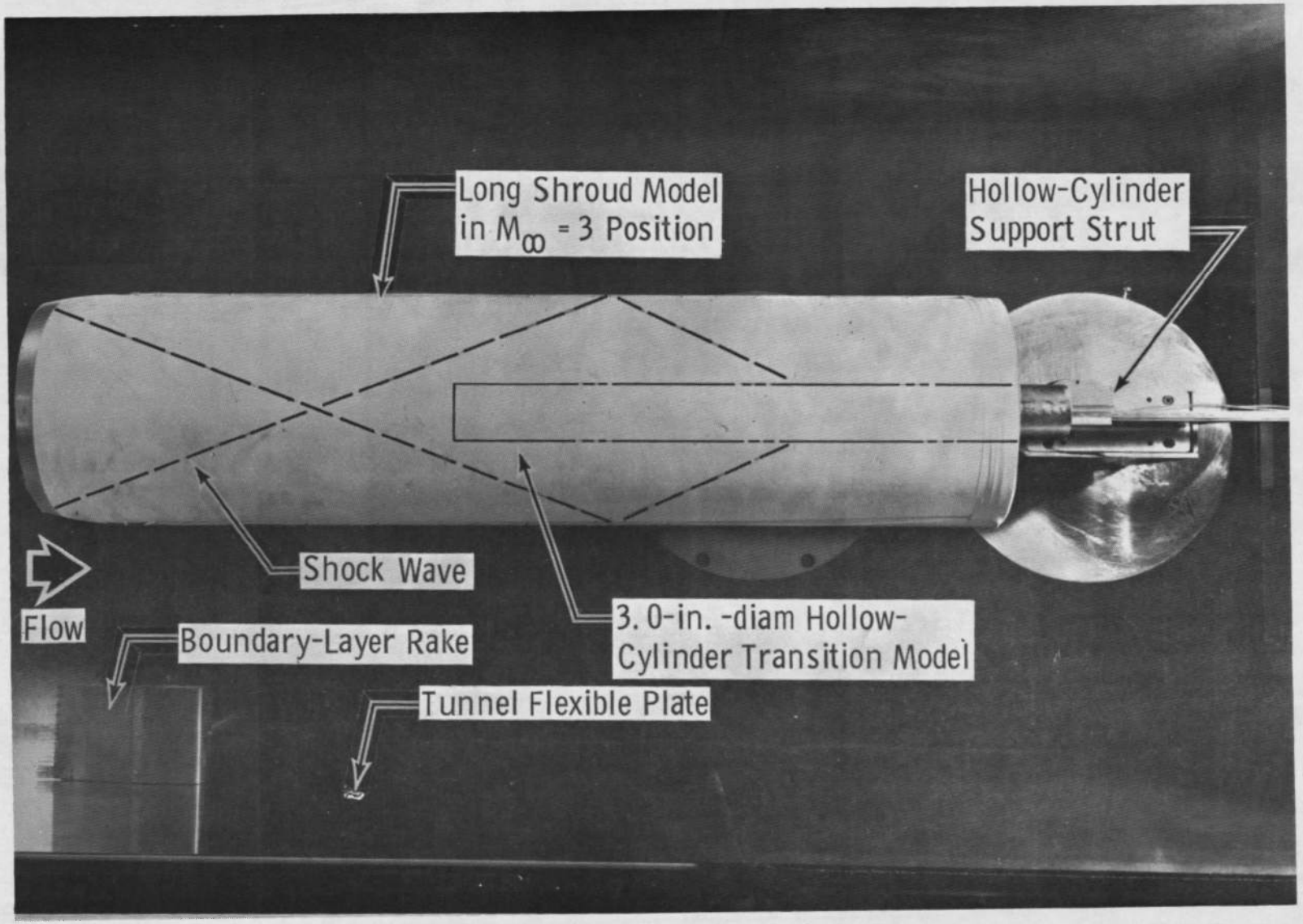

Fig. 2 Long Shroud Installation in the AEDC-VKF Tunnel A

SECTION III
BASIC TRANSITION RESULTS

Experimental transition studies were conducted in the AEDC-VKF Tunnels A and D and the AEDC-PWT-16S tunnel to provide data from the largest range of wind-tunnel sizes available and, thereby, test the validity of the proposed correlation of transition Reynolds numbers.

Comparisons of typical pitot pressure data obtained in the AEDC-VKF 12-in. Tunnel D, 40-in. Tunnel A and the AEDC-PWT 16-ft supersonic tunnel are shown in Fig. 3 for $M_\infty = 3.0$. These data clearly show the large increase in transition location, and consequently transition Reynolds number (Re_t), with increasing tunnel size and confirm the earlier results of Schueler (Ref. 13). This increase in Re_t with increasing tunnel size is in accordance with the aerodynamic noise philosophy discussed in Sections I and V.

The location of transition used in this report is defined as the peak in the pitot pressure profile as indicated in Fig. 3. This method of transition detection is generally accepted as being near the end of the transition process and has been established as one of the more repeatable and reliable methods of selecting a particular and finite location for transition (see Refs. 13, 17, and 18).

Basic transition Reynolds number results from the AEDC-VKF Tunnels D and A and the AEDC-PWT-16S tunnel for $M_\infty = 3.0$ are presented in Fig. 4 for the test unit Reynolds number range and various leading-edge geometries. The large increase in the transition Reynolds numbers with increasing tunnel size is again clearly shown. The AEDC-PWT transition data in Fig. 4 represent the average value of Re_t determined from the four independent pitot probes. The transition Reynolds numbers for each probe location are tabulated in Appendix I. Agreement between the four sets of Re_t values for a given test condition was good and in general agreement with the leading-edge thickness variation of approximately $\pm$ 0.0005 in. around the leading-edge circumference. The standard deviation of Re_t determined using each individual probe Re_t value and the mean Re_t curves in Fig. 4 for $\bar{b}$ = 0.0015, 0.0050, and 0.0090 in. was $Re_t = \pm 0.011 \times 10^6$. Good agreement also existed between the AEDC-VKF Tunnels D and A Re_t data from these experiments and the previous results of Potter and Whitfield (Ref. 17) and Schueler (Ref. 13), respectively, for $\bar{b}$ = 0.003 in.

All of the basic transition Reynolds number data obtained in the AEDC-PWT-16S tunnel and the AEDC-VKF Tunnels A and D are tabulated and plotted in Appendixes I, II, and IV, respectively.

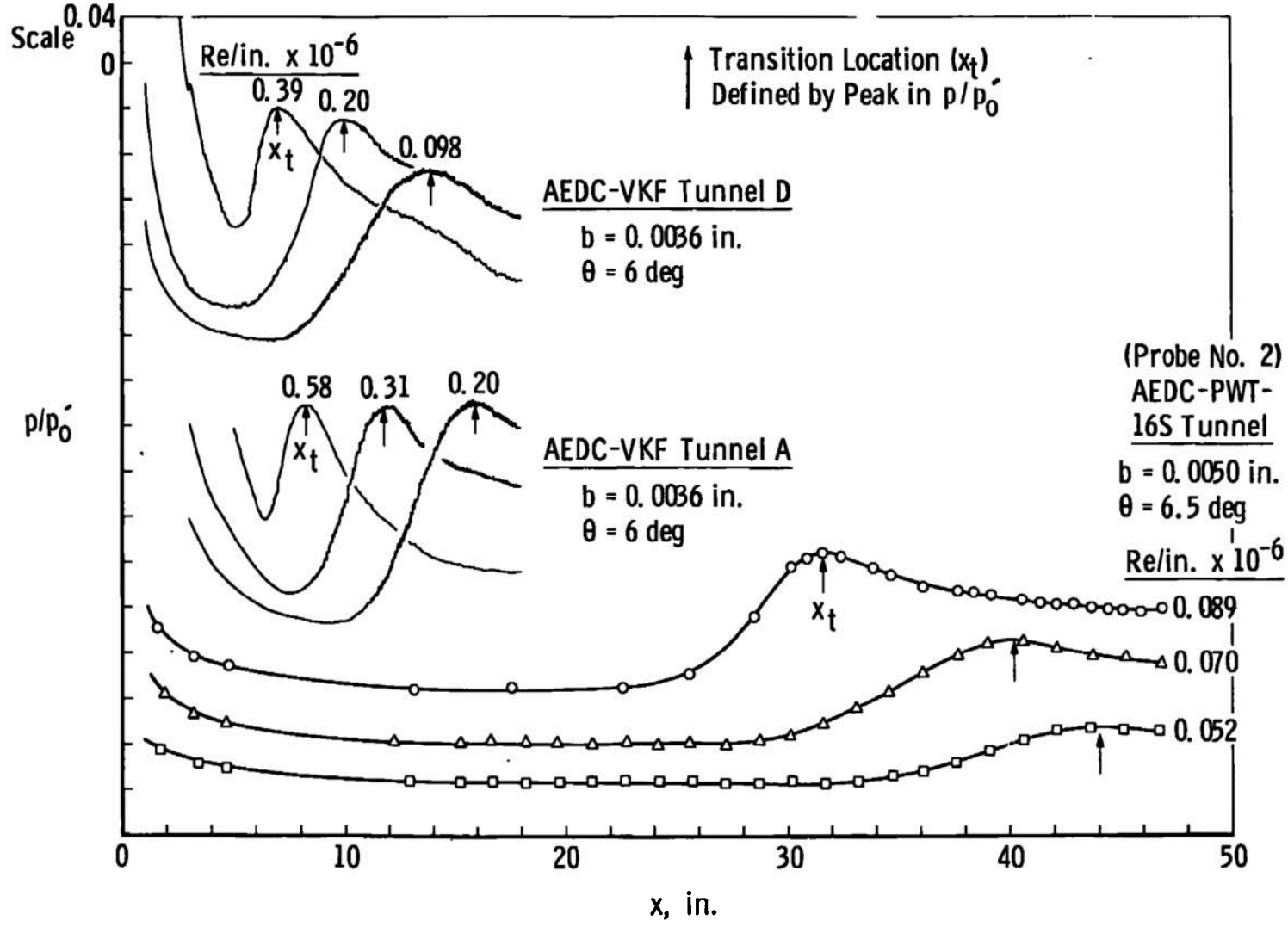

Fig. 3 Comparison of Probe Pressure Transition Traces in the AEDC-VKF Tunnels A and D and AEDC-PWT-16S for M_∞ = 3.0

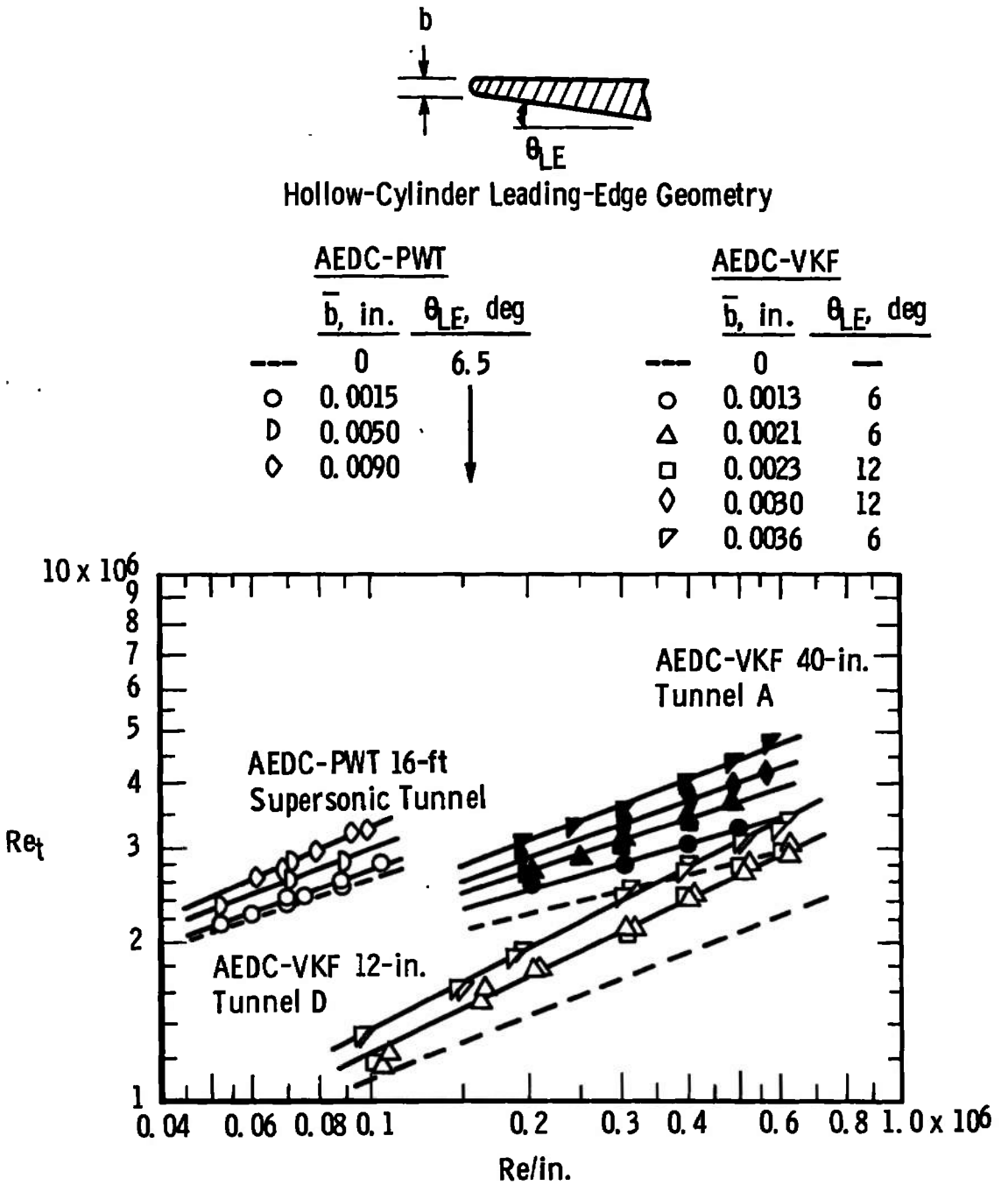

Fig. 4 Basic Transition Reynolds Number Data from the AEDC-VKF 12-in. Tunnel D and 40-in. Tunnel A and the AEDC-PWT 16-ft Supersonic Tunnel at $M_\infty = 3.0$

Brinich in Ref. 19 reported that the effect of leading-edge bevel (θ_{LE} = 5 and 30 deg) on boundary-layer transition was negligible at M_∞ = 3. However, Potter and Whitfield (Ref. 17) correlated three sets of M_∞ = 3 transition data using the bevel angle as a parameter. Unfortunately, the three sets of data were from three different wind tunnels. Later experiments by Whitfield and Potter (Ref. 18) at a Mach number of eight showed no bevel angle effect. Therefore, in order to use transition data in this research from various sources, it was felt necessary to determine conclusively if the leading-edge bevel angle has an influence on transition at supersonic speeds. The data in Fig. 4 from the AEDC-VKF Tunnels A and D for bevel angles of 6 and 12 deg clearly show no bevel angle effect at M_∞ = 3. Similar results were also obtained at M_∞ = 4 and 5 in Tunnel A (see Appendix II). Therefore, it was concluded that there is no leading-edge bevel-angle effect on transition Reynolds numbers from sharp-leading-edge models at supersonic and hypersonic speeds.

SECTION IV
SHROUD TRANSITION AND NOISE RESULTS

Previous experiments using two concentric hollow cylinders with the outer cylinder serving as a shield to protect the smaller hollow cylinder from the tunnel radiated aerodynamic noise were reported in Ref. 20. The idea was to measure the transition point on the inside of the smaller shroud using a pitot probe and, thereby, provide some measure of the effect that a radiated pressure field had on transition. Unfortunately, the presence of the outer cylinder introduced disturbances in the flow, and the results were inconclusive.

Based on the negative results of those experiments, a somewhat different approach was used in this investigation. The experimental apparatus employed to demonstrate the effects of radiated aerodynamic noise generated by a turbulent boundary layer consisted of a 12-in.-diam shroud model placed concentrically around the 3.0-in.-diam hollow cylinder transition model, as shown in Fig. 2 and Fig. III-1 in Appendix III. This design was selected primarily because it allowed a controlled boundary-layer environment to be maintained on the shroud inner wall upstream of the transition model. Also the shroud provided some protection from the noise radiating from the turbulent boundary layer on the wall of the 40-in. Tunnel A. The procedure was to measure the location of transition on the 3.0-in.-diam model as the boundary layer on the shroud inner wall upstream of the transition model changed from laminar to turbulent.

From the earlier experiments of Laufer (Refs. 7, 11, and 20) and Morkovin (Refs. 3 and 5) it was anticipated that when the shroud wall boundary layer changed from laminar through transitional to fully turbulent then the radiated aerodynamic noise would increase and adversely influence the location of transition on the internal 3.0-in.-diam transition model.

Experimental results from the shroud test in the AEDC-VKF Tunnel A are presented in Figs. 5 and 6 for M_∞ = 3.0 and 5.0, respectively. Figures 5a and 6a are sketches showing the location of transition on the shroud inner surface for various unit Reynolds numbers. With a boundary trip in position 1/8-in. from the shroud leading edge, the flow was turbulent very near the trip for M_∞ = 3.0 and Re/in. $\geq 0.2 \times 10^6$ (Fig. 5a). The effectiveness of the trip (serrated fiber glass tape) at M_∞ = 3 was determined from separate studies conducted in the AEDC-VKF Tunnel D, as shown in Fig. IV-4 in Appendix IV. From the results shown in Fig. 6b, it was concluded that the trip was not effective at M_∞ = 5.0.

Large changes in the transition Reynolds numbers on the 3.0-in.-diam, hollow-cylinder model (as compared to the no shroud case) were obtained as the shroud boundary layer upstream of the 3.0-in. model was changed from laminar to turbulent by using the trip and/or by increasing the unit Reynolds number as are clearly and distinctly shown in Figs. 5b and 6b. The no-shroud basic Re_t data are presented for comparison. It is suggested from 5b that the decrease in the no-trip Re_t results with increasing Re/in. values and the large reduction in Re_t with the trip in position are directly related to the formation of the turbulent boundary layer on the inside shroud wall and the resulting generation of radiated pressure fluctuations (aerodynamic noise).

It is of interest to note that the M_∞ = 5 transition Reynolds number results in Fig. 6b exhibited the characteristic decrease in Re_t with a decrease in leading-edge bluntness ($\bar{b}$) even when exposed to the intensified field of radiated noise.

Static pressure measurements on the shroud inner surface and the 3.0-in., hollow-cylinder, external surface confirmed that the flow was supersonic at all times. The impingement of the shroud leading-edge shock wave was downstream of the transition area ($0 < x_t \lesssim 15.5$ in.), as confirmed by the surface probe pressure data and the hollow-cylinder surface static pressures. The strength of the leading-edge shock was equivalent to approximately a 1.0-deg, two-dimensional wedge shock. For example, at M_∞ = 3.0 the shroud static pressure ratios near the leading edge were on the order of p_s/p_∞ = 1.06,

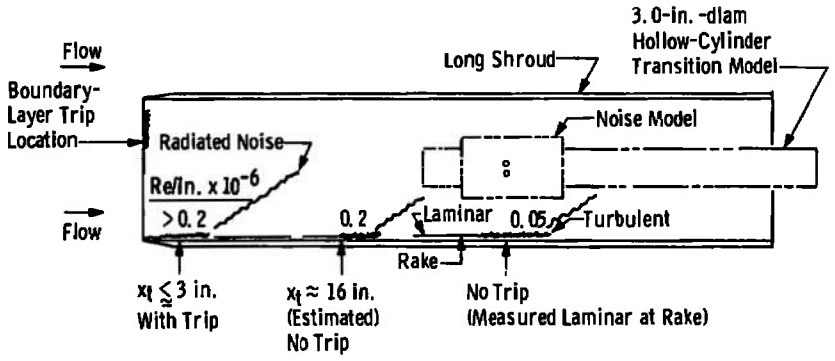

a. Boundary-Layer Development inside Long Shroud

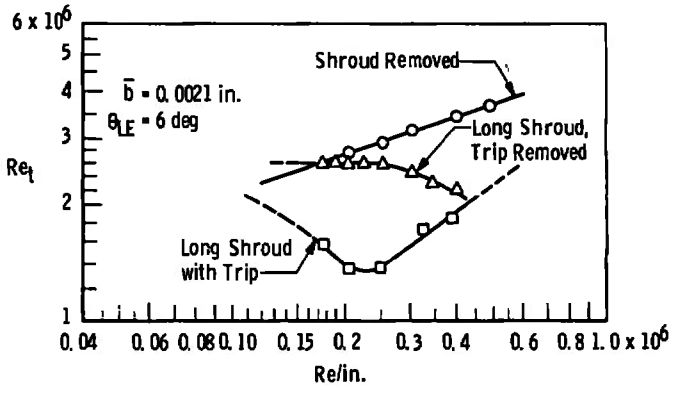

b. Transition Reynolds Numbers on the 3.0-in.-diam Hollow-Cylinder Model

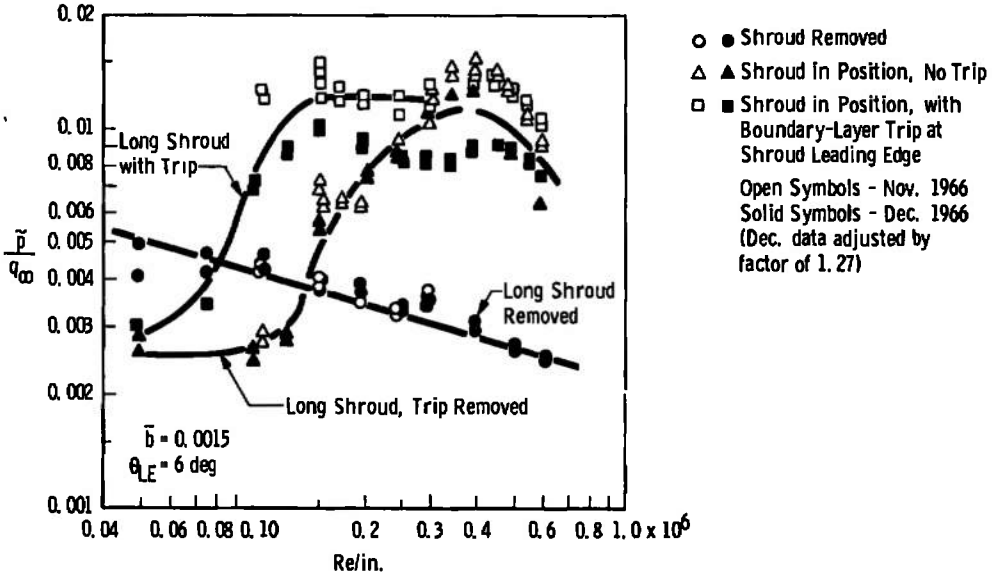

c. Root-Mean-Squore Radiated Pressure Fluctuations

Fig. 5 Comparisons of Transition Reynolds Numbers and Root-Mean-Square Radiated Pressure Fluctuations at M_∞ = 3.0

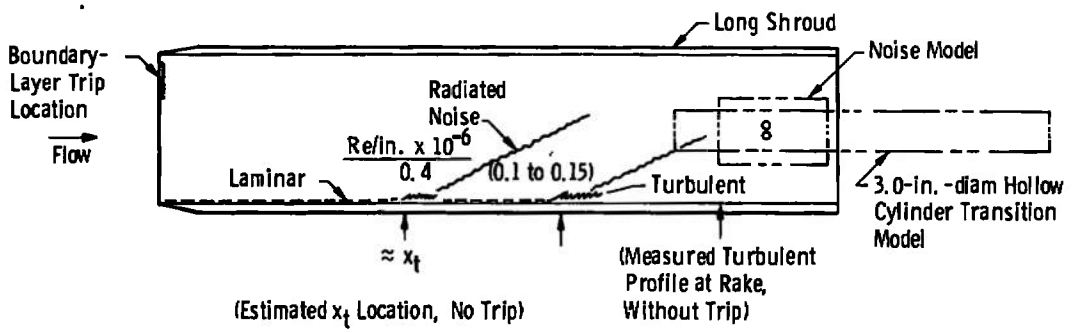

a. Boundary-Layer Development inside Long Shroud

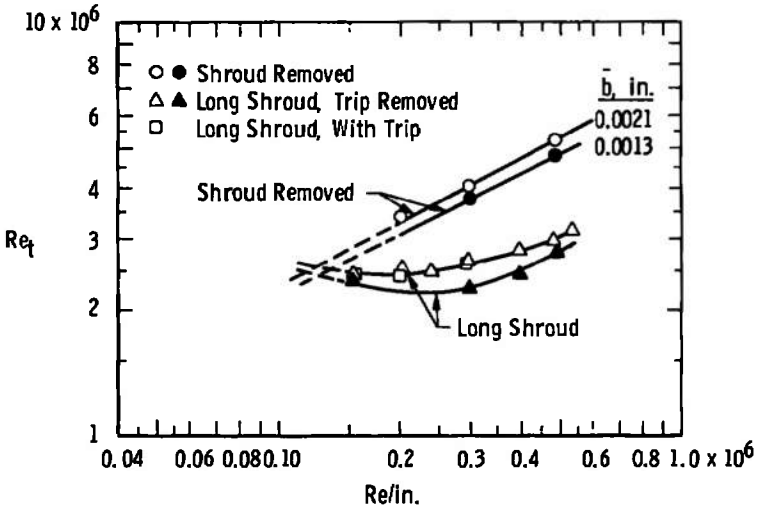

b. Transition Reynolds Numbers on the 3.0-in.-diam Hollow-Cylinder Model

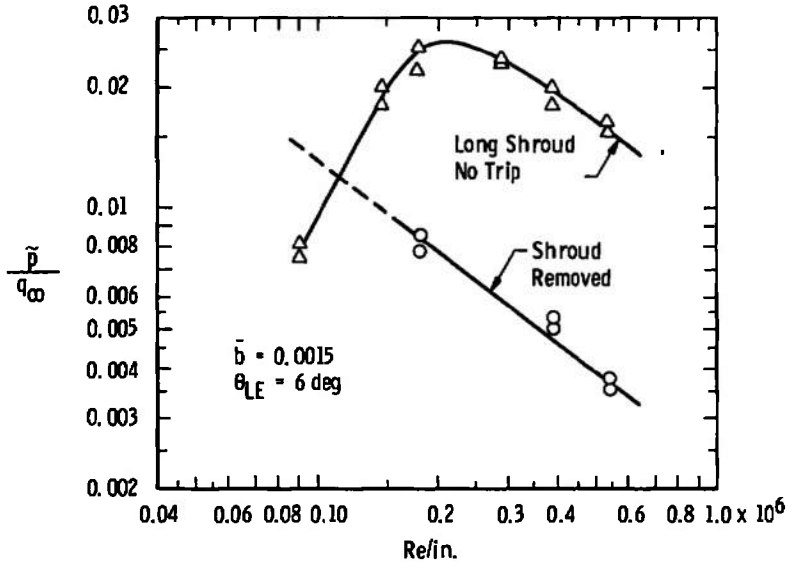

c. Root-Mean-Square Radiated Pressure Fluctuations

Fig. 6 Comparisons of Transition Reynolds Numbers and Root-Mean-Square Radiated Pressure Fluctuations at $M_\infty = 5.0$

and the corresponding hollow-cylinder and flat-plate surface static pressure ratios were equal to $p_s/p_\infty = 1.15$. Hollow-cylinder static pressure ratios with the shroud removed were equal to $p_s/p_\infty = 1.02$ at $M_\infty = 3$.

Additional information on the surface pressure distributions inside the long shroud, typical surface probe pitot transition profiles, the transition Reynolds number values obtained inside the shroud, and the shroud inner wall measured boundary-layer characteristics are presented in Appendix III for $M_\infty = 3$, 4, and 5.

Confirmation of the proposed effects of aerodynamic noise on the shroud transition results was provided by an 8- by 5-in. sharp-leading-edge flat plate ($\bar{b} = 0.0015$ in., $\theta_{LE} = 6$ deg) microphone model located as shown in Figs. 5a and 6a. The flat-plate model was instrumented with two commercially available 1/4-in.-diam condenser microphones having a frequency response range from zero to one-hundred-thousand cycles per second. One microphone was mounted flush with the plate surface, and the second was mounted internally to record model vibrational effects on the microphone response. Vibrational effects were found to be insignificant. The microphone data were recorded visually from two RMS voltage meters and also recorded on magnetic tape. The uncorrected RMS pressure fluctuations received by the surface microphone are plotted in Figs. 5c and 6c as a function of the tunnel Re/in. values for the conditions of shroud off and shroud on. The shroud-on configuration was tested with and without a boundary-layer trip in position near the shroud leading edge. It is clearly seen that the RMS radiated pressure fluctuations in Figs. 5c and 6c were a mirror image of the transition data in Figs. 5b and 6b, respectively; i.e., as the aerodynamic noise increased, the Re_t decreased. Furthermore, the trends and intersection points of the radiated pressure data were in good agreement with the Re_t results. For example, the $M_\infty = 3$, long shroud, no-trip Re_t data in Fig. 5b intersected the shroud-removed data at a Re/in. value near 0.15×10^6 and intersected the trip Re_t data at approximately 0.40×10^6. Correspondingly, the $\overline{p}/q_\infty$ data in Fig. 5c exhibited very nearly identical points of intersection. Details of the microphone model and additional information on the microphone are included in Appendix III.

For the no-shroud case, it is of interest to note the decrease in the noise results and the corresponding increase in the Re_t data with increasing unit Reynolds number. This trend adds support to the tentative suggestion that a part of the Re_t variation with unit Reynolds number in supersonic and hypersonic tunnels is a result of decreasing radiated pressure fluctuations with increasing unit Reynolds number.

Similar transition results with and without the shroud configuration were also obtained in Tunnel A at $M_\infty = 4$. At a unit Reynolds number value of 0.34×10^6 the AEDC-VKF Tunnel D $\tilde{p}/q_\infty$ data obtained using the same microphone model and instrumentation were approximately three to four times higher than the Tunnel A noise results for Mach $M_\infty = 3$ and 4.

It is felt that these data show conclusively the strong effect of radiated aerodynamic noise generated by a turbulent boundary layer on boundary-layer transition.

The tunnel radiated pressure fluctuations ($\tilde{p}/q_\infty$) without the shroud presented in Figs. 5c and 6c were in qualitative agreement in both magnitude and trend with the hot-wire, RMS, $\tilde{p}/q_\infty$ data of Laufer published in Refs. 7 and 11. Also the Tunnel A, no-shroud, $M_\infty = 3$ data scaled with the wall turbulent shear stress and were independent of unit Reynolds number as were the hot-wire results of Laufer (Ref. 11) and the microphone data of Kistler (Ref. 10).

SECTION V
TRANSITION CORRELATION

Theoretical and experimental studies contributing to the basic understanding of the radiated pressure field generated by a turbulent boundary layer were reviewed in Section I. These investigations determined that the major factors which influence the radiated fluctuating pressures are the turbulent-boundary-layer wall mean shear and thickness, the Mach number, and the tunnel test-section size. Using these factors as a guide and employing the premise that transition Reynolds numbers in supersonic ($M_\infty \geq 3$) and hypersonic wind tunnels are influenced primarily by the radiated aerodynamic noise, a correlation of transition Reynolds numbers was developed.

The correlation was based on two-dimensional, hollow-cylinder transition data obtained in these experiments from the AEDC-VKF 12-in. and 40-in. and the AEDC-PWT 16-ft tunnels and from previously published hollow-cylinder data from the AEDC-VKF 12-in. and 40-in. tunnels and hollow-cylinder and flat-plate transition data published from six other wind tunnels of various sizes. The test conditions covered a Mach number range from 3 to 8 and a unit Reynolds number range from 0.05×10^6 to 1.1×10^6 per inch.

The nine wind-tunnel facilities that provided transition data used in the correlation are tabulated in Table I along with the specific range of test conditions and pertinent model details.

Values of the transition Reynolds numbers used in the correlation correspond to the location determined from the peak in the surface pitot probe pressure trace and are for a zero leading-edge bluntness. Transition data from other sources which were not obtained using a pitot probe were adjusted according to Refs. 17 and 18, as listed in Table I. The zero-bluntness Re_t data were obtained by extrapolating the transition values from sharp, but finite leading-edge models (see Table I) to b = 0. It is desirable to correlate data for b = 0 since this in effect removes the model leading-edge geometric influences.

Transition Reynolds number data from the nine wind tunnels are presented in Fig. 7 as a function of the wall, mean turbulent, skin-friction coefficient (C_F), the wall boundary-layer displacement thickness (δ^*), and the tunnel circumference (c). The parameter $Re_t \sqrt{\delta^*/c}$ is seen to have correlated the data as a function of C_F for a particular size tunnel; however, the results show a definite and regular behavior with increasing tunnel size. The mean skin-friction coefficient was determined from Ref. 21 using the model locations (ℓ_m) listed in Table I. When the experimental δ^* values in the tunnel test section were not available, then empirical δ^* values were determined using the correlation method presented in Ref. 22. Table I provides additional information on the source of values used for δ^*. Appendix V gives additional information on experimental and theoretical (Ref. 21) mean skin-friction coefficients and the δ^* correlation method of Ref. 22.

The normalized parameter

$$Re_t \sqrt{\frac{\delta^*}{c}} \Bigg/ \left(Re_t \sqrt{\frac{\delta^*}{c}} \right)_{c_1=48 \text{ in.}}$$

is plotted in Fig. 8 for the four basic size tunnels. A linear fairing of these data provides a method for collapsing all the Re_t data in Fig. 7 onto a single correlation curve.

Figure 9 presents the final correlation of the transition Reynolds number data. It should be noted that the correlation was independent of unit Reynolds number and Mach number and depended only on the aerodynamic noise parameters, C_F, δ^*, and c. The transition data used in Fig. 9 covered the full Mach number and unit Reynolds number ranges of each data source. An empirical equation can be written for the data correlation in Fig. 9 as

$$Re_t = \frac{0.0141 \, (C_F)^{-2.55} \left[0.56 + 0.44 \, \frac{c_1}{c} \right]}{\sqrt{\frac{\delta^*}{c}}}$$

TABLE I
SOURCE AND RANGE OF DATA USED IN THE CORRELATION

Ref.	Sym	M_∞	$\bar{L} \times 10^{+3}$, in.	θ_{LE}, deg	(Re/in.) Range $\times 10^{-6}$	Model Config.	Tunnel	Test Section Size	Method of Transition Detection	Amount of Adjustment	l_m, in.	Method of δ^* Determination
Present Study & 17	○	3.0	1.3, 2.1, 2.3 3.0, 3.6	6, 12	0.1 to 0.6	HC	AEDC-VKF-D	12- by 12-in.	Maximum p	No adjustment	48 5	Flexible Plate, Rake Profiles, (l_r = 56 in.) from Ref. 33
17	△	4.0	3, 8	6	0.1 to 0.6							
17	□	5.0	3, 8	6	0.1 to 0.4							
25	▱	5.0	1	10	0.2 to 1.0	FP	AEDC-VKF-E	12- by 12-in.	Maximum p		64	$\bar{\delta}^*$ Correlation Ref. 22 (l_r = 64 in.) from Fig. V-1, Appendix V
26	◇	6.1	1.1, 2, 4	15	0.3 to 1.1	FP					60	
	◁	7.1	1.1, 2, 4		0.2 to 0.7							
	○	8.0	1.1, 2		0.3 to 0.5							
Present Study & 13	●	3.0	1.3, 2.1, 2.3 3.0, 3.6, 8	6, 12	0.15 to 0.6	HC	AEDC-VKF-A	40- by 40-in.	Maximum p		231 and 213	Flexible Plate, Rake Profiles (l_r = 208 in.) from Fig. II-3 Appendix II
	▲	4.0	2.1, 3, 3.6, 8	6	0.15 to 0.6							
	■	5.0	1.3, 2.1, 3, 3.6, 8	6, 12	0.15 to 0.6							
18	◖	8.0	0.6 to 9.4	5.6, 12.5	0.1 to 0.3	HC	AEDC-VKF-B	50-in Diam	Maximum p		232	Rake Profiles (l_r = 244 in.) from Unpublished AEDC Data and Ref. 35
31	○	3.7	≤1	15	0.1 to 0.4	FP	JPL 20-in. SWT	18- by 20-in.	Maximum τ_w		≈118	Flexible Plate, Rake Profiles (l_r = 117 in.) from Ref. 34
31	◇	4.6	≤1	15	0.1 to 0.4	FP	JPL 20-in. SWT	18- by 20-in.	Maximum τ_w		≈118	
28	◊	6.0	≤2	20	0.59, 0.69	FP	NASA-Langley	20- by 20-in.	Maximum $\dot{q}$	1.1*	≈90	$\bar{\delta}^*$ Correlation from Fig. V-1, Appendix V
27	◆	6.0	1	20	0.14, 0.27	FP	AEDC-VKF-B	50-in. Diam	Maximum p	No adjustment	≈232	Rake Profiles (l_r = 244 in.) from Unpublished AEDC Data and Ref. 35
27	◖	8.0	1	20	0.2	FP	AEDC-VKF-B	50-in. Diam	Maximum p	No adjustment	≈232	
29	▱	3.1	0.8 to 8.0	5	0.1 to 0.6	HC	NACA-Lewis	12- by 12-in.	Maximum T_w	1.2*	40.5	$\bar{\delta}^*$ Correlation from Fig. V-1, Appendix V
30	◊	5.0	1, 5, 10	15	0.15 to 0.4	HC	NASA-Lewis	12- by 12-in.	Maximum T_w	1.15*	47	
Present Study	⊕	3.0	1.5, 5, 9	6.5	0.05 to 0.11	HC	AEDC-PWT-16S	16- by 16-ft	Maximum p	No adjustment	792	Flexible Plate, Rake Profiles (l_r = 839 in.) from Fig. I-3, Appendix I

Symbols correspond to data in Figs. 7 and 9.

HC - Hollow Cylinder
FP - Flat Plate

*Adjustment based on results from Refs. 17 and 18

τ_w - Surface Shear Stress
$\dot{q}$ - Heat Transfer
p - Maximum Surface Pitot Probe Pressure
T_w - Maximum Surface Temperature

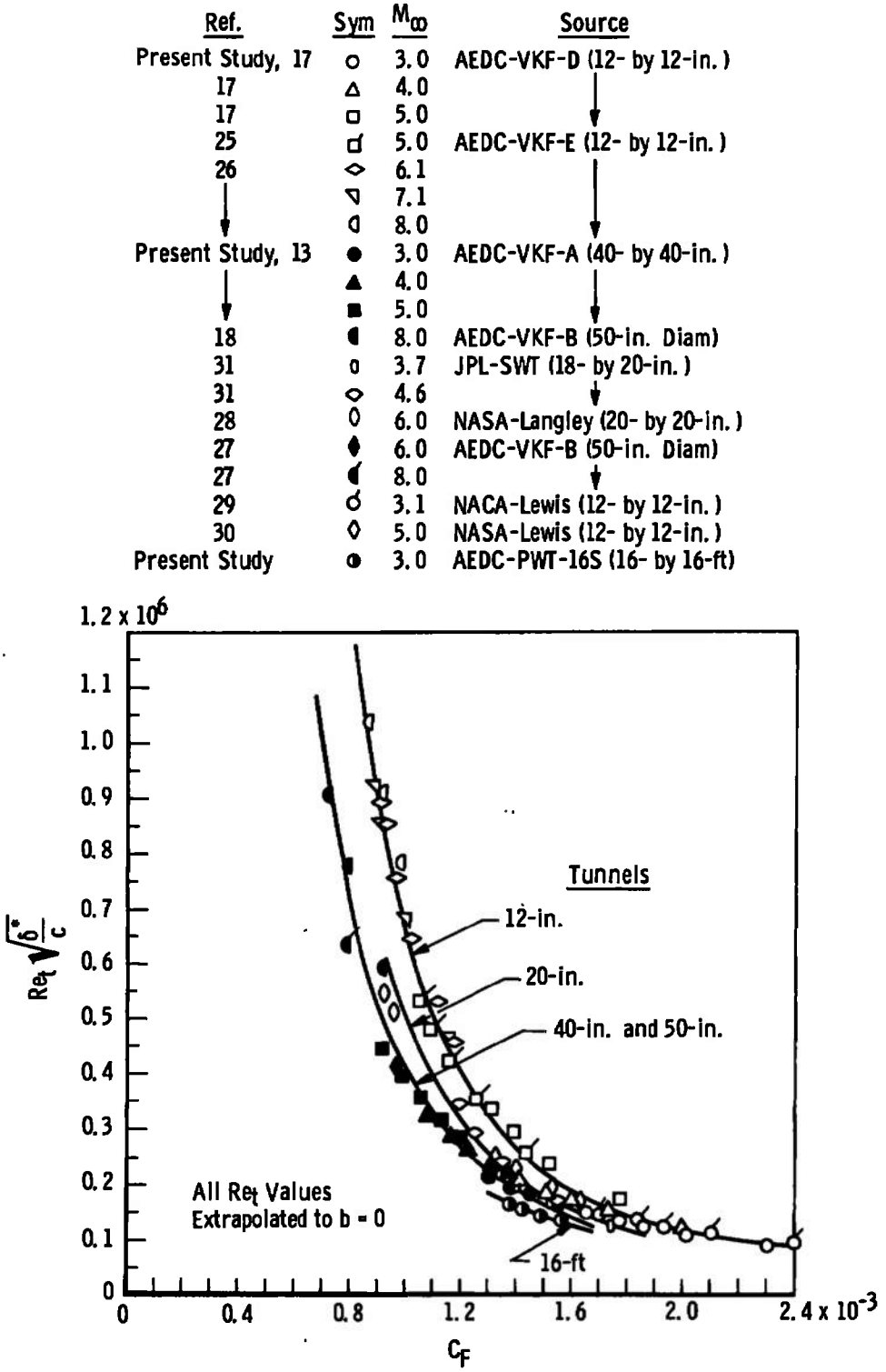

Fig. 7 Influence of Tunnel Size on the Boundary-Layer Transition Reynolds Number Correlation

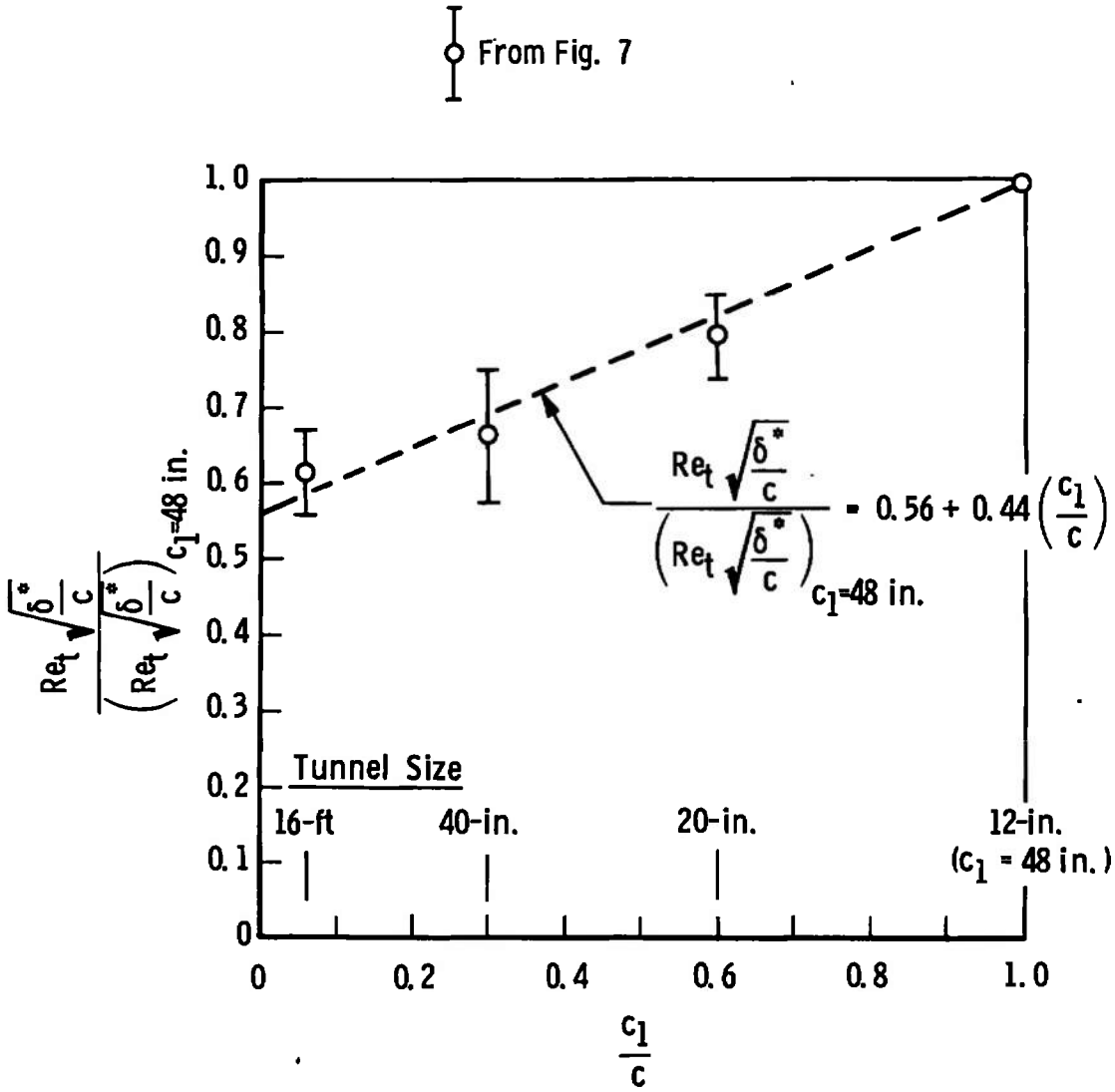

Fig. 8 Tunnel Size Parameter

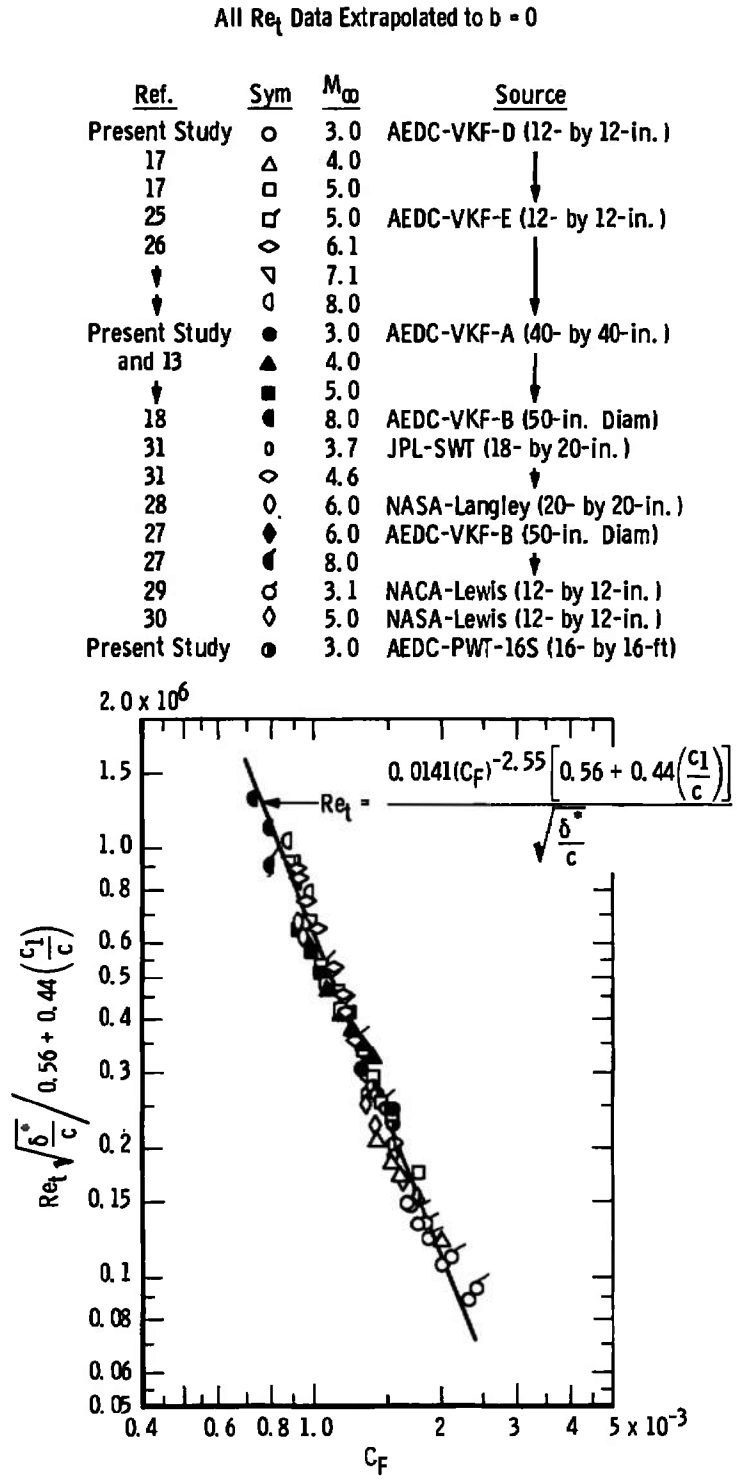

Fig. 9 Correlation of Transition Reynolds Number

The aerodynamic noise parameters (C_F, δ^*, and c) appearing in the correlation and empirical equation are the same factors that have been shown by previous investigators to be significant factors in turbulent-boundary-layer-generated aerodynamic noise.

The reader is reminded that the transition Reynolds number correlation presented in Fig. 9 and the resulting empirical equations are applicable only to wind tunnels having turbulent boundary layers on the walls. The correlation cannot be applied to ballistic ranges or free flight because of the obvious restrictions imposed by C_F and δ^*. Similarly, since the correlation was developed for finite-size wind tunnels and the proper boundary conditions for free flight are not included, conclusions relative to fundamental influences on transition in free flight cannot be drawn, i.e., the influence of Mach number and unit Reynolds number, per se. The correlation does, however, clearly establish that a major and, perhaps, dominant influence of aerodynamic noise exists in wind-tunnel transition experiments.

SECTION VI
COMPARISONS OF CORRELATION PREDICTIONS WITH EXPERIMENTAL RESULTS

6.1 INFLUENCE OF UNIT REYNOLDS NUMBER, MACH NUMBER, AND TUNNEL SIZE

Typical transition Reynolds number data are presented in Figs. 10, 11, and 12 to illustrate the variation of Re_t with changes in the unit Reynolds number, tunnel size, and tunnel Mach number. The increase in Re_t with increasing tunnel Mach number (Figs. 10a and 12) and unit Reynolds number (Fig. 10a) is a characteristic trend shown previously by many investigators, but the increase in Re_t with tunnel size presented in Figs. 10b, 11, and 12 has not been shown previously. The experimental noise results presented in Figs. 5 and 6, along with the general success of the correlation and the good agreement between the experimental Re_t data in both magnitude and trend with estimates from the empirical equation, suggest that the increase in Re_t with the unit Reynolds number in supersonic and hypersonic wind tunnels is directly related to the radiated aerodynamic noise emanating from the tunnel wall turbulent boundary layer. Although this is suggested by the wind-tunnel results and the correlation, it cannot be definitely concluded because of the results from the VKF range (Ref. 23).

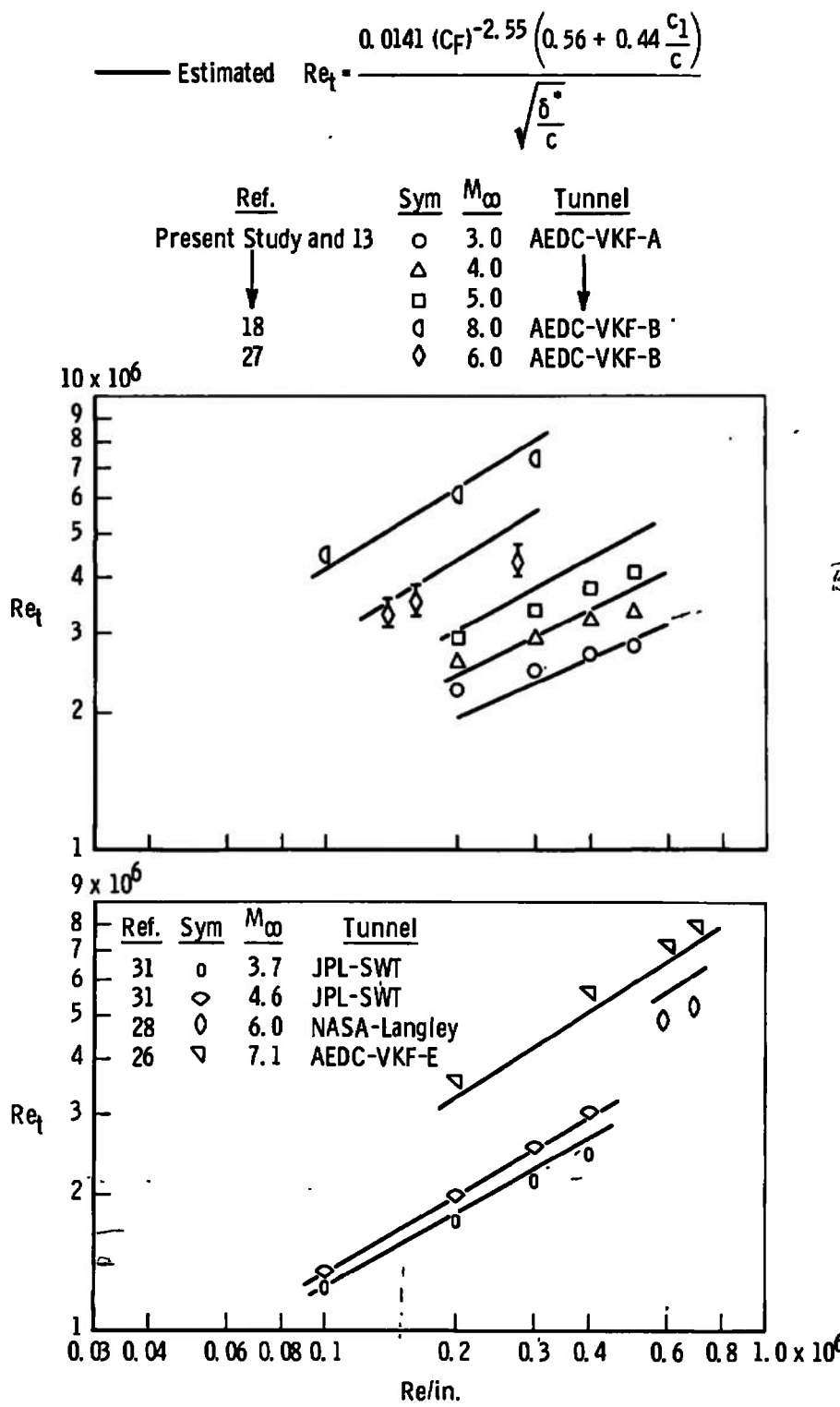

a. Mach Number and Unit Reynolds Number Effects (b = 0)

Fig. 10 Comparison of Measured and Estimated Transition Reynolds Numbers from Several Tunnels for Various Mach Numbers and Unit Reynolds Numbers

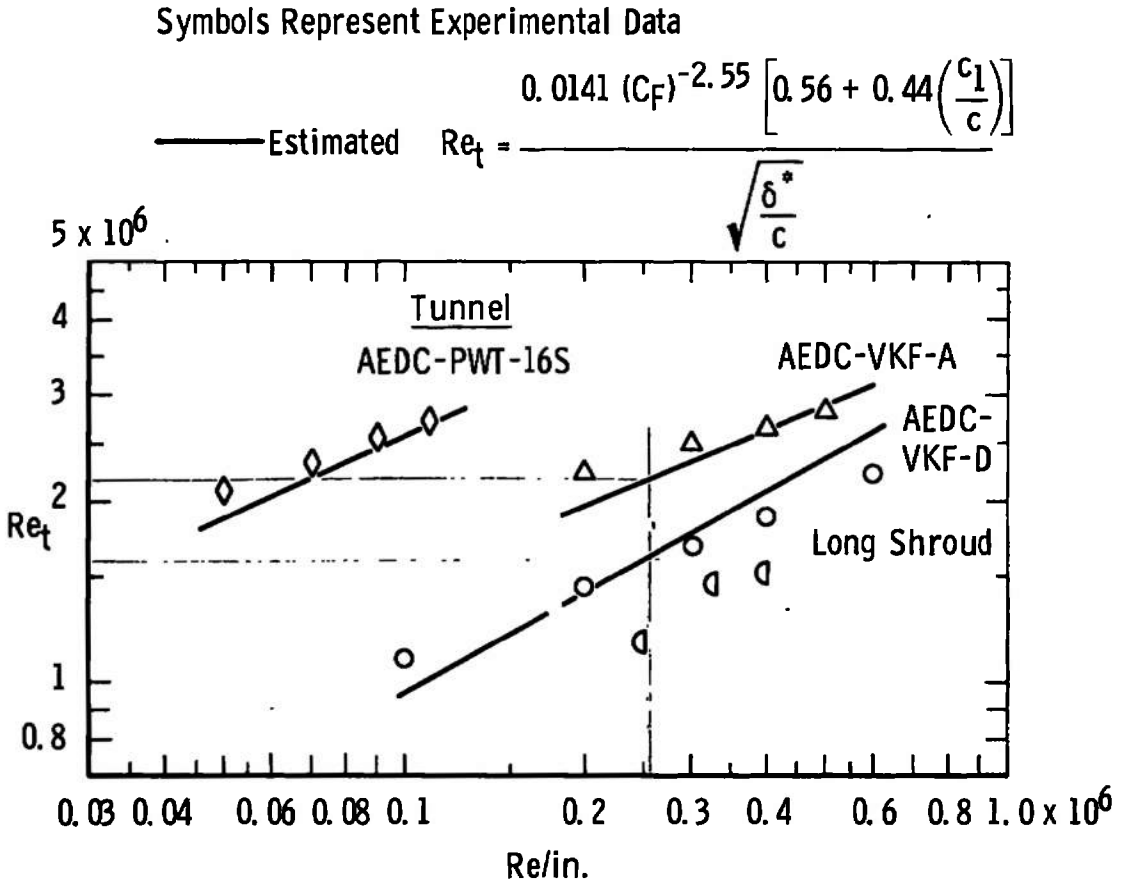

b. Tunnel Size and Unit Reynolds Number Effect at $M_\infty = 3$, $b = 0$

Fig. 10 Concluded

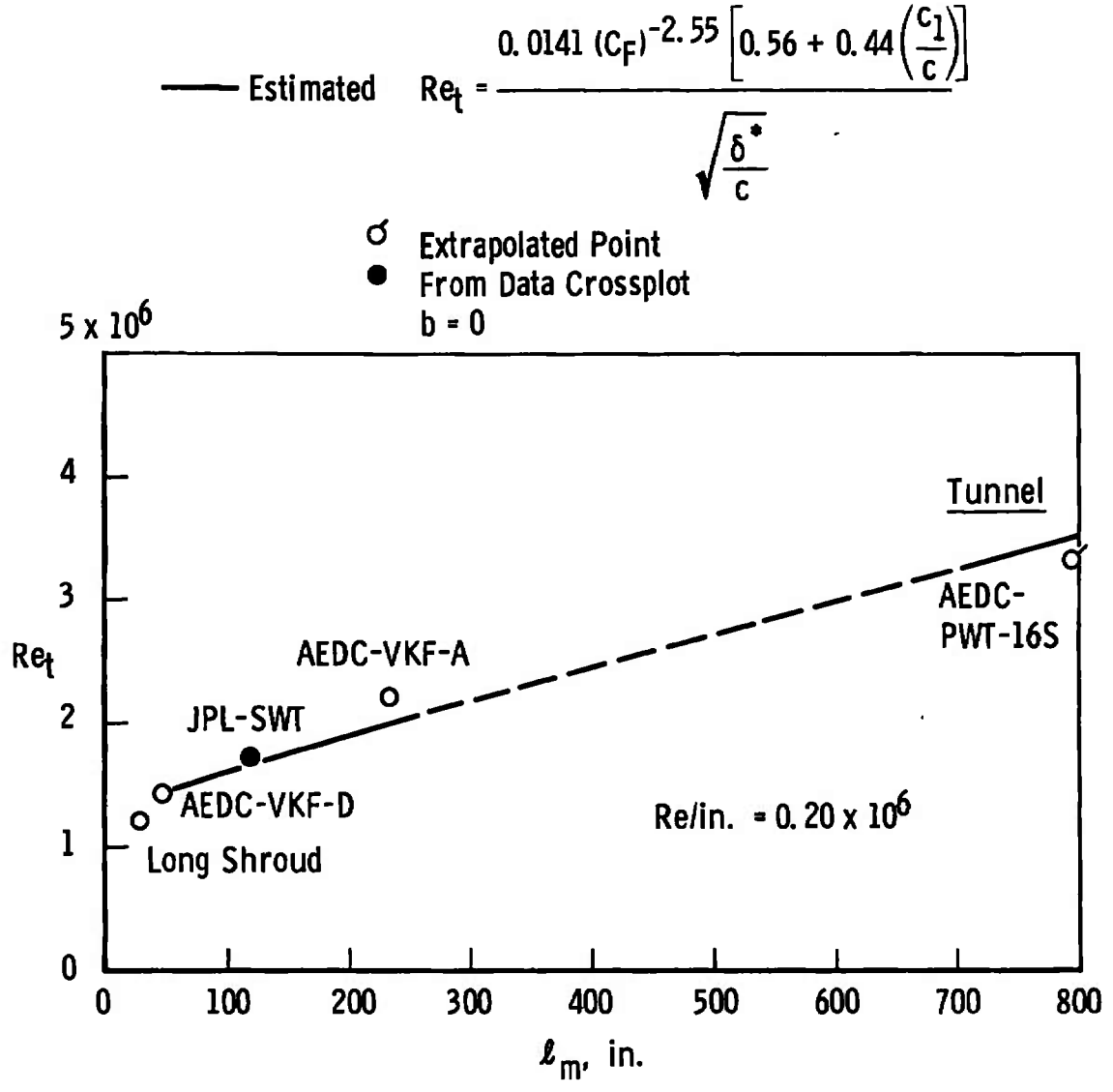

Fig. 11 Effect of the Tunnel Size on Transition at $M_\infty = 3$

Ref.	Sym	Tunnel	Test-Section Size
Present Study, 13	●	AEDC-VKF-A	40- by 40-in.
18	▲	AEDC-VKF-B	50-in. Diam
27	◤	AEDC-VKF-B	50-in. Diam
Present Study, 17	□	AEDC-VKF-D	12- by 12-in.
25, 26	◊	AEDC-VKF-E	12- by 12-in.
31	◹	JPL-SWT	18- by 20-in.
Present Study	◊	AEDC-PWT-16S	16- by 16-ft

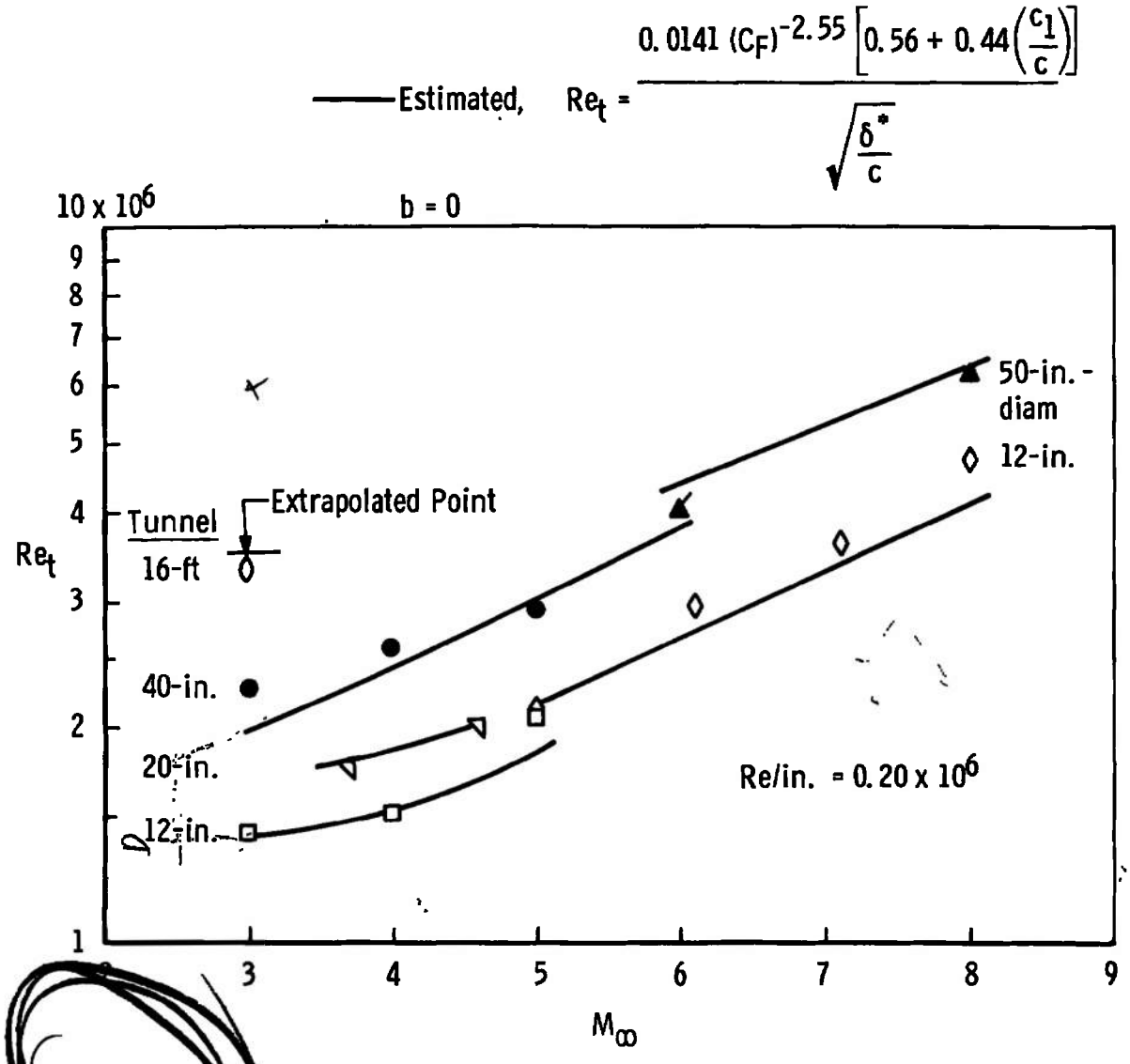

Fig. 12 Variation of Transition Reynolds Number with Increasing Tunnel Mach Number

If it is assumed that noise from various sources in a range is small compared to the wind tunnel, one would not expect a variation in transition Reynolds number with unit Reynolds number in the range as a result of noise. Potter's results presented in Ref. 23 for a 10-deg half-angle, 1.75-in.-diam cone with a 0.005-in. nose radius (one model with a 2.3-in. diameter), a local Mach number of approximately 4.34 and a wall temperature ratio of approximately 0.184 show a unit Reynolds number effect in the range.

6.2 MACH NUMBER EFFECT

Comparisons of the measured and estimated transition Reynolds numbers with increasing Mach number from several wind tunnels are presented in Fig. 12. Several important conclusions are drawn from this figure. First, it is obvious that transition data from different size wind tunnels cannot be used to establish a trend of Re_t with Mach number. Second, the correlation using C_F, δ^*, and c produced Re_t values in good agreement with the experimental results. The question that naturally arises as a result of this is concerned with what is the true Mach number effect. There are experimental data that may provide some insight into this question.

Figure 13a presents Re_t data as a function of local cone Mach number for a free-stream Mach number of eight. The data for the 7.5- and 15.8-deg cones were published in Ref. 24. The data for the 5- and 20.1-deg cones were obtained through personal correspondence with Mr. Stainback. For a given free-stream Mach number, there are two cone angles which will produce equivalent local unit Reynolds numbers but significantly different local Mach numbers. Figure 13a shows that when the local Mach number was changed from approximately 4 to 7 for constant free-stream conditions, there was no significant upward trend with Mach number except for the lowest unit Reynolds number. Stainback in Ref. 24 concluded that perhaps there was not a Mach number effect on cones as contrasted to Mach number effects on two-dimensional models similar to the results presented in Fig. 12. The conclusions of Ref. 24 are in agreement with the implications of the correlation presented herein.

It should be pointed out that the 5- and 20.1-deg cone angles produce equivalent local unit Reynolds numbers as do the 7.5- and 15.8-deg cones. However, for the local unit Reynolds number conditions to have been constant for both sets of cone values as listed in Fig. 13a, there would necessarily have been a 10- to 15-percent difference in the free-stream conditions. A 15-percent difference in Re/in. would produce a maximum change in Re_t of approximately 10 percent, and this is well within the scatter of the data.

Sym	$(Re/in.)_\delta \times 10^{-6}$	θ_c, deg: 5, 20.1 $(Re/in.)_\infty \times 10^{-6}$	θ_c, deg: 7.5, 15.8 $(Re/in.)_\infty \times 10^{-6}$
○	0.116	0.092	0.082
■	0.224	0.18	0.16
◇	0.483	0.38	0.34
▲	1.17	0.93	0.83

$(Re_t)_\delta = (Re/in.)_\delta \, x_t$

x_t determined from heat transfer data obtained using fusible paint.

Data from Ref. 24

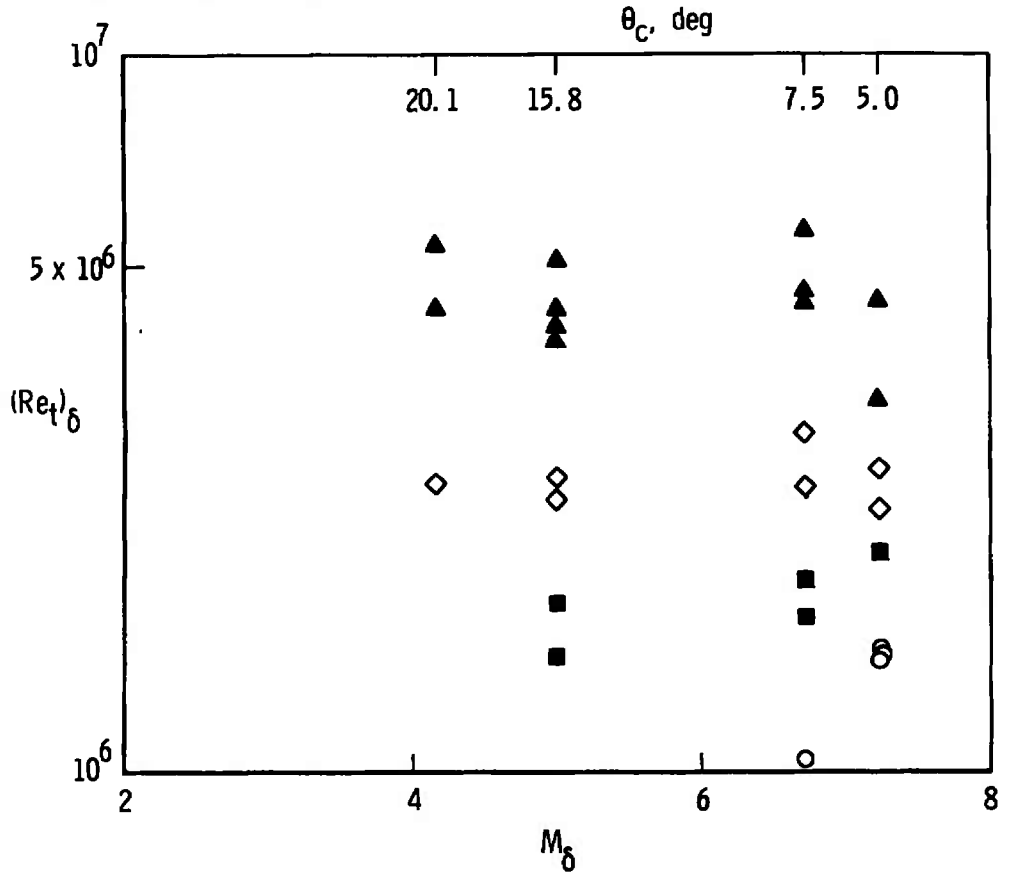

a. Sharp Cones at $M_\infty = 8$

Fig. 13 Transition Reynolds Numbers as a Function of Local Mach Number for Sharp Cones and Pitched Flat Plates

	Ref.	Sym	M_∞	α, deg	$(Re/in.)_\infty \times 10^{-6}$	$(Re/in.)_\delta \times 10^{-6}$
Hollow Cylinder	17	●	4.0	0	0.68	0.68
↓	25	○	5.0	0	0.68	0.68
↓	26	○	6.1, 7.1, 8.0	0	0.68	0.68
Flat Plate	28	△	6.0	0	0.58	0.58
↓	28	▲	6.0	8	0.58	0.87
↓	28	□	6.0	0	0.68	0.68
↓	28	■	6.0	8	0.68	1.02

$(Re_t)_\delta = (Re/in.)_\delta \, x_t$

x_t Based on Peak Pitot Location

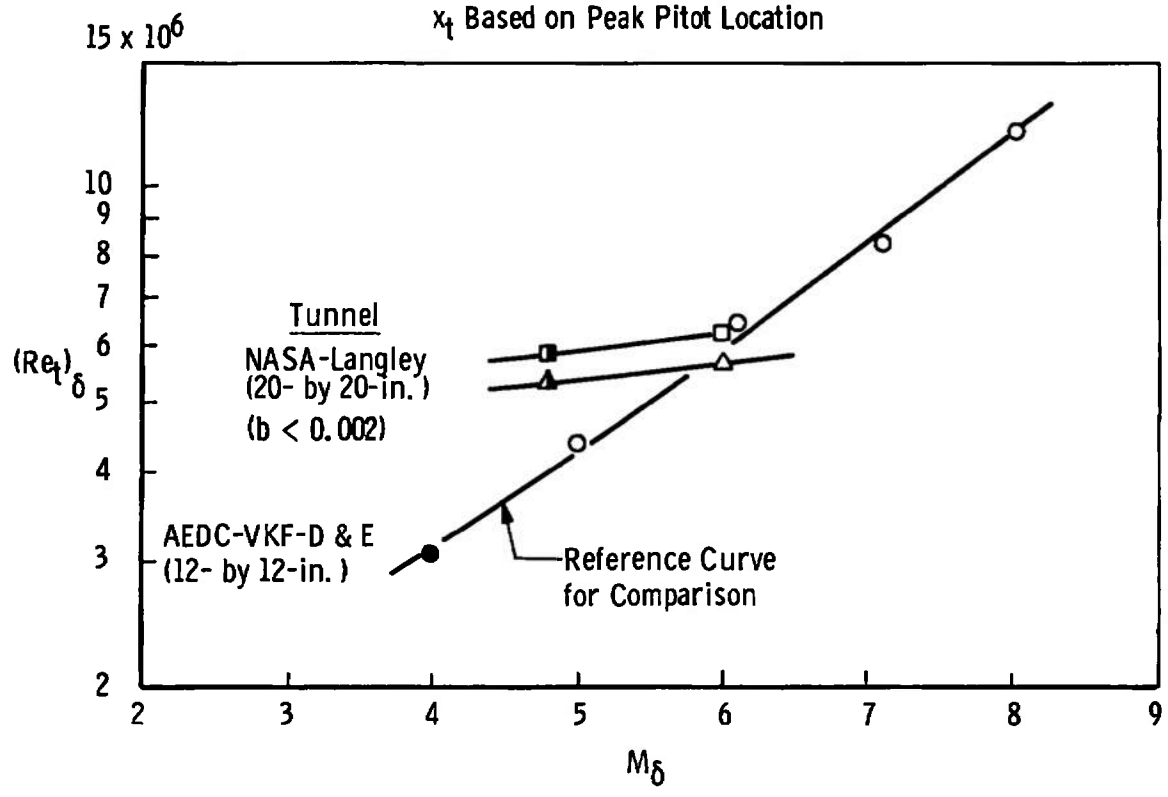

b. Pitched Flat Plate at $M_\infty = 6.0$

Fig. 13 Continued

Ref.	Sym	M_∞	M_δ	α, deg	$(Re/in.)_\infty \times 10^{-6}$	$(Re/in.)_\delta \times 10^{-6}$
27	▲	6.0	6.0	0	0.175	0.175
	▲	6.0	6.73	-4.5		0.131
	▲	6.0	5.77	1.5		0.193
	▲	6.0	4.95	7.5		0.246
	▲	6.0	3.97	15		0.259
	●	8.0	8.0	0		0.175
	●	8.0	5.82	10		0.262
	●	8.0	4.72	15		0.248

$(Re_t)_\delta = (Re/in.)_\delta \, x_t$

x_t Based on Peak Pitot Location

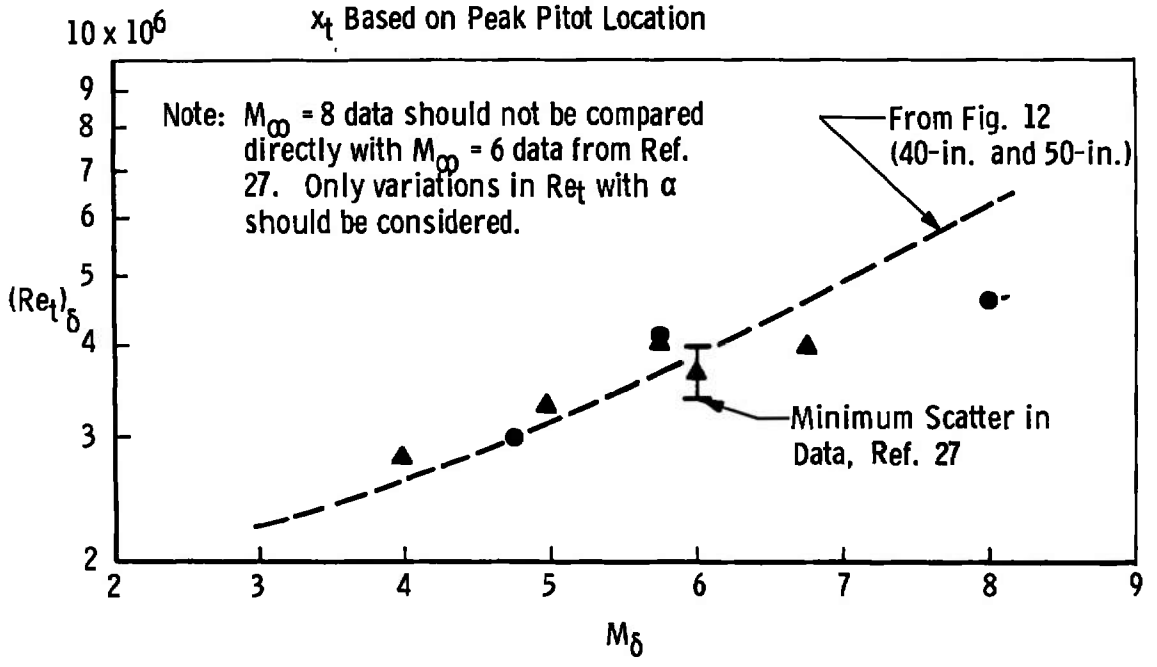

c. Pitched Flat Plate at M_∞ = 6 and 8

Fig. 13 Concluded

Consequently, it seems justified to compare the four sets of cone data directly.

Additional transition data on flat plates pitched to change the local conditions are presented in Figs. 13b and c. The results in Fig. 13b show for constant free-stream tunnel conditions there was no increase (or small increase) in Re_t with increasing local Mach number. Figure 13c suggests perhaps a linear increase in Re_t with increasing Mach number, but the rate of increase is less than indicated in Fig. 12 for increasing tunnel Mach number. Hollow cylinder data obtained at different tunnel Mach numbers are included in Figs. 13b and c for comparison.

Cone and pitched flat-plate transition data should be plotted for a constant free-stream unit Reynolds number to show the influence of Mach number since this is the case where the radiated aerodynamic noise is constant. It should be noted that in Fig. 13a the local unit Reynolds number remained constant between the cone models for a given free-stream unit Reynolds number, but for the flat plate (Figs. 13b and c) the local unit Reynolds number varied because the pitch angles were not selected with the intended purpose of producing a constant local unit Reynolds number.

These results indicate that if a true Mach number effect on transition Reynolds number exists at supersonic and hypersonic speeds, it appears doubtful that the trend could be established by comparing transition data at different Mach numbers obtained in wind tunnels having turbulent boundary layers because of the influence of radiated aerodynamic noise.

SECTION VII
CONCLUDING REMARKS

The significant results and conclusions obtained from this research, which was directed toward an investigation of the effect of radiated aerodynamic noise on boundary-layer transition on models in supersonic and hypersonic wind tunnels, are summarized as follows:

1. Boundary-layer transition measurements at Mach number three on sharp-leading-edge, hollow-cylinder models in the AEDC-VKF 12-in. and 40-in. Tunnels D and A and the AEDC-PWT 16-ft supersonic tunnel have shown conclusively a significant and continuous increase in transition Reynolds numbers (Re_t) with increasing tunnel size. This increase in Re_t is explained by a decrease in the radiated aerodynamic noise emanating from the tunnel wall, turbulent boundary layer as the tunnel size increases.

2. Results from a shroud configuration placed concentrically around a hollow-cylinder transition model in the AEDC-VKF Tunnel A demonstrated a significant change in the magnitude and trend in transition Reynolds number with unit Reynolds number, as compared to transition Reynolds numbers without the shroud, when the boundary layer on the shroud wall changed from laminar to turbulent.

3. A flat-plate model equipped with a microphone confirmed that a significant increase in the RMS radiated pressure fluctuations accompanied the decrease in the transition Reynolds numbers between the AEDC-VKF 40-in. and 12-in. tunnels and the decrease in transition Reynolds number as the shroud wall boundary layer changed from laminar to turbulent.

4. From transition data obtained in these investigations and data from six other wind tunnels, a correlation of transition Reynolds numbers was developed. The correlation was based on zero-bluntness, flat-plate, and hollow-cylinder transition data which covered a Mach number range from 3 to 8 and a unit Reynolds number range from 0.05 to 1.1 x 10^6. The correlation was independent of Mach number and unit Reynolds number and was dependent only on parameters known to have an influence on radiated aerodynamic noise. These included wall turbulent, mean skin-friction coefficient (C_F), boundary-layer displacement thickness (δ^*), and the tunnel test-section circumference (c).

5. Transition data on sharp cones and flat plates pitched to angles of attack have indicated that for high tunnel unit Reynolds numbers the transition Reynolds number (Re_t) is perhaps invariant with local Mach number, provided the tunnel Mach number remains constant. This is in agreement with the transition correlation of wind-tunnel data and suggests that possibly a major part of the increase in Re_t with increasing tunnel Mach number is related to the radiated aerodynamic noise.

6. If a true Mach number effect on transition Reynolds numbers exists at supersonic and hypersonic speeds, it appears doubtful that the trend can be established by comparing transition data at different Mach numbers obtained in wind tunnels having turbulent wall boundary layers because of the influence of radiated aerodynamic noise.

7. The experimental, radiated noise results and the success of the correlation of wind-tunnel data suggest that a major part of the heretofore unexplained unit Reynolds number effect in supersonic and hypersonic wind tunnels having turbulent boundary layers on the walls may be the result of radiated aerodynamic noise.

8. Based on transition Reynolds number data presented in this report and data from two other sources, it is concluded that there is no leading-edge internal bevel-angle effect on transition Reynolds numbers from sharp leading-edge models at supersonic and hypersonic speeds.

REFERENCES

1. Czarnecki, K. R. and Sinclair, Archibald R. "Factors Affecting Transition at Supersonic Speeds." NACA RM L53118a, November 4, 1953.

2. Kovasznay, Leslie, S. G. "Turbulence in Supersonic Flow." Journal of the Aeronautical Sciences, Vol. 20, No. 10, October 1953.

3. Morkovin, M. V. "On Supersonic Wind Tunnels with Low Free-Stream Disturbances." Journal of Applied Mechanics, Paper No. 59--APM-10, Vol. 26.

4. Laufer, John. "Factors Affecting Transition Reynolds Numbers on Models in Supersonic Wind Tunnels." Journal of the Aeronautical Sciences, 21 (No. 7), July 1954.

5. Morkovin, M. V. "On Transition Experiments at Moderate Supersonic Speeds." Journal of the Aeronautical Sciences, 24 (No. 7), July 1957, pp. 480-486.

6. Laufer, J. "Sound Radiation from a Turbulent Boundary Layer." Jet Propulsion Laboratory Technical Report No. 32-119, November 1961.

7. Laufer, John. "Aerodynamic Noise in Supersonic Wind Tunnels." JPL Progress Report No. 20-378, February 1959 and Journal of the Aerospace Sciences, Vol. 28, 1961, pp. 685-692.

8. Vrebalovich, Thomas. Discussion: "On Supersonic Wind Tunnels with Low Freestream Disturbances." by M. V. Morkovin, Journal of Applied Mechanics, June 1960.

9. Phillips, O. M. "On the Generation of Sound by Supersonic Turbulent Shear Layers." Journal of Fluid Mechanics, Vol. 9, 1960, pp. 1-28.

10. Kistler, A. L. and Chen, W. S. "The Fluctuating Pressure Field in a Supersonic Turbulent Boundary Layer." Jet Propulsion Laboratory Technical Report No. 32-277, August 1962.

11. Laufer, J. "Some Statistical Properties of the Pressure Field Radiated by a Turbulent Boundary Layer." The Physics of Fluids, Vol. 7, No. 8, August 1964.

12. Schueler, C. J. "Comparison of the Aerodynamic Characteristics of AGARD Model A from Tests in 12-in. and 40-in. Supersonic Wind Tunnels." AEDC-TN-61-8 (AD 251477), February 1961.

13. Schueler, C. J. "A Comparison of Transition Reynolds Numbers from 12-in. and 40-in. Supersonic Tunnels." AEDC-TDR-63-57 (AD 299290), March 1963.

14. Nichols, J. H. "Supplemental Aerodynamic Calibration Results for the AEDC-PWT 16-ft Supersonic Tunnel." AEDC-TDR-64-76 (AD 435732), April 1964.

15. Coats, Jack D. "Flow Characteristics of a 40-in. Wind Tunnel at Mach Numbers 1.5 to 6." AEDC-TDR-62-130 (AD 277289), June 1962.

16. Anderson, A. "Flow Characteristics of a 12-in. Intermittent Supersonic Tunnel." AEDC-TDR-63-203 (AD 418578), September 1963.

17. Potter, J. Leith and Whitfield, Jack D. "Effects of Unit Reynolds Number, Nose Bluntness, and Roughness on Boundary-Layer Transition." AEDC-TR-60-5 (AD 234478), March 1960.

18. Whitfield, Jack D. and Potter, J. Leith. "The Influence of Slight Leading-Edge Bluntness on Boundary-Layer Transition at a Mach Number of Eight." AEDC-TDR-64-18 (AD 431533), March 1964.

19. Brinich, Paul F. "Effect of Leading-Edge Geometry on Boundary-Layer Transition at Mach 3.1." NACA TN 3659, March 1956.

20. Laufer, John and Marte, Jack E. "Results and a Critical Discussion of Transition Reynolds Number Measurements on Insulated Cones and Flat Plates in Supersonic Wind Tunnels." JPL Report No. 20-96, November 1955.

21. Van Driest, E. R. "Turbulent Boundary Layer in Compressible Fluids." Journal of the Aeronautical Sciences, Vol. 18, No. 3, March 1951, pp. 145-160, 216.

22. Maxwell, H. and Jacocks, J. L. "Nondimensional Calculation of Turbulent Boundary-Layer Development in Two-Dimensional Nozzles of Supersonic Wind Tunnels." AEDC-TN-61-153 (AD 270596), January 1962.

23. Potter, J. Leith. "The Influence of Ambient Pressure on Boundary-Layer Transition in an Aeroballistic Range." Paper Presented at the Aerospace Boundary-Layer Transition Specialists' Study Group Meeting at San Bernardino, California, July 11-12, 1967.

24. Stainback, Calvin P. "Some Effects of Roughness and Variable Entrophy on Transition at a Mach Number of 8." AIAA Paper No. 67-132 Presented at AIAA 5th Aerospace Sciences Meeting, New York, N.Y., January 23-26, 1967.

25. AEDC-VKF Tunnel Calibration Data (Unpublished).

26. Rhudy, J. P. "Investigation of Uncooled Leading-Edge Effect on Cooled-Wall Hypersonic Boundary-Layer Transition." AEDC-TR-68-61, to be published.

27. Nagel, A. L., Savage, R. T., and Wanner, R. "Investigation of Boundary Layer Transition in Hypersonic Flow at Angle of Attack." AFFDL-TR-66-122, August 1966.

28. Holloway, Paul F. and Sterrett, James R. "Effect of Controlled Surface Roughness on Boundary-Layer Transition and Heat Transfer at Mach Numbers of 4.8 and 6.0." NASA TN D-2054, April 1964.

29. Brinich, Paul F. and Sands, Norman. "Effect of Bluntness on Transition for a Cone and a Hollow Cylinder at Mach 3.1." NACA TN 3979, May 1957.

30. Brinich, Paul F. "Recovery Temperature, Transition and Heat Transfer Measurements at Mach 5." NASA TN D-1047, August 1961.

31. Coles, Donald. "Measurements of Turbulent Skin Friction on a Smooth Flat Plate in Supersonic Flow." Journal of the Aeronautical Sciences, 21 (No. 7), 1954, pp. 433-448.

32. Jones, Jerry. "An Investigation of the Boundary-Layer Characteristics in the Test Section of a 40 by 40-Inch Supersonic Tunnel." AEDC-TN-60-189 (AD 245362), October 1960.

33. Bell, D. R. "Boundary-Layer Characteristics at Mach Numbers 2 through 5 in the Test Section of the 12-Inch Supersonic Tunnel (D)." AEDC-TDR-63-192 (AD 418711), September 1963.

34. Jet Propulsion Laboratory Research Summary No. 36-6, Vol. II, January 1961.

35. Sivells, J. C. and Payne, R. G. "A Method of Calculating Turbulent Boundary Layer Growth at Hypersonic Mach Numbers." AEDC-TR-59-3 (AD 208774), March 1959.

36. Winter, K. G., Smith, K. G., and Gaudet, L. "Measurements of Turbulent Skin Friction at High Reynolds Numbers at Mach Numbers of 0.2 and 2.2." AGARD Specialistics' Meeting on Recent Developments in Boundary Layer Research, May 1965. AGARDograph 97, Part II.

37. Tucker, Maurice. "Approximate Calculation of Turbulent Boundary Layer Development in Compressible Flow." NACA TN 2337, April 1951.

APPENDIXES

I. TRANSITION DATA AND TUNNEL WALL BOUNDARY-LAYER CHARACTERISTICS FROM THE AEDC-PWT-16S TUNNEL
II. TRANSITION REYNOLDS NUMBER DATA AND TUNNEL WALL BOUNDARY-LAYER CHARACTERISTICS FROM THE AEDC-VKF TUNNEL A
III. EXPERIMENTAL RESULTS FROM THE LONG AND SHORT SHROUD CONFIGURATIONS INSTALLED IN THE AEDC-VKF TUNNEL A
IV. TRANSITION REYNOLDS NUMBER RESULTS FROM THE AEDC-VKF TUNNEL D
V. DISPLACEMENT THICKNESS CORRELATION AND TURBULENT SKIN-FRICTION COEFFICIENTS

APPENDIX I
TRANSITION DATA AND TUNNEL WALL BOUNDARY-LAYER CHARACTERISTICS FROM THE AEDC-PWT-16S TUNNEL

1.1 AEDC-PWT-16S TUNNEL AND MODEL DETAILS

A sketch of Tunnel 16S is presented in Fig. I-1. Information on the tunnel operating range can be found in Section II. The position of the hollow-cylinder transition model and the locations of the two wall boundary-layer rakes relative to the test section and the tunnel throat are shown in Fig. I-1b.

Details of the hollow-cylinder model, model support, and probe drive mechanism are shown in Fig. I-2. Small variations in the model leading-edge thickness existed, and these bluntness values are tabulated in the table included in Fig. I-2 as a function of the model circumferential location. The leading-edge bluntness was determined by making bluntness impressions (impression depth approximately two to four times bluntness value) in thin (sharpened) soft lead sheet and viewing the profile on a 100-power comparator. The individual bluntness values (b) listed in Fig. I-2 for each model leading-edge location are the average of several impressions. Additional comments concerning the accuracy of this method are given in Appendix II.

1.2 AEDC-PWT-16S BOUNDARY-LAYER CHARACTERISTICS

The tunnel wall boundary-layer characteristics presented in Fig. I-3 were determined using the fourteen-rake pitot pressures and the tunnel free-stream static pressure in conjunction with the usual assumptions that the total temperature and the static pressure remain constant through the boundary layer.

The following equations were used to define the two-dimensional displacement and momentum thickness, respectively:

$$\delta^* = \int_0^\delta \left(1 - \frac{\rho u}{\rho_\infty U_\infty}\right) dy$$

$$\theta = \int_0^\delta \frac{\rho u}{\rho_\infty U_\infty}\left(1 - \frac{u}{U_\infty}\right) dy$$

1.3 AEDC-PWT-16S TRANSITION RESULTS

Surface pitot probe pressure traces from probe No. 1 (bluntness value b of 0.0012 in.) are presented in Fig. I-4 for M_∞ = 2.0, 2.5, and 3.0 and several tunnel unit Reynolds number values. These data serve to show the quality of the probe data obtained. As explained in Section III, the location of transition was defined as the peak in the pitot pressure profile.

The transition Reynolds number results as determined by the maximum surface pitot pressure value are presented in Fig. I-5 for M_∞ = 2.0, 2.5, and 3.0 for the average bluntness values ($\bar{b}$) of 0.0015, 0.0050, and 0.0090-in. These data show the familiar increase in Re_t with Re/in., which is a characteristic exhibited by most other supersonic wind tunnel data.

Figure I-6 presents the Re_t values plotted versus $\bar{b}$ for several Re/in. values and the three Mach numbers tested. These plots were used to obtain the $\bar{b}$ = 0 value used in the correlation presented in Section V.

The slight variation in leading-edge bluntness that existed around the model circumference was apparently sufficient to influence the location of transition. Figure I-7a shows the pitot pressure traces obtained simultaneously from the four surface probes and variations in the x_t values are clearly evident. Figures I-7b and c show a systematic variation of Re_t with the local leading bluntness value (b), and the slope is in agreement with the slope of the data presented in Fig. I-6. This would indicate that the small variation in Re_t that existed between the four pitot probes is traceable to variations in the model leading-edge bluntness rather than to individual probe effects or from any tunnel flow angularity. The model internal lip pressures indicated that a free-stream flow angle less than approximately ±0.1 deg existed, and this is in general agreement with Ref. 16.

The variation in the AEDC-PWT-16S transition data with Mach number is shown in Fig. I-8a. Coles' data from Ref. 31 obtained in the JPL 20-in. supersonic tunnel is presented in Fig. I-8b. These data indicate that the increase in Re_t with decreasing Mach number in the $1.5 < M_\infty < 3.0$ range is the rule rather than the exception. However, it is to be remembered that for $M_\infty < 3$ the tunnel stilling chamber turbulence level will have a strong influence on the location of transition as discussed in Section I. It is of further interest to note the decreasing effect of Mach number on Coles' data for $M_\infty > 3$ as the unit Reynolds number decreases. This type trend is also evident in Schueler's data (Ref. 13). It is, therefore, possible that the decreasing influence

of Mach number ($M_\infty > 3$) as Re/in. decreases is also connected to the radiated aerodynamic noise effects discussed in Sections I, IV, V, and VI.

All of the AEDC-PWT-16S transition Reynolds number data obtained in this investigation are tabulated in Table I-1.

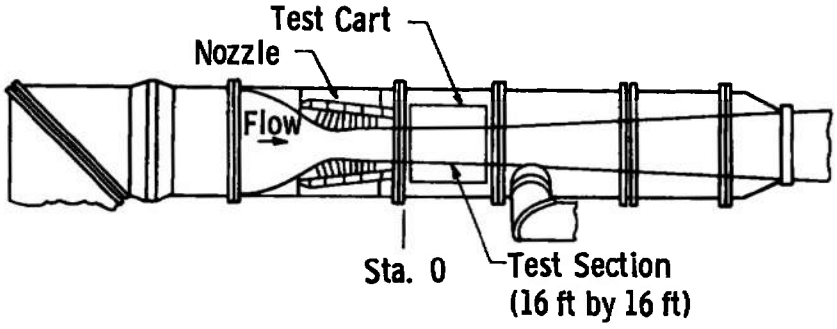

a. Plan View

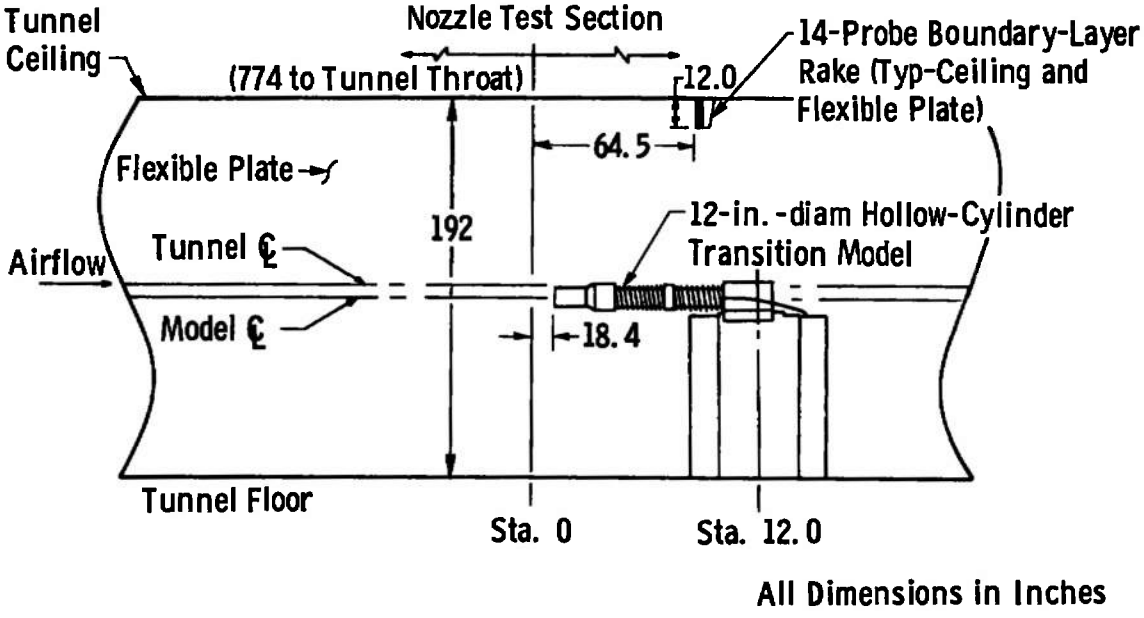

b. Test Section

Fig. I-1 Sketch of AEDC-PWT 16-foot Supersonic Tunnel

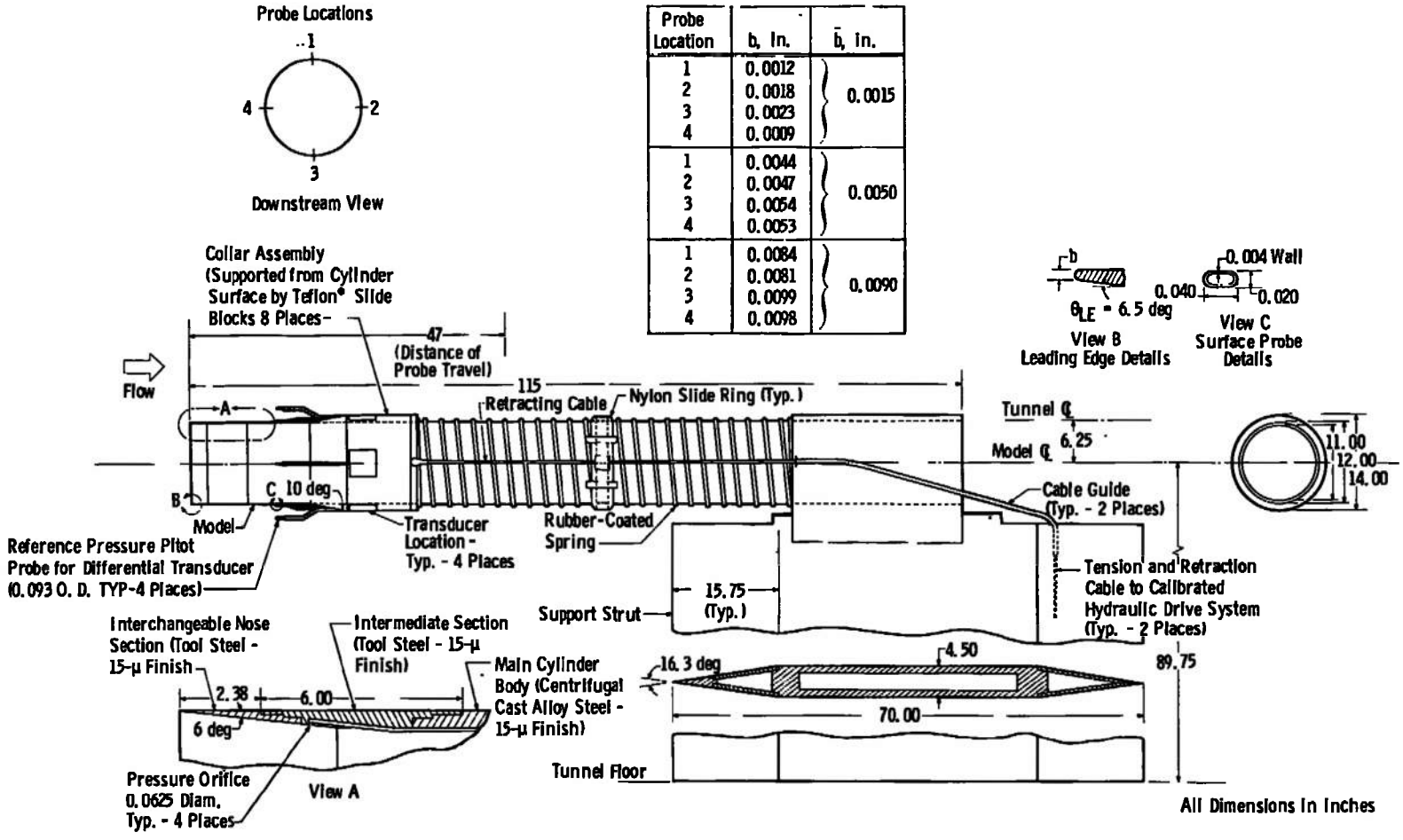

Fig. 1-2 12-in.-Diam. Hollow Cylinder Transition Model Details - AEDC-PWT 16S

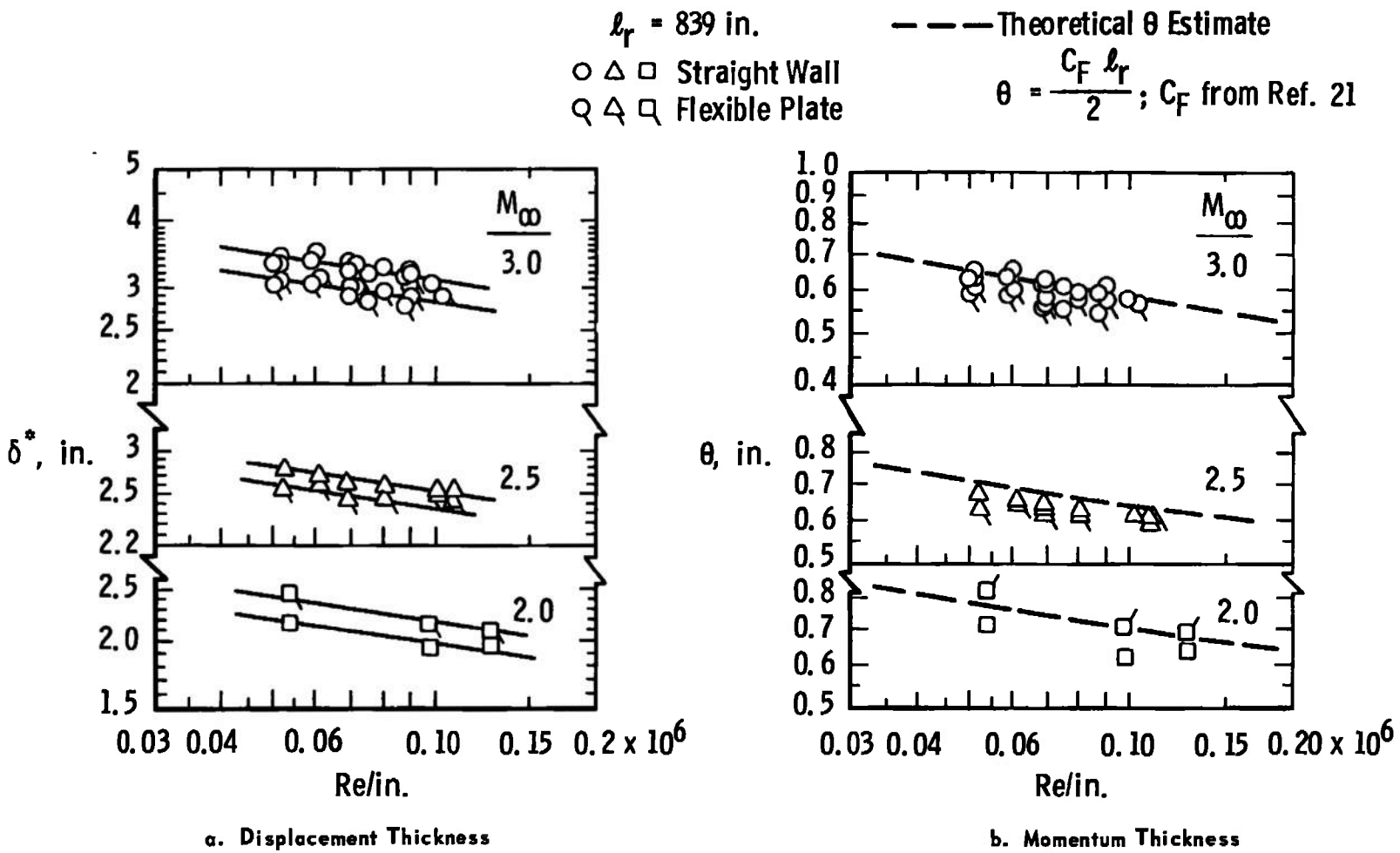

a. Displacement Thickness

b. Momentum Thickness

Fig. I-3 AEDC-PWT-16S Boundary-Layer Characteristics

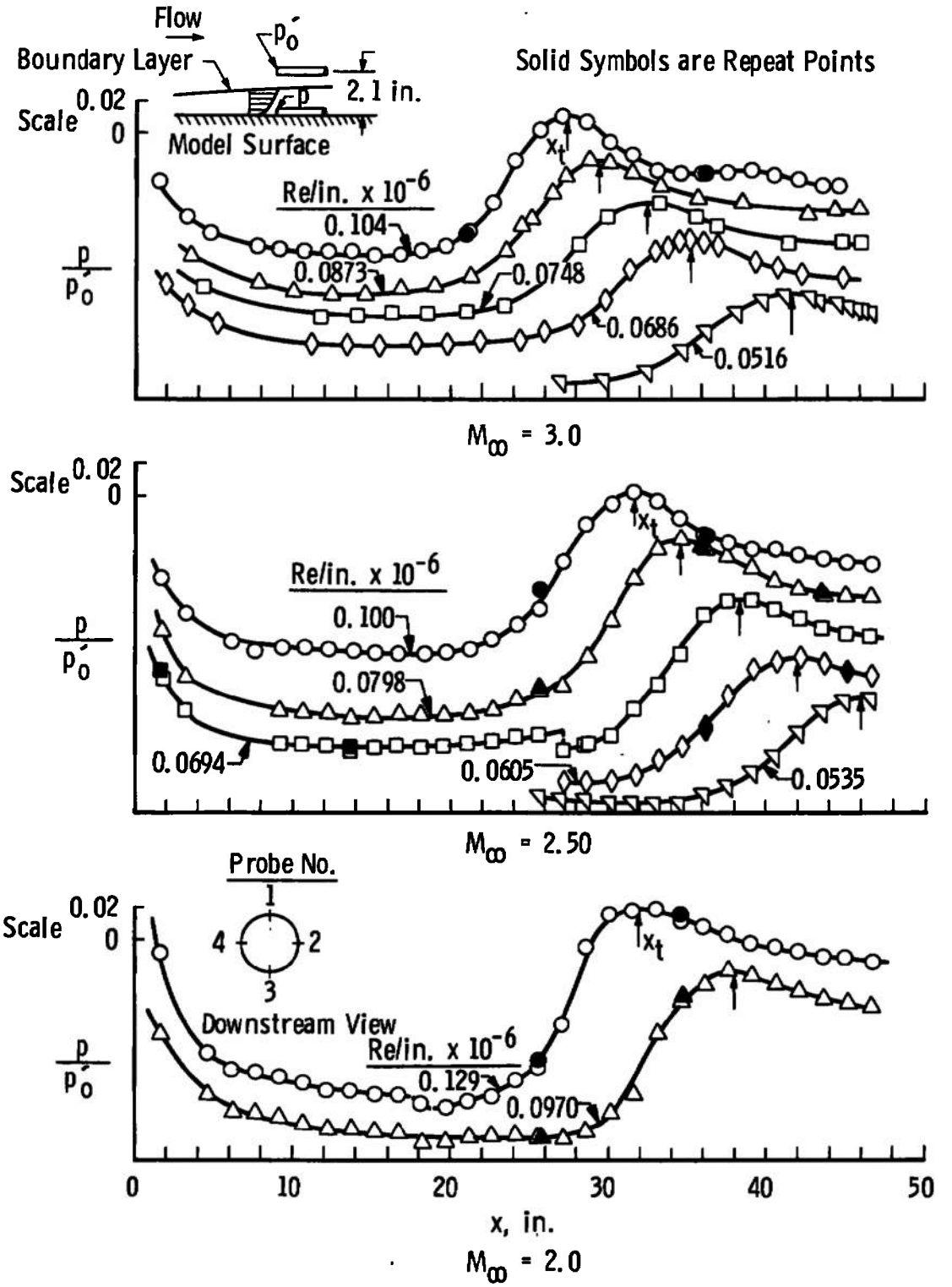

Fig. I-4 Probe Pressure Data Showing the Location of Boundary-Layer Transiton on the 12-in.-diam Hollow-Cylinder Model in the AEDC-PWT-16S Tunnel for M_∞ = 2.0, 2.5, and 3.0, Probe No. 1, b = 0.0012 in., θ_{LE} = 6.5 deg

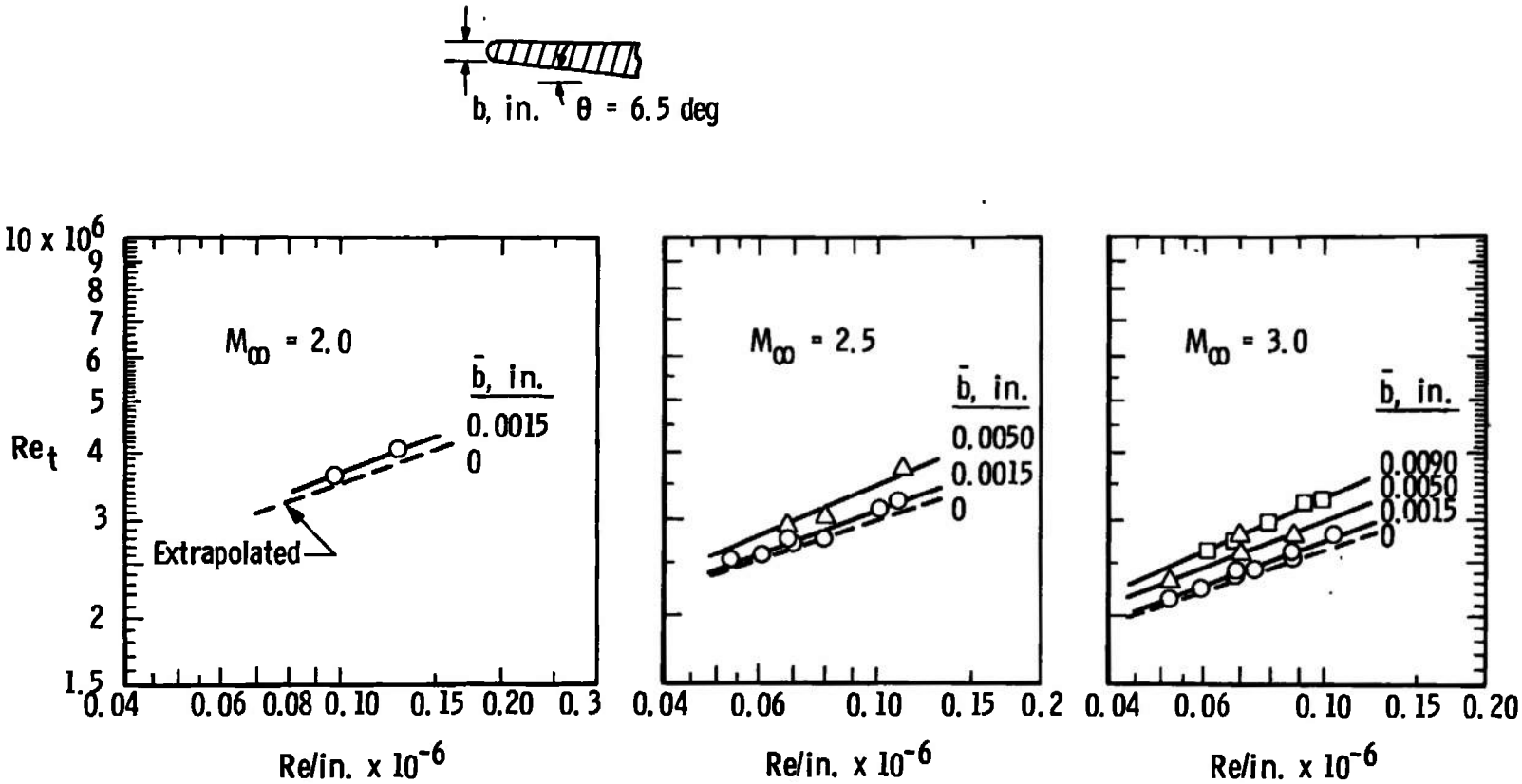

Fig. 1-5 Basic Transition Reynolds Number Data from the 12-in.-diam Hollow Cylinder Model in the AEDC-PWT-16S Tunnel for M_∞ = 2.0, 2.5, and 3.0 and $\bar{b}$ = 0.0015, 0.0050, and 0.0090 in.

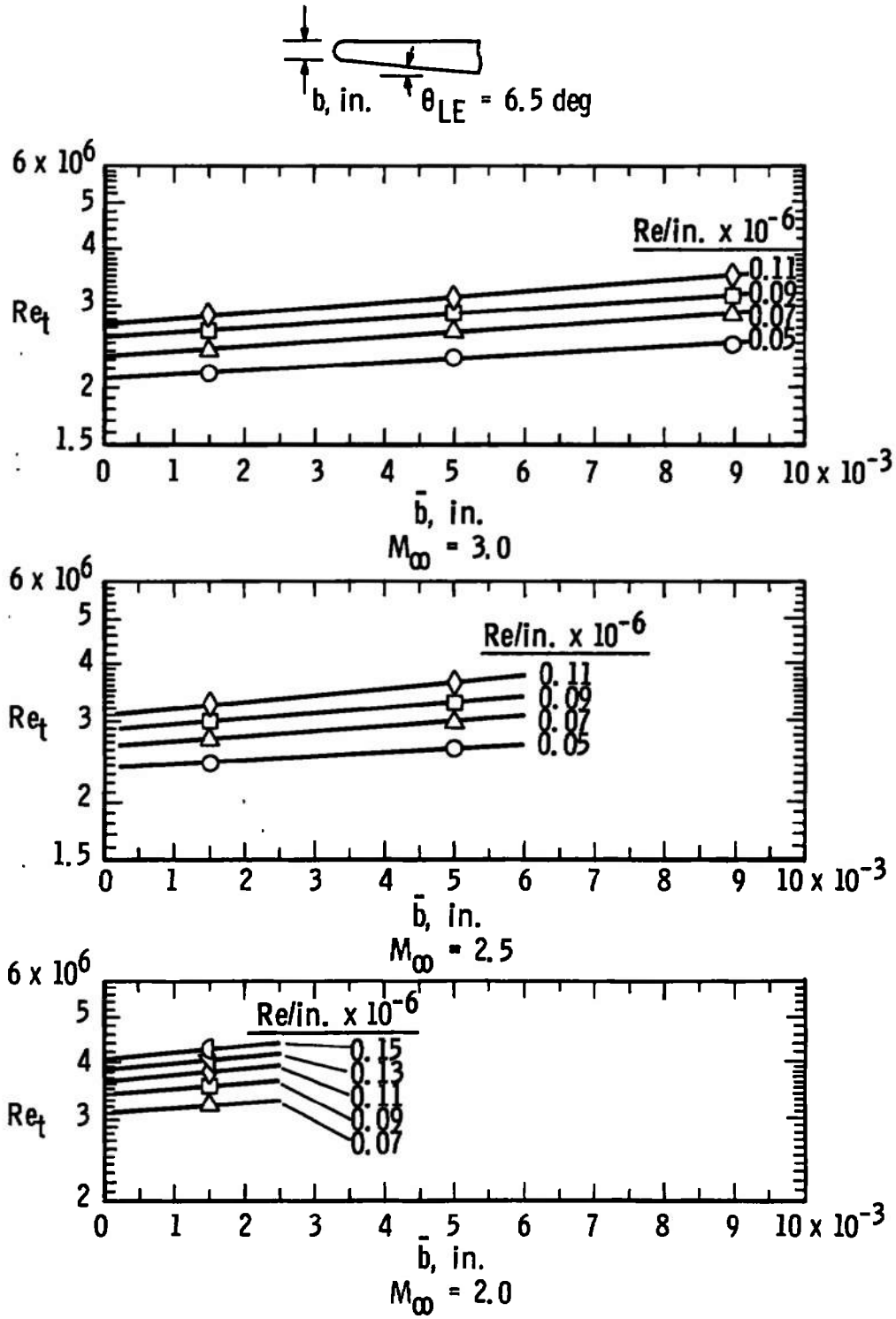

Fig. 1-6 AEDC-PWT-16S Transition Results, Re_t versus $\bar{b}$ for M_∞ = 2.0, 2.5, and 3.0

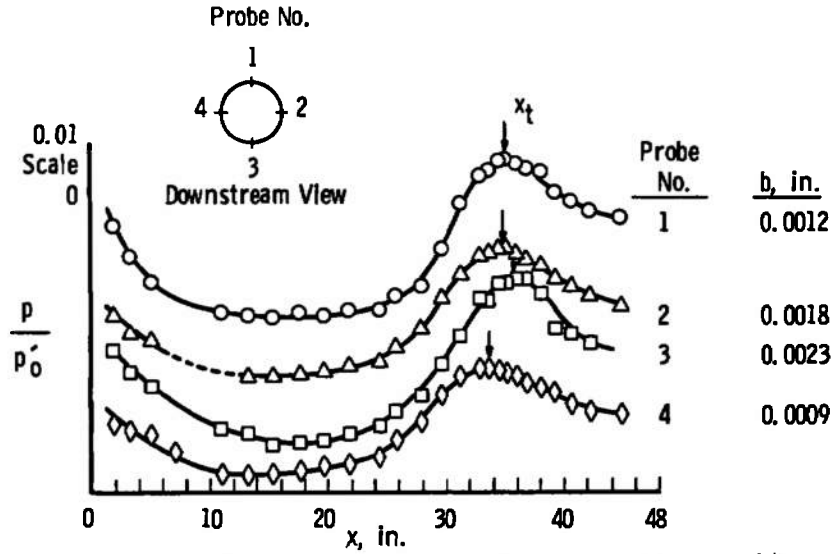

a. Surface Probe Pressure Trace, M_∞ = 3, Re = 0.069 × 10^6/in.

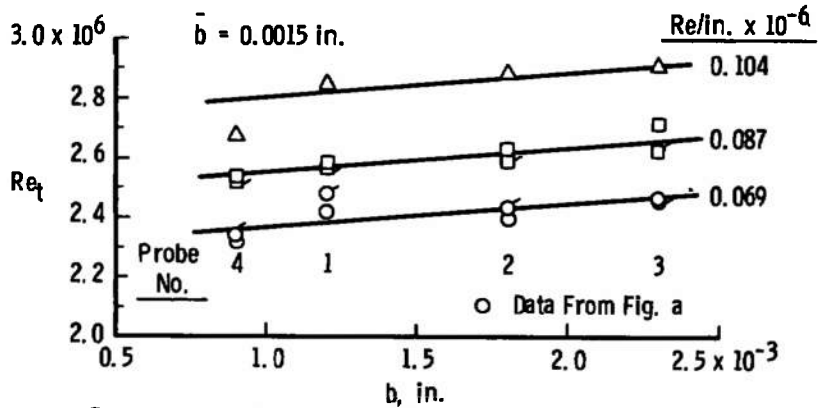

b. Circumferential Transition Reynolds Number Distribution, M_∞ = 3.0

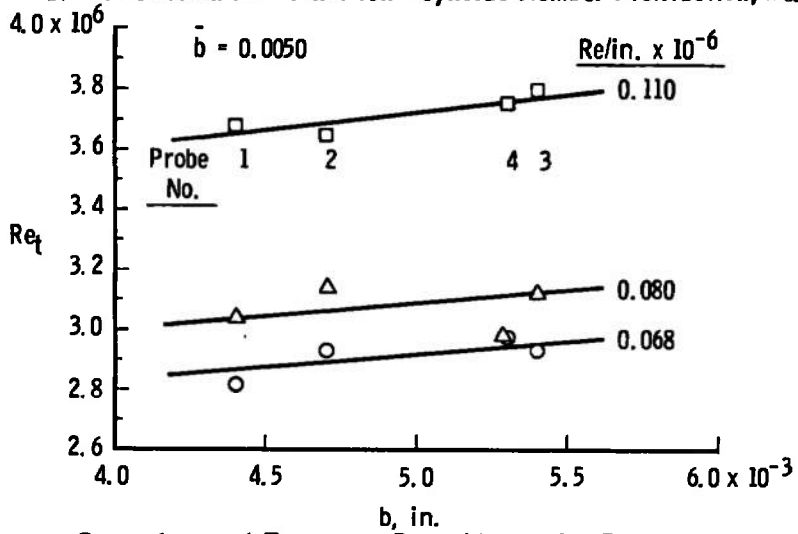

c. Circumferential Transition Reynolds Number Distribution, M_∞ = 2.5

Fig. I-7 Circumferential Transition Locations on the AEDC-PWT-16S Hollow-Cylinder Model

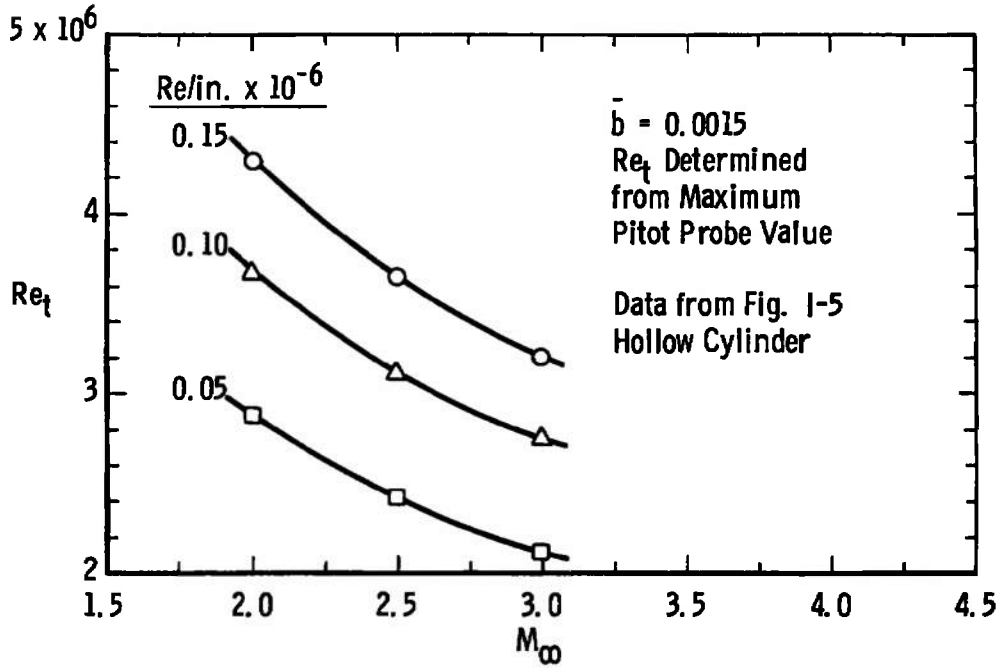

a. AEDC-PWT-16S Transition Data

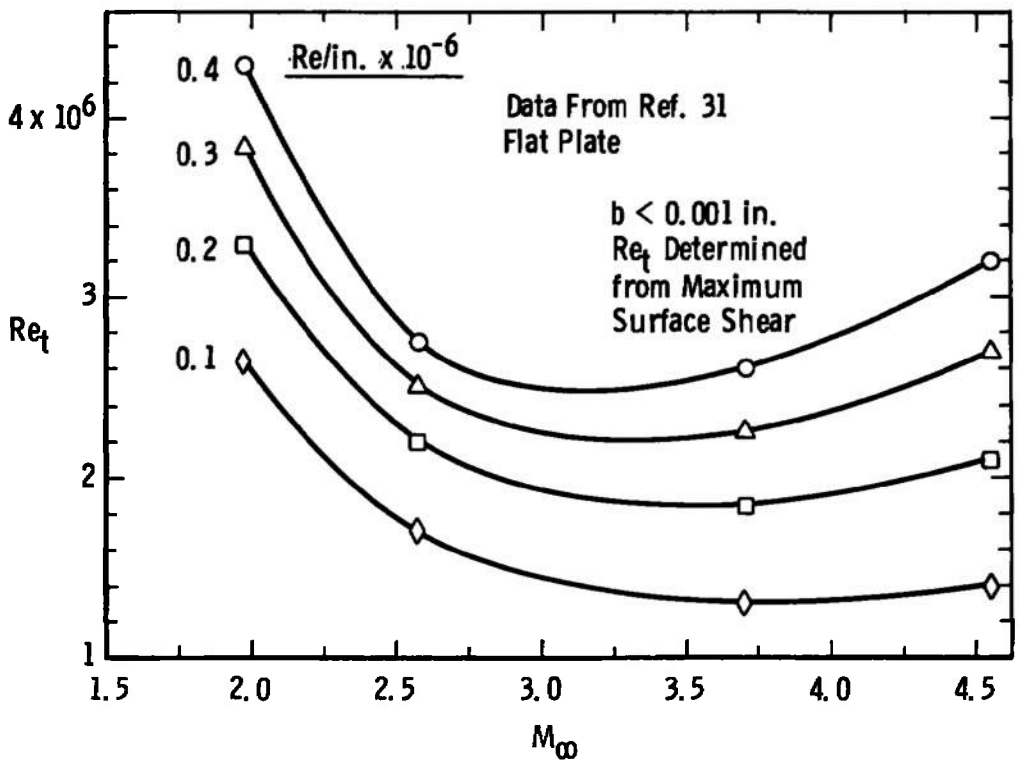

b. JPL Transition Data

Fig. I-8 Variation Transition Reynolds Number with Tunnel Mach Number

TABLE I-1
AEDC-PWT-16S TUNNEL BASIC TRANSITION REYNOLDS NUMBER DATA,
12.0-IN.-DIAM HOLLOW CYLINDER

M_∞	p_o, psia	T_o, °R	Re/in. x 10^{-6}	Re_{t_1} x 10^{-6}	Re_{t_2} x 10^{-6}	Re_{t_3} x 10^{-6}	Re_{t_4} x 10^{-6}	Average Ret x 10^{-6}	Average $\bar{b}$, in.
3.00	5.23	647	0.0516	2.16	2.16	--	2.12	2.15	0.0015
3.00	6.21	666	0.0591	2.26	2.26	--	2.26	2.26	↓
3.01	7.09	656	0.0686	2.42	2.40	2.47	2.32	2.40	↓
3.01	7.06	653	0.0689	2.48	2.43	2.46	2.34	2.43	↓
3.00	7.93	669	0.0748	2.43	2.42	2.54	2.40	2.45	↓
3.00	9.27	671	0.0873	2.57	2.59	2.62	2.53	2.58	↓
3.00	9.27	669	0.0876	2.59	2.63	2.72	2.54	2.62	↓
3.00	10.92	667	0.104	2.85	2.88	2.91	2.68	2.83	↓
3.00	5.09	645	0.0517	--	2.30	2.36	2.32	2.33	0.0050
3.00	7.12	649	0.0701	2.64	--	2.64	2.54	2.61	0.0042
3.00	7.17	655	0.0700	--	2.82	--	2.88	2.85	0.0050
3.00	9.28	664	0.0888	--	2.81	2.84	2.77	2.81	0.0050
3.00	6.22	658	0.0603	2.53	2.63	2.77	2.63	2.64	0.0090
3.00	7.05	657	0.0686	2.75	2.81	--	2.75	2.77	↓
3.03	8.36	659	0.0794	2.94	3.05	3.08	2.91	2.99	↓
3.00	9.20	644	0.0920	3.26	3.36	3.40	3.18	3.27	↓
3.03	10.52	659	0.0998	3.19	3.39	3.36	3.23	3.29	↓
2.50	4.06	641	0.0535	2.52	2.52	--	--	2.52	0.0015
2.51	4.62	642	0.0605	2.54	2.60	2.64	--	2.59	↓
2.50	5.34	654	0.0685	2.71	2.81	2.81	2.81	2.78	↓
2.50	5.46	655	0.0694	2.66	2.70	2.77	--	2.71	↓
2.50	6.31	657	0.0798	2.76	2.71	2.87	--	2.78	↓
2.50	7.82	654	0.1003	3.18	3.08	3.29	3.12	3.16	↓
2.50	8.57	658	0.1089	3.32	3.16	3.38	3.16	3.25	↓
2.50	5.38	658	0.0684	2.82	2.93	2.93	2.98	2.91	0.0050
2.50	6.26	655	0.0799	3.04	3.14	3.12	2.98	3.07	↓
2.50	8.65	656	0.1105	3.68	3.65	3.80	3.76	3.72	↓
2.00	5.62	632	0.0970	3.68	3.40	3.83	3.64	3.64	0.0015
2.00	7.45	631	0.1286	4.12	3.73	4.38	4.12	4.09	0.0015
3.0	--	-	0.050	--	--	--	--	2.09	0*
↓	↓	↓	0.070	↓	↓	↓	↓	2.32	↓
↓	↓	↓	0.090	↓	↓	↓	↓	2.54	↓
↓	↓	↓	0.11	↓	↓	↓	↓	2.71	↓
2.5	↓	↓	0.050	↓	↓	↓	↓	2.38	↓
↓	↓	↓	0.070	↓	↓	↓	↓	2.64	↓
↓	↓	↓	0.090	↓	↓	↓	↓	2.89	↓
↓	↓	↓	0.11	↓	↓	↓	↓	3.09	↓
2.0	↓	↓	0.090	↓	↓	↓	↓	3.40	↓
↓	↓	↓	0.11	↓	↓	↓	↓	3.65	↓
↓	↓	↓	0.13	↓	↓	↓	↓	3.86	↓

*Extrapolated Values of Re_t from Fig. I-6.

APPENDIX II
TRANSITION REYNOLDS NUMBER DATA AND TUNNEL WALL BOUNDARY-LAYER CHARACTERISTICS FROM THE AEDC-VKF TUNNEL A

2.1 AEDC-VKF TUNNEL A AND TRANSITION MODEL DETAILS

Some of the pertinent design and geometrical features of the 40- by 40-in. Tunnel A are illustrated in Fig. II-1. Information on the tunnel operating range can be found in Section II.

Details of the 3.0-in.-diam hollow-cylinder transition model are given in Fig. II-2. The model leading-edge nose bluntness was determined from impressions (depth equal to approximately two to four times the bluntness value) in thin (sharpened) soft lead sheet and from rubber molds made from General Electric Company RTV 60® silicone rubber compound. Both methods were nondestructive to the model leading edge. Profiles of the lead impressions and slices (approximately 0.04-in. in width) from the rubber mold were then read on a 100-power comparator to determine the leading-edge bluntness. Several lead impressions and several cuts from each of the rubber molds were averaged to obtain the bluntness value at each of several circumferential stations around each of the leading-edge sections. The maximum difference between average bluntness values obtained using lead impressions and rubber molds was ±0.0002-in. Measurements with the lead impressions were repeatable to within +0.0002-in., and measurements with the rubber molds were repeatable to within ±0.0001-in. The circumferential variation in bluntness around the model leading edge was ±0.0001-in.

The flexible plate which forms the lower nozzle wall in the Tunnel A was damaged on October 10, 1961. The damage (Figs. II-1 and II-3) occurred in the converging region of the nozzle upstream of the throat where several of the lugs which connected the flexible plate to automatically controlled actuators were broken or cracked. Repair of the plate required new lugs to be bolted to the plate as were the original lugs. A total of 160 steel bolt heads, protruding 0.158-in. above the plate surface, was required (Fig. II-3). Details of the replacement lugs, bolt heads, and plate damage can be found in Ref. 15.

Test results presented in Ref. 15 show that the connecting bolt heads had no significant effect on the uniformity of the free-stream flow but increased the boundary-layer displacement thickness (δ^*) on the repaired plate by a factor of approximately 1.5 at a freestream Mach number (M_∞) of 1.5 and had no effect on δ^* at $M_\infty = 5.0$.

To obtain more information on the effects of the bolt heads on the bottom plate boundary-layer growth and to provide information on δ^* to be used in the transition correlation (discussed in Section V), additional boundary-layer profile measurements were made on the repaired bottom flexible plate and the top (undamaged) flexible plate using a 23-probe rake. These results are presented in Fig. II-3 and confirm the results of Ref. 15, which showed no bolt head effects on the bottom plate at $M_\infty = 5.0$. Likewise, there was no effect at $M_\infty = 4.0$ and only about a six-percent increase in δ^* at $M_\infty = 3.0$ when compared with the results from Ref. 32.

Since this research was directed toward investigating the effects of radiated aerodynamic noise on transition, it was felt necessary to determine if the plate repair produced any noticeable differences on model transition. Therefore, a set of duplicate rubber bolt heads were glued to the top flexible plate, and the boundary-layer characteristics on the top plate and the transition location on the 3.0-in. diam hollow-cylinder model were measured with and without these rubber bolt heads. These results are presented in Figs. II-3 and II-4. Calculation of the displacement and momentum thickness was in accordance with equations in Appendix I.

2.2 AEDC-VKF TUNNEL A TRANSITION RESULTS

Figures II-4 and II-5 present the transition Reynolds number data obtained on the 3.0-in.-diam hollow-cylinder model. The permanent steel bolt heads or the duplicate set of rubber bolt heads produced no discernible effect on Re_t. Also, there was no effect of the internal bevel (θ_{LE}) angle on Re_t. Figure II-5 provided the zero bluntness values of Re_t for use in the transition correlation presented in Section V. All of the basic Tunnel A transition results obtained in this investigation along with the corresponding tunnel flow conditions and model leading-edge geometry are tabulated in Table II-1.

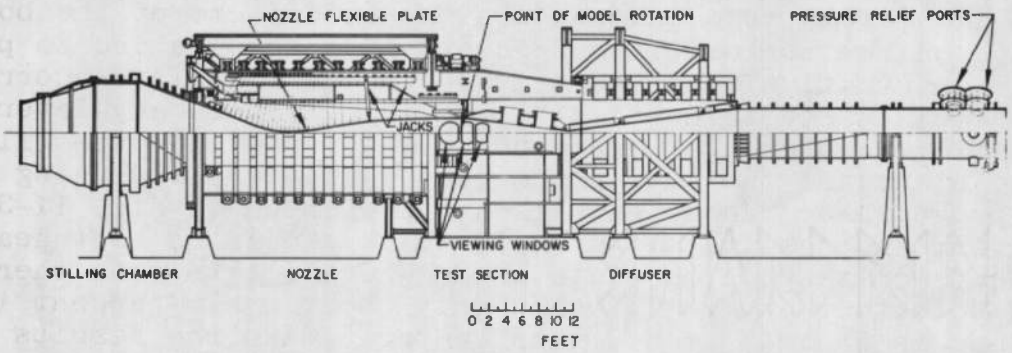

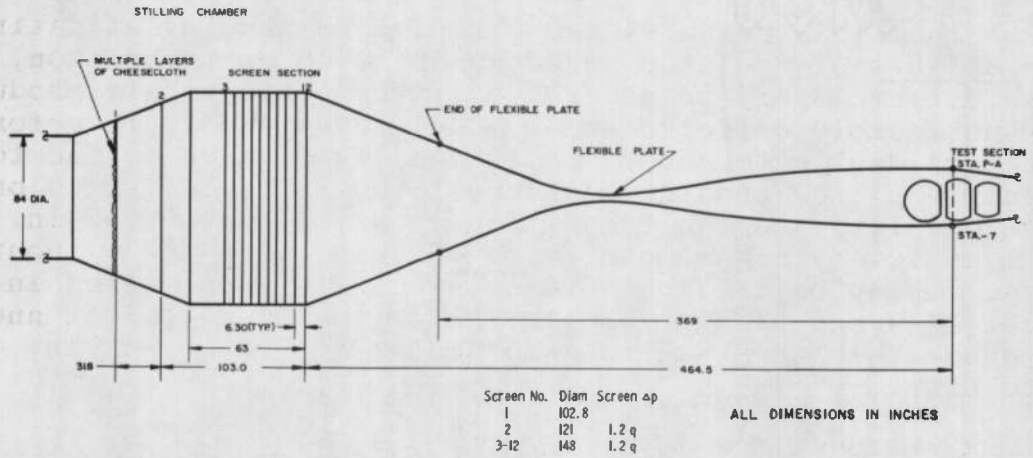

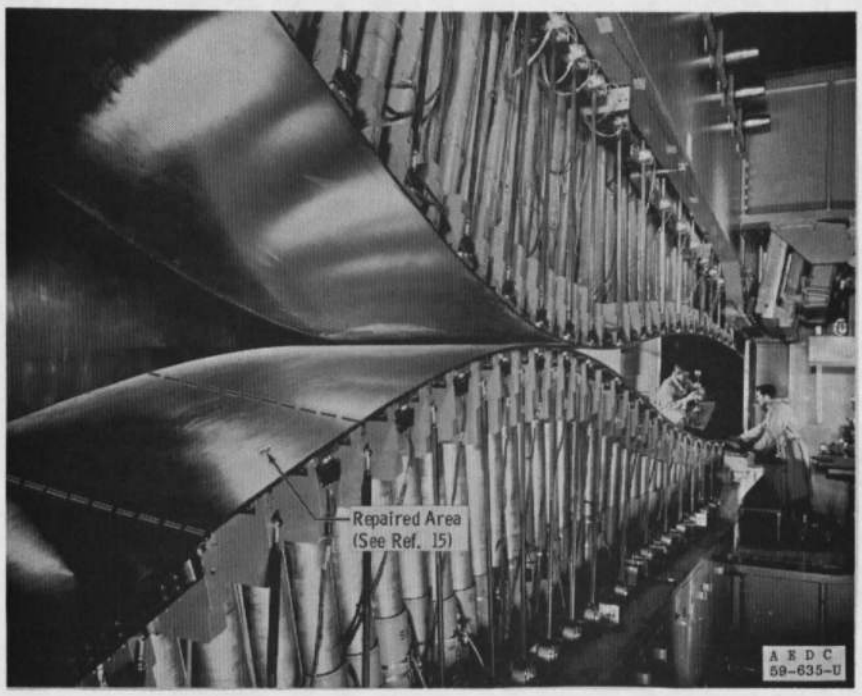

Fig. 11-1 AEDC-VKF Tunnel A (40-by 40-in. Test Section)

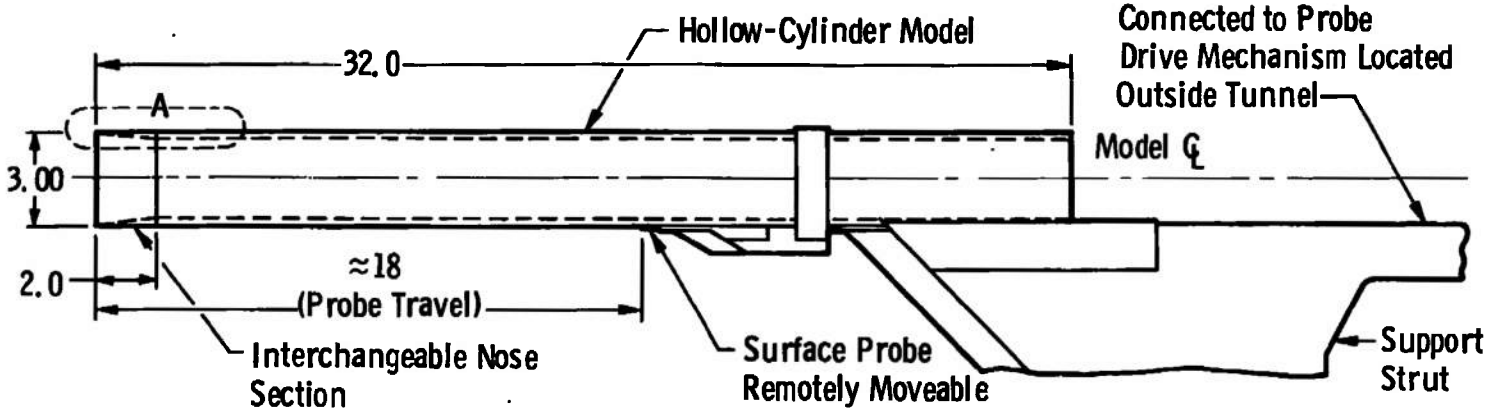

Model Details

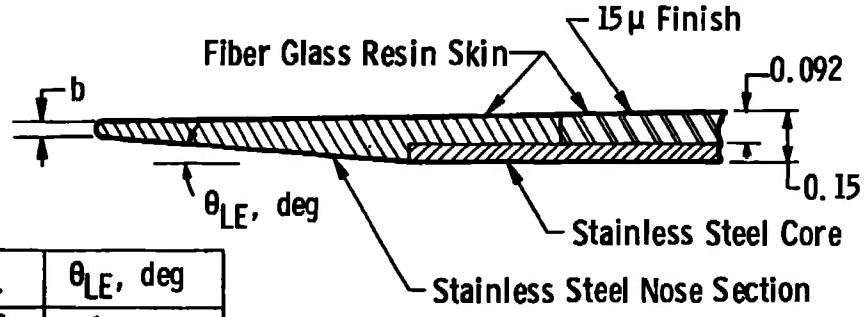

View A

$\bar{b}$, in.	θ_{LE}, deg
0.0021	6
0.0036	6 *
0.0013	12
0.0023	12
0.0030	12

*Original Nose Used in Refs. 13 and 17 (Maximum Deviation of ±0.0001 in. around Leading-Edge Circumference)

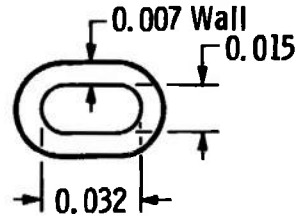

Probe "A" Tip Detail

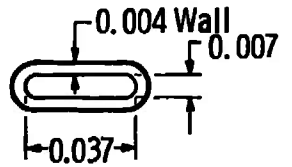

Probe "B" Tip Detail

All Dimensions in Inches

Fig. 11-2 3.0-in.-diam Hollow-Cylinder Transition Model

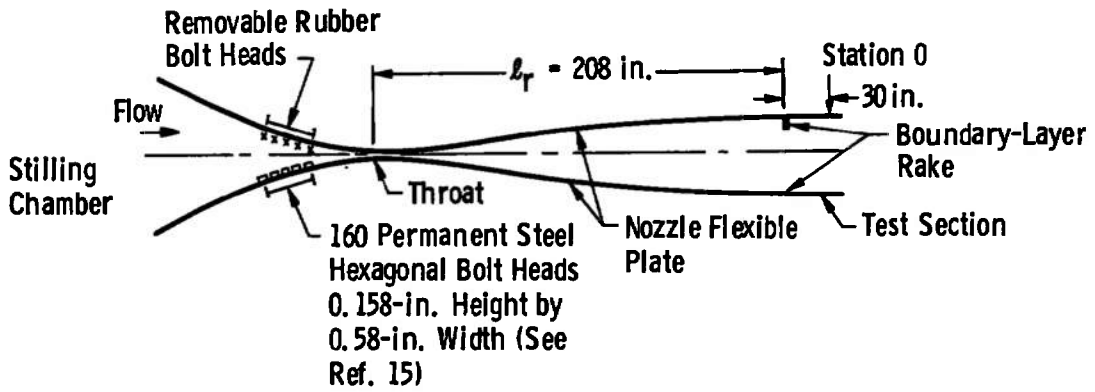

AEDC-VKF Tunnel A Profile

Rake Location	Remarks
○ △ □ Top Plate	With Rubber Bolt Heads
● ▲ ■ Top Plate	Without Rubber Bolt Heads
◌ ◬ ◻ Bottom Plate	With Steel Bolt Heads
◑ ◭ ◨ Bottom Plate	Before Plate Repair, Ref. 32

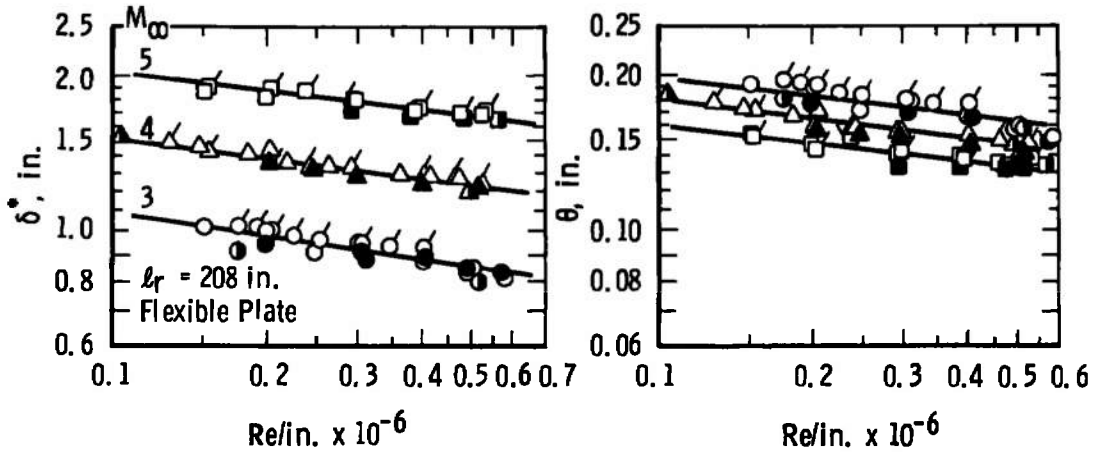

a. Displacement Thickness

b. Momentum Thickness

Fig. II-3 AEDC-VKF Tunnel A Boundary-Layer Characteristics

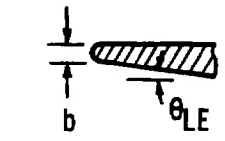

Leading-Edge Geometry

Flagged Symbols Represent Data Obtained with Duplicate Set of Rubber Bolt Heads on Top Plate (See Fig. 11-3)

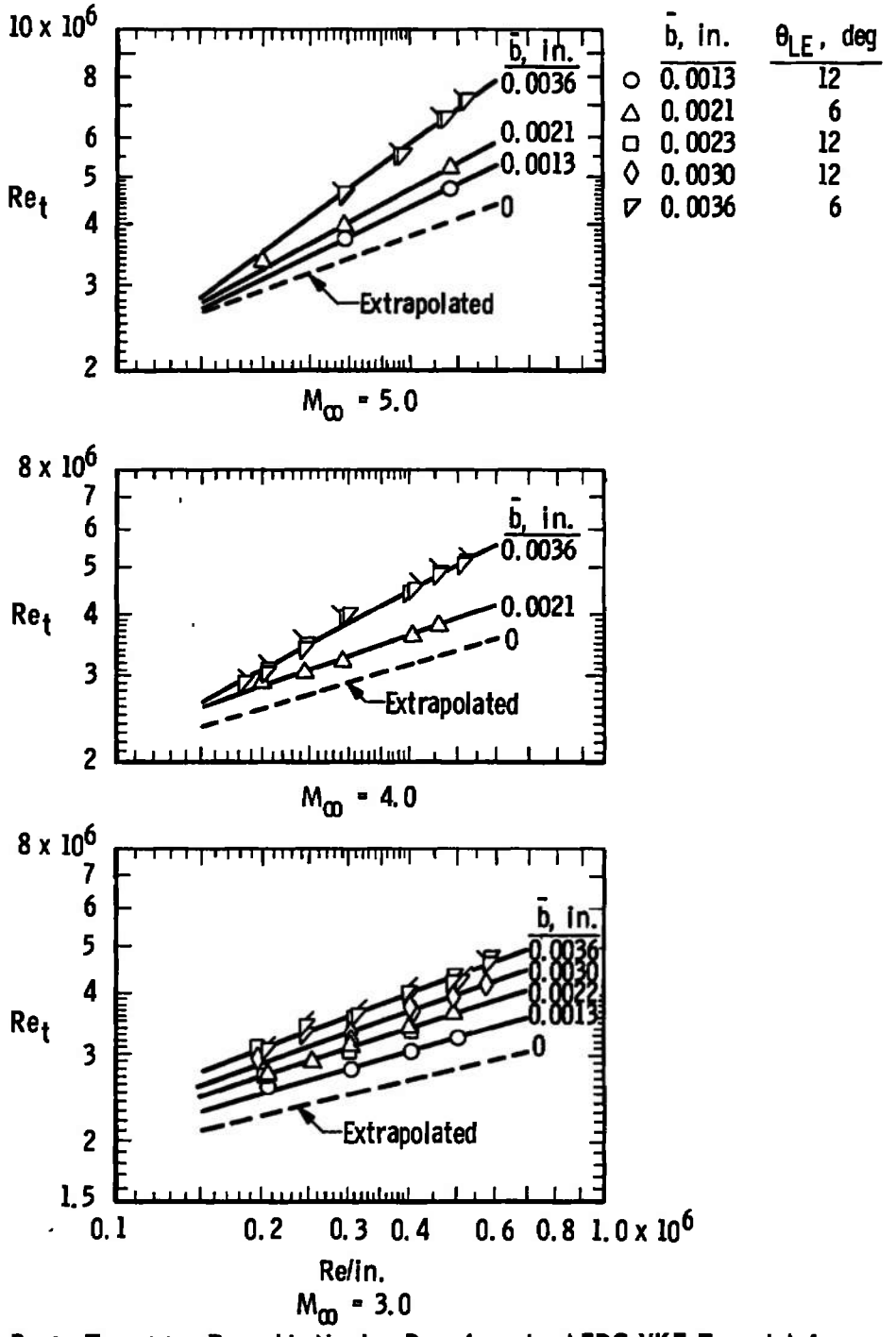

Fig. 11-4 Basic Transition Reynolds Number Data from the AEDC-VKF Tunnel A for M_∞ = 3, 4, and 5 and Variable $\bar{b}$ and θ_{LE}

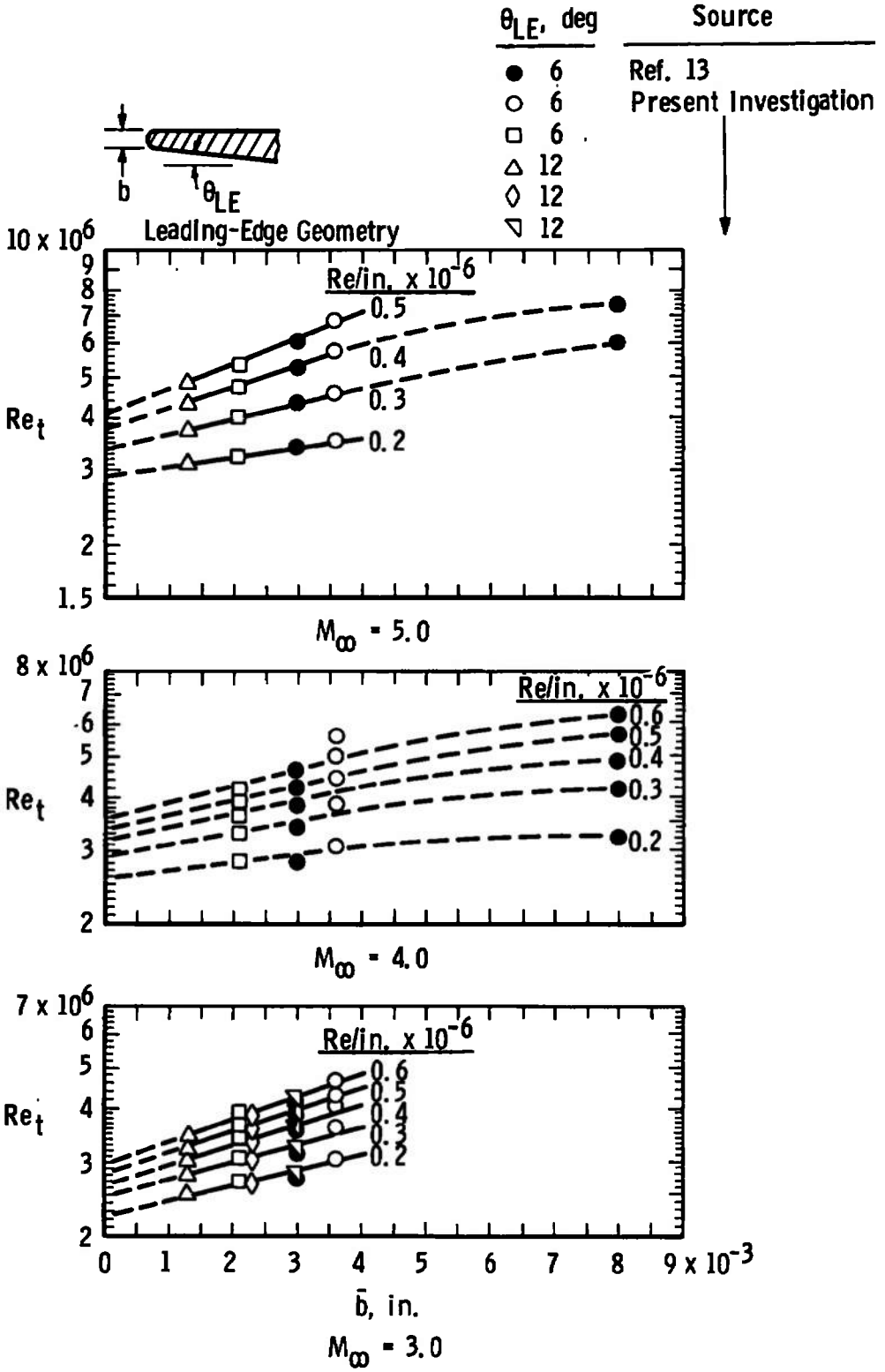

Fig. II-5 AEDC-VKF Tunnel A Re_t Values versus $\bar{b}$ for M_∞ = 3, 4, and 5

TABLE II-1
AEDC-VKF TUNNEL A TRANSITION REYNOLDS NUMBER DATA,
3.0-IN.-DIAM HOLLOW-CYLINDER

M_∞	p_o, psia	T_o, ^oR	Re_t x 10^{-6}	x_t, in.	Re_t x 10^{-6}	$\bar{b}$, in.	θ_{LE}, deg	Remarks
2.98	16.6	560	0.206	13.3	2.74	0.0021	6	
2.99	20.5	560	0.253	11.5	2.91	↓	↓	
2.99	24.8	564	0.303	10.5	3.18			
2.99	32.8	565	0.400	8.6	3.44			
3.00	40.7	566	0.493	7.5	3.69			
4.02	28.0	565	0.200	14.6	2.92			
4.02	34.1	563	0.244	12.6	3.08			
4.02	41.0	565	0.292	11.0	3.22			
4.02	56.5	562	0.405	9.1	3.69			
4.02	64.5	565	0.459	8.4	3.85			
5.04	50.95	603	0.200	17.0	3.40			
5.04	81.96	640	0.294	13.6	4.00			
5.06	136.7	644	0.484	10.9	5.26			
2.98	16.2	572	0.195	16.0	3.12	0.0036	6	
2.99	20.5	571	0.246	13.5	3.32	↓	↓	
2.99	25.6	570	0.308	11.7	3.60			
2.99	33.3	571	0.400	10.0	4.00			
2.99	41.4	573	0.494	9.0	4.45			
3.00	49.2	575	0.581	8.3	4.82			
2.98	12.2	560	0.151	--	--			Duplicate Set of Rubber Bolt Heads on Top Plate
2.98	16.4	560	0.203	15.2	3.09			
2.99	25.2	561	0.311	11.7	3.64			
2.99	41.4	565	0.505	8.5	4.29			
2.99	20.2	567	0.245	14.2	3.48			
2.99	33.2	569	0.400	10.2	4.08			
3.00	49.3	575	0.582	8.1	4.71			
2.99	41.4	575	0.491	8.7	4.28	↓	↓	↓
4.02	28.4	563	0.203	15.0	3.04	0.0036	6	
4.02	34.3	561	0.246	14.0	3.44	↓	↓	
4.02	41.5	561	0.298	13.5	4.02			
4.02	56.3	562	0.404	11.3	4.56			
4.02	73.4	567	0.518	10.0	5.18			
4.00	20.3	563	0.147	--	--			Duplicate Set of Rubber Bolt Heads on Top Plate
4.01	28.2	563	0.205	15.0	3.08			
4.02	34.3	564	0.245	14.3	3.50			
4.02	41.3	561	0.297	13.5	4.01			
4.02	56.2	564	0.401	11.3	4.53			
4.02	73.3	566	0.520	10.0	5.20			
4.02	64.8	566	0.460	10.8	4.96			
4.01	25.3	560	0.183	16.0	2.93	↓	↓	↓
5.05	81.5	638	0.292	16.0	4.67	0.0036	6	
5.06	109.9	645	0.386	14.5	5.60	↓	↓	
5.06	137.1	647	0.478	14.0	6.69			
5.05	150.5	649	0.526	13.8	7.26			

TABLE II-1 (Concluded)

M_∞	p_o, psia	T_o, ^oR	Re/in. x 10^{-6}	x_t, in.	Re_t x 10^{-6}	$\bar{b}$, in.	θ_{LE}, deg	Remarks
5.04	50.2	604	0.197	--	--	0.0036	6	Duplicate
5.04	81.6	634	0.297	15.5	4.61	↓	↓	Set of
5.06	110.5	648	0.385	14.5	5.59			Rubber
5.06	137.1	651	0.475	14.0	6.65			Bolts on
5.05	150.4	649	0.525	13.8	7.25			Top Plate
3.00	41.0	563	0.503	6.5	3.27	0.0013	12	
2.99	32.9	563	0.403	7.6	3.06	↓	↓	
2.99	24.8	562	0.305	9.2	2.81			
2.98	16.7	562	0.206	12.5	2.58			
5.06	136.4	642	0.483	9.9	4.78			
5.04	82.3	640	0.296	12.7	3.76			
2.98	16.5	565	0.203	13.4	2.72	0.0023	12	
2.99	32.7	563	0.401	8.4	3.37	↓	↓	
2.99	24.7	562	0.304	10.0	3.04			
2.98	16.2	566	0.198	15.0	2.97	0.0030	12	
2.99	25.4	566	0.309	10.7	3.31			
2.99	33.6	568	0.407	9.2	3.74			
2.99	40.9	571	0.491	8.0	3.93			
3.00	48.7	573	0.578	7.3	4.22			
2.99	33.1	564	0.404	9.3	3.76			
2.99	25.0	565	0.305	10.6	3.24			
3.0	--	≈560	0.15	--	2.10	0*	--	Extrapolated
↓	↓	↓	0.2	↓	2.25	↓	↓	Value of Re_t
			0.3		2.49			↓
			0.4		2.68			
			0.5		2.82			
			0.6		2.96			
4.0	--	≈560	0.15	--	2.37	0*	--	Extrapolated
↓	↓	↓	0.20	↓	2.60	↓	↓	Value of Re_t
			0.30		2.92			↓
			0.40		3.20			
			0.50		3.41			
			0.60		3.60			
5.0	--	--	0.15	--	2.64	0*	--	Extrapolated
↓	↓	↓	0.20	↓	2.91	↓	↓	Value of Re_t
			0.30		3.38			↓
			0.40		3.80			
			0.50		4.12			
			0.60		4.40			

*From Figs. II-4 and II-5

APPENDIX III
EXPERIMENTAL RESULTS FROM THE LONG AND SHORT SHROUD CONFIGURATIONS INSTALLED IN THE AEDC-VKF TUNNEL A

3.1 SHROUD MODEL AND MICROPHONE MODEL

Long and short shrouds (11.42-in. ID) (Fig. III-1) were used to shield the 3.0-in.-diam hollow-cylinder model. The short shroud was maintained at a fixed position, and the long shroud was repositioned axially to prevent shroud leading shock interference in the region of transition measurements on the transition model.

The microphone model (Fig. III-2) was an 8- by 5-in. sharp leading-edge flat plate instrumented with two 1/4-in.-diam microphones and two static orifices. One microphone was mounted flush with the model surface and the other mounted internally to record model vibrations.

The microphone model was tested in the freestream of the AEDC-VKF Tunnels A and D and inside the long shroud in Tunnel A. The microphone model locations inside the long shroud (Fig. III-3) were similar to the 3.0-in.-diam transition model locations, and the shroud model was repositioned with changes in free-stream Mach number to prevent the shroud leading-edge generated shock wave from impinging on the model surface.

3.2 MICROPHONE

The microphone instrumentation employed to measure the radiated aerodynamic noise consisted of two Brüel and Kjar® 1/4-in.-diam condenser microphones (Model No. 4136) used in conjunction with a Brüel and Kjar root-mean-square (RMS) voltmeter and an Ampex® (Model No. FR1300) analog tape recorder. The lower and upper limit of the microphone dynamic range was from 70 and 180 db, respectively, and the frequency range was from 0 to 100 kHz. The RMS pressure fluctuations were read directly from the RMS voltmeter during test operation. The microphone output was also recorded on the Ampex data tape system and later checked for verification of the on-line RMS values.

Microphone interference from model vibration was minimized by providing a nylon insert around the surface microphone, using insulator strips on the mounting plate, and filling the microphone cable cavity with cotton. Model vibrations as determined from the internally mounted microphone were found to be negligible.

3.3 LONG SHROUD INNER WALL BOUNDARY-LAYER CHARACTERISTICS AND PRESSURE DISTRIBUTIONS

A pitot rake having fifteen probes was used to determine the long shroud inner-wall boundary-layer characteristics at the microphone model leading-edge location (Fig. III-4c). At $M_\infty = 3.0$ and 5.0, the boundary layer (no trip) was fully turbulent at the rake location for Re/in. $\geq 0.15 \times 10^6$, as shown in Figs. III-4a and b and III-5b and c. For $M_\infty = 3.0$ and Re/in. $= 0.05 \times 10^6$, the boundary layer was laminar at the rake for the no-trip condition. When an equivalent length concept ($x_{eq.}$) was used as outlined in Fig. III-4d, the experimentally no-trip, momentum thickness (θ) data were in good agreement with the theoretical results, as shown in Fig. III-4b.

The shroud inner-wall boundary-layer displacement and momentum thicknesses were evaluated using the following equations:

$$\delta^* = \int_0^\delta \left(1 - \frac{\rho u}{\rho_L U_L}\right)\left(1 - \frac{y}{r}\right) dy$$

$$\theta = \int_0^\delta \frac{\rho u}{\rho_L U_L}\left(1 - \frac{u}{U_L}\right)\left(1 - \frac{y}{r}\right) dy$$

The local boundary-layer velocity (u) was determined using the rake probe total pressures and the shroud static pressure. The static pressure (measured shroud static) and total temperature was assumed to remain constant through the boundary layer. The local flow velocity (U_L) outside the shroud boundary layer was calculated using T_o with the measured shroud static and the pitot pressure from the outermost probe on the rake which was outside the shroud boundary layer.

Figure III-6 presents the measured pressure distributions inside the long shroud for $M_\infty = 3$ and 5 as determined from static pressure orifices located on the shroud inner surface near the shroud leading edge, from orifices on the 3.0-in.-diam hollow-cylinder transition model, and from orifices on the flat plate microphone model. These data confirm that the shroud internal flow was supersonic at all times. A fairly good theoretical estimate of the static pressure distribution inside the shroud was obtained assuming that a 1-deg, two-dimensional shroud lip shock existed.

3.4 LONG SHROUD TRANSITION RESULTS

Typical surface pitot pressure traces from which transition locations on the 3.0-in.-diam hollow cylinder were determined are presented in Figs. III-7 and III-8. The pitot probe was remotely controlled, and a continuous pitot pressure trace was provided by an X-Y plotter. In accordance with the previous discussions in Section III and Appendix I, the location of transition was defined as the peak in the pitot pressure trace. When the boundary-layer trip was placed on the shroud lip inner surface, the large decrease in the location of transition as a result of the increase in the radiated aerodynamic noise emanating from the shroud inner wall turbulent boundary layer is clearly seen in Fig. III-7. The impingement location of the long shroud lip shock (x_s) on the 3.0-in.-diam hollow-cylinder model (Fig. III-7) was clearly visible on the probe pressure trace and was near the anticipated station.

In addition to the long shroud, a short shroud configuration was also tested. The purpose of this configuration was to maintain laminar flow on the inner wall and attempt to shield some of the radiated aerodynamic noise from the walls of the 40-in. Tunnel A from the 3.0-in.-diam transition model. However, it was suspected that this short shroud configuration would not shield an appreciable amount of radiation since the radiated pressure fluctuations travel along incline rays similar to, but somewhat steeper than, Mach waves (see Ref. 6). Again the leading-edge shock impingement (x_s) was clearly visible on the probe pressure traces presented in Fig. III-8 and occurred on the 3.0-in.-diam model near the anticipated location.

Figure III-9 presents the transition Reynolds number results obtained without the shroud configuration and with the short and long shroud configurations placed concentrically around the 3.0-in.-diam hollow-cylinder model for M_∞ = 3,4, and 5 and the allowable Re/in. range. These data were taken with and without the boundary-layer trip on the long shroud inner surface at M_∞ = 3 and 5. However, the trip was not effective at M_∞ = 5 which was not unexpected.

All of the transition results obtained in this investigation are tabulated in Table III-1.

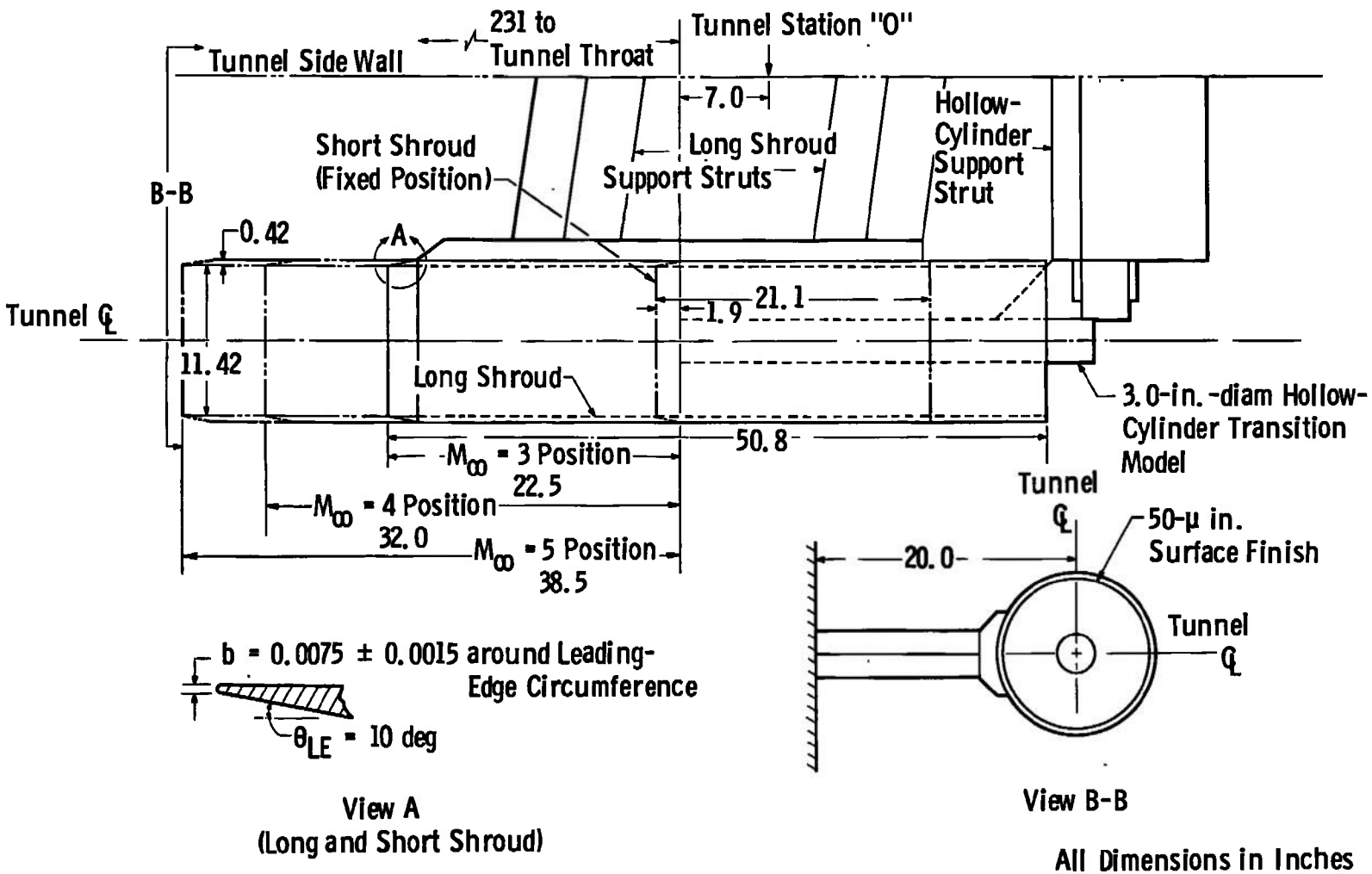

Fig. III-1 AEDC-VKF Tunnel A Long and Short Shroud Configurations

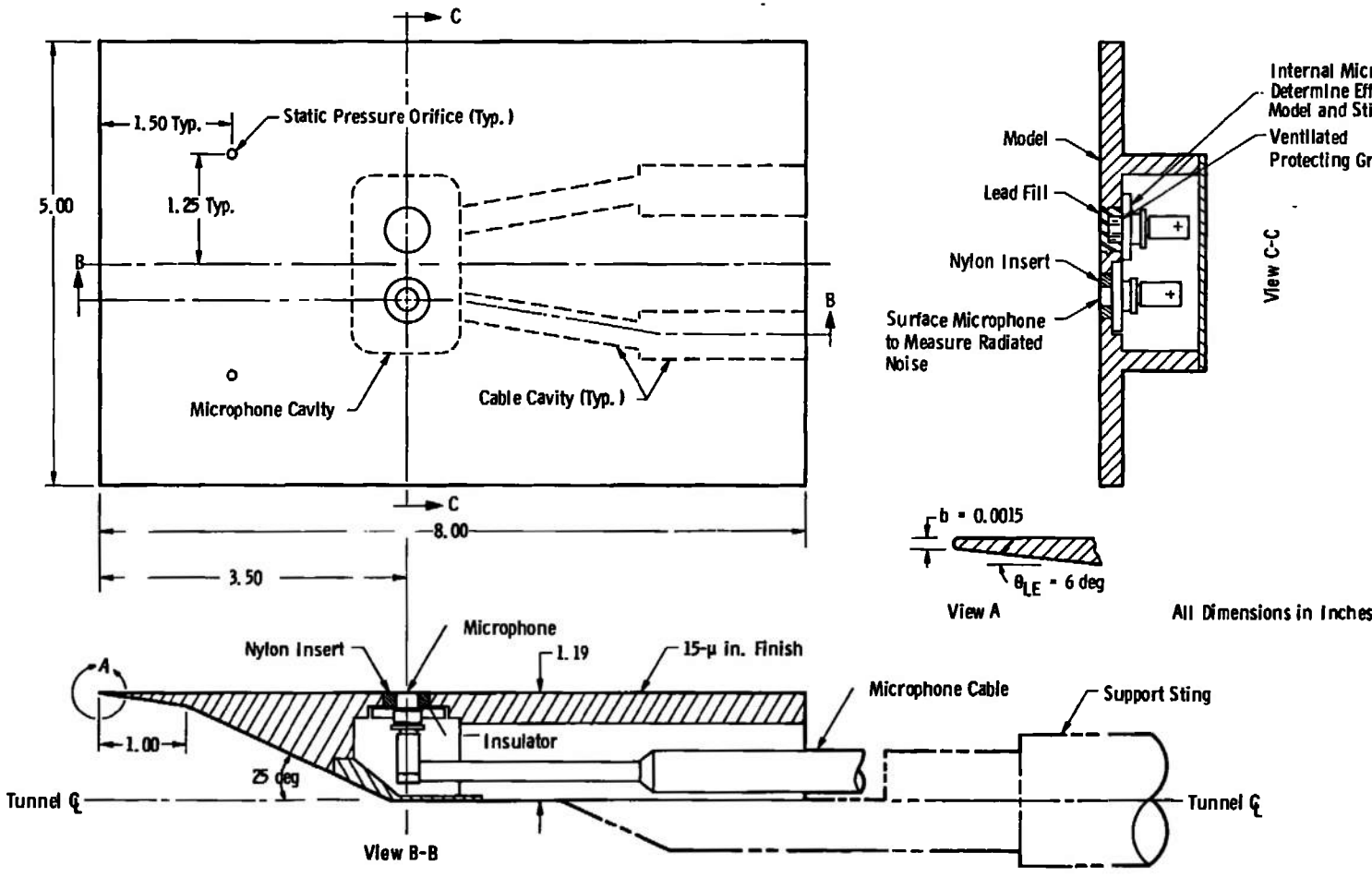

Fig. III-2 Flat Plate Microphone Model

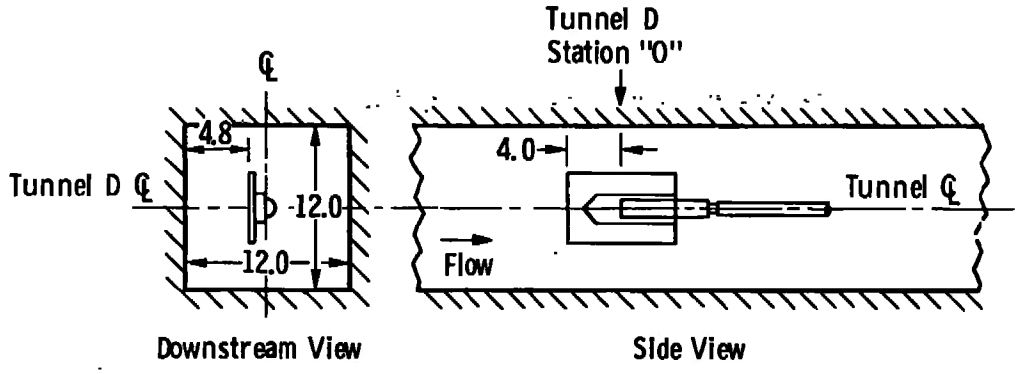

a. Tunnel D Installation

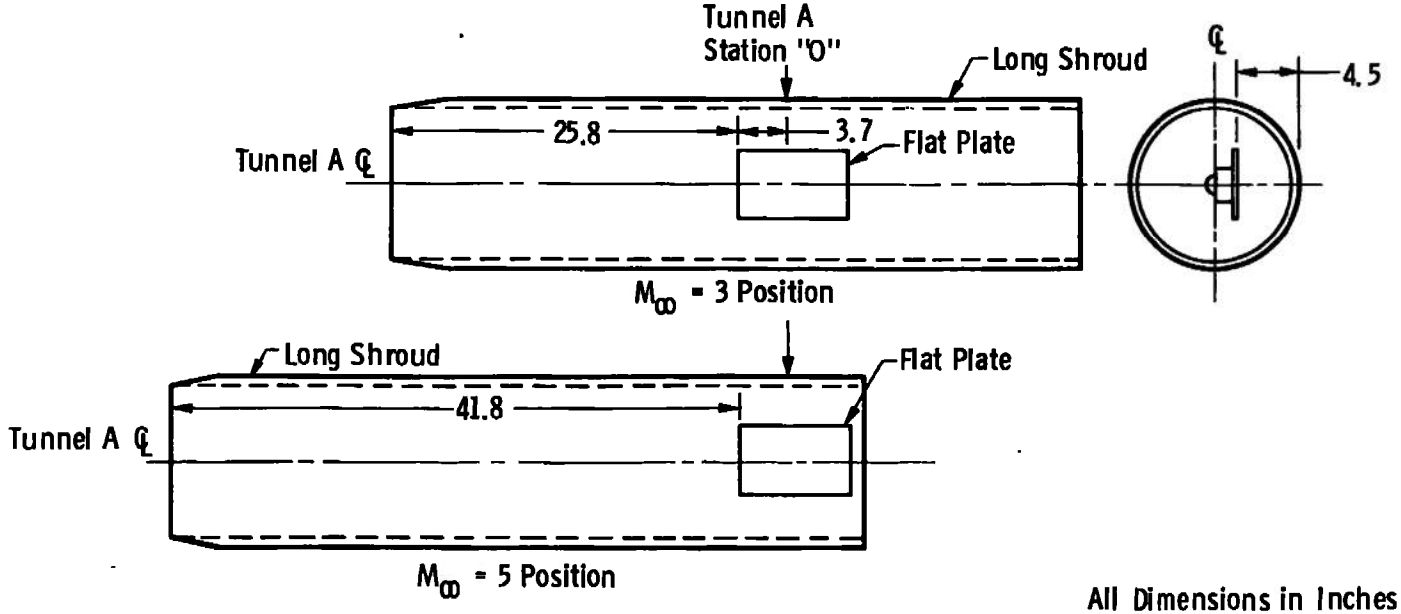

b. Tunnel A Installation

Fig. III-3 AEDC-VKF Tunnels A and D Microphone-Flat-Plate Installation

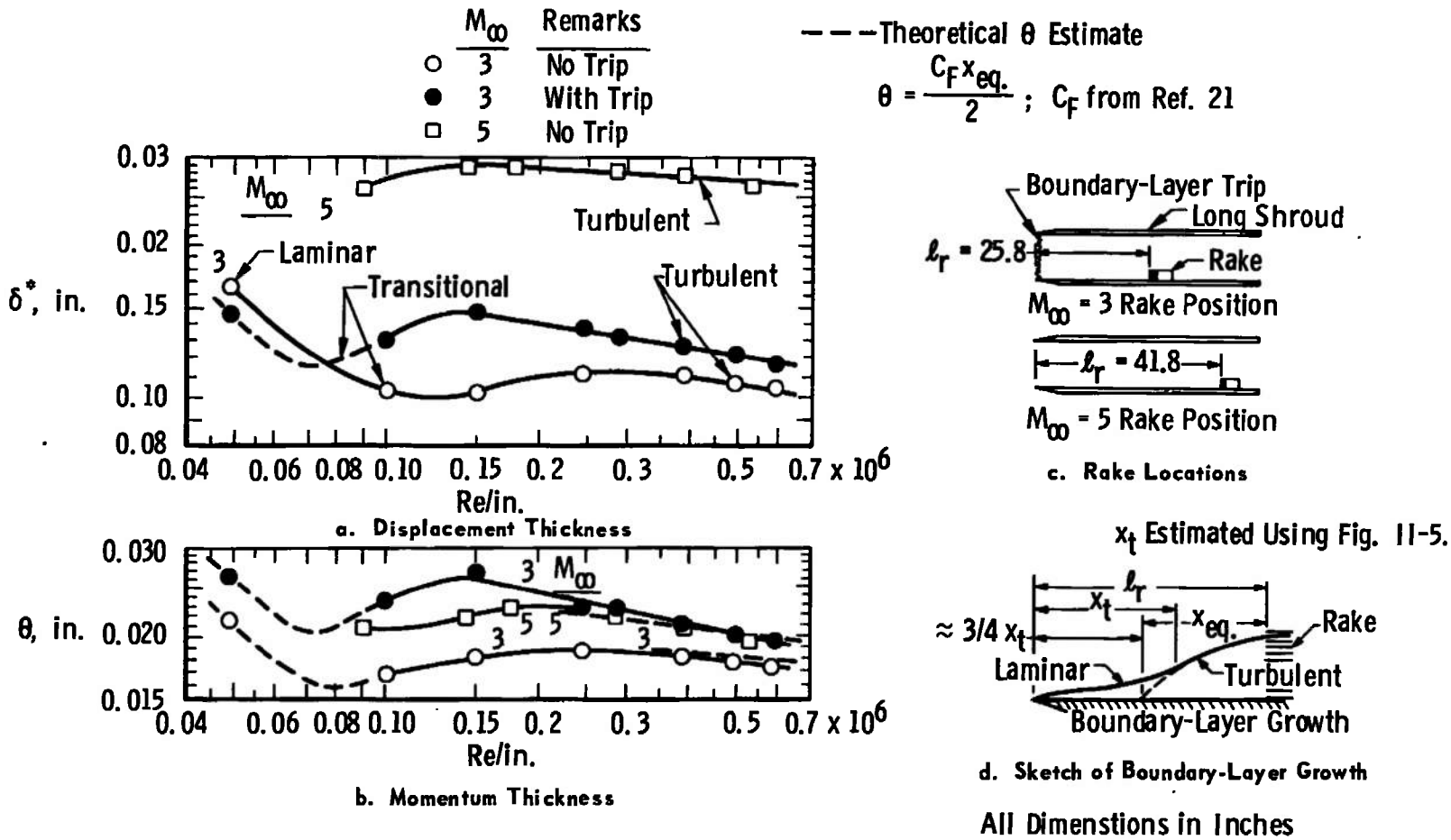

Fig. III-4 Long Shroud Boundary-Layer Characteristics

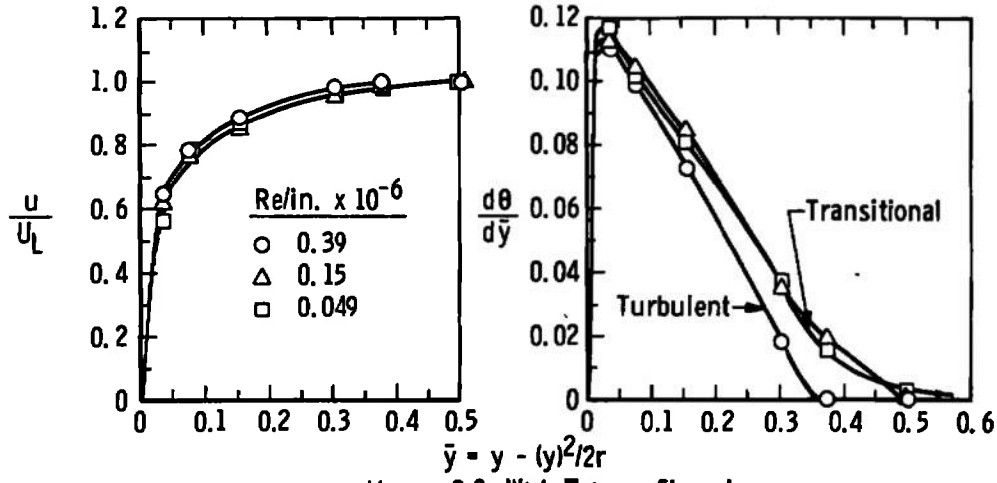

a. M_∞ = 3.0, With Trip on Shroud

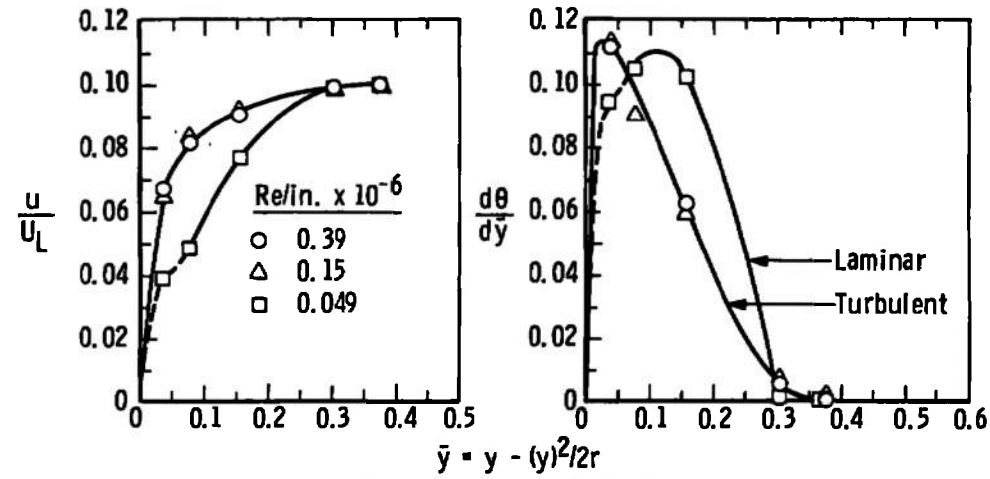

b. M_∞ = 3.0, No Trip on Shroud

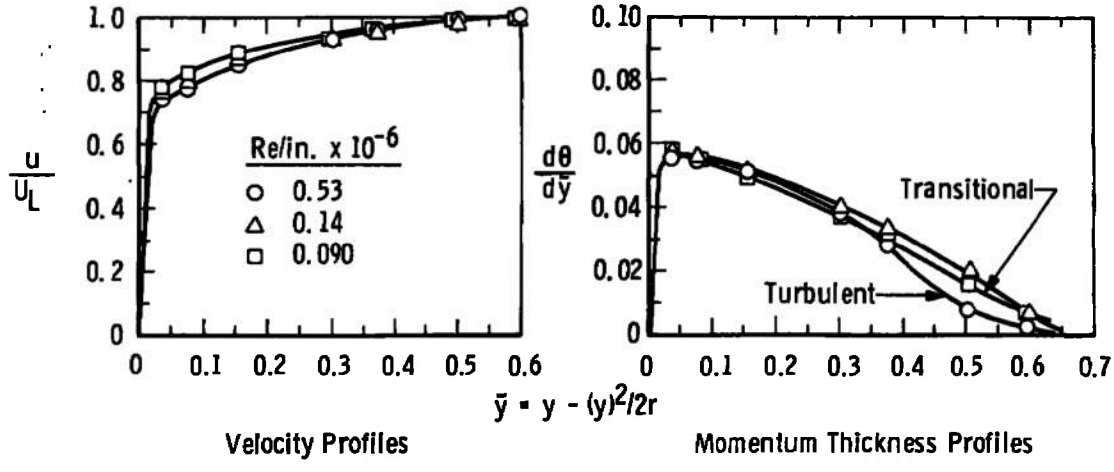

c. M_∞ = 5.0, No Trip on Shroud

Fig. III-5 Boundary-Layer Profiles on Inner Wall of Long Shroud

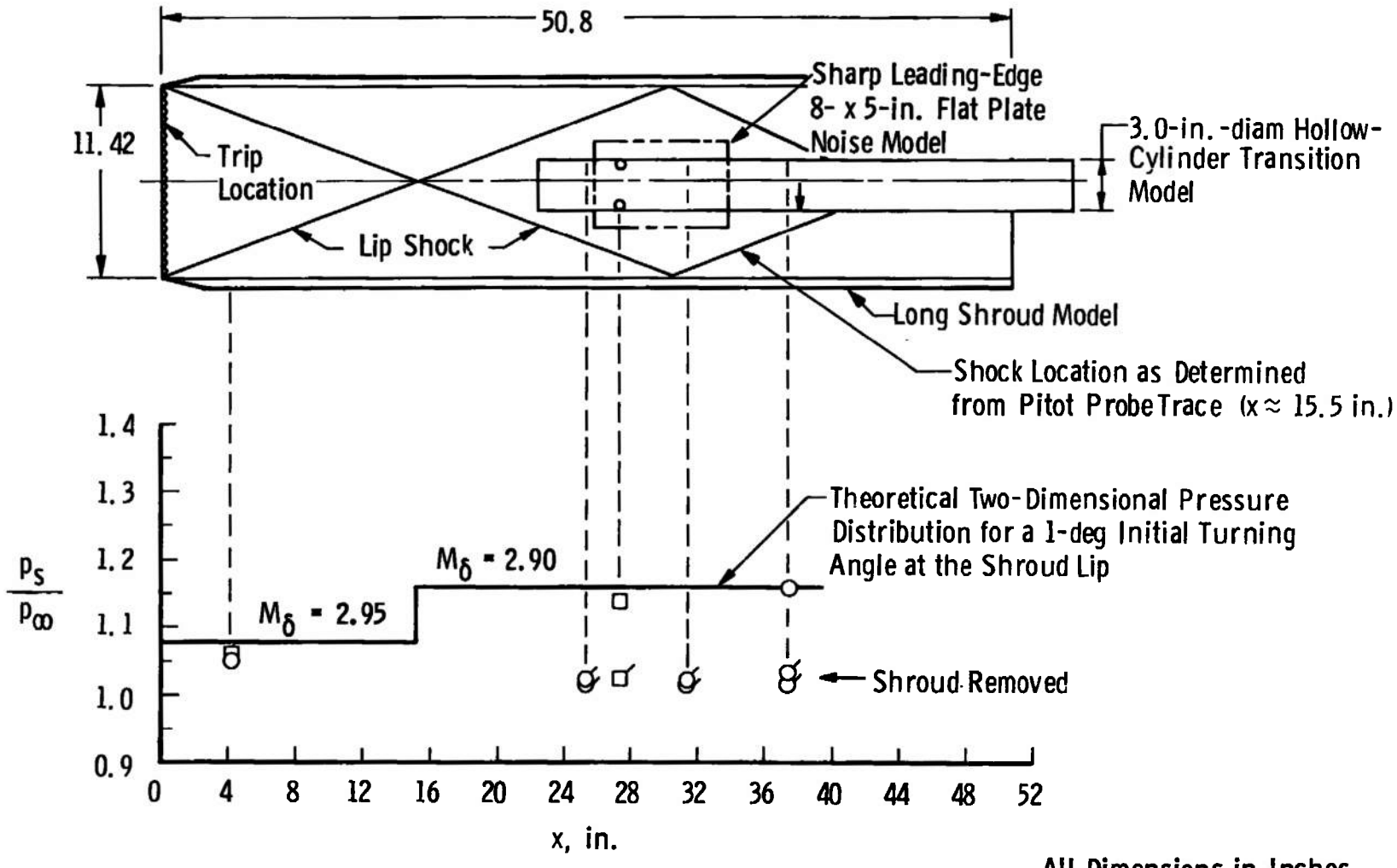

a. M_∞ = 3.0, Re/in. = 0.30 × 10^6

Fig. III-6 Inviscid Pressure Distribution inside Long Shroud

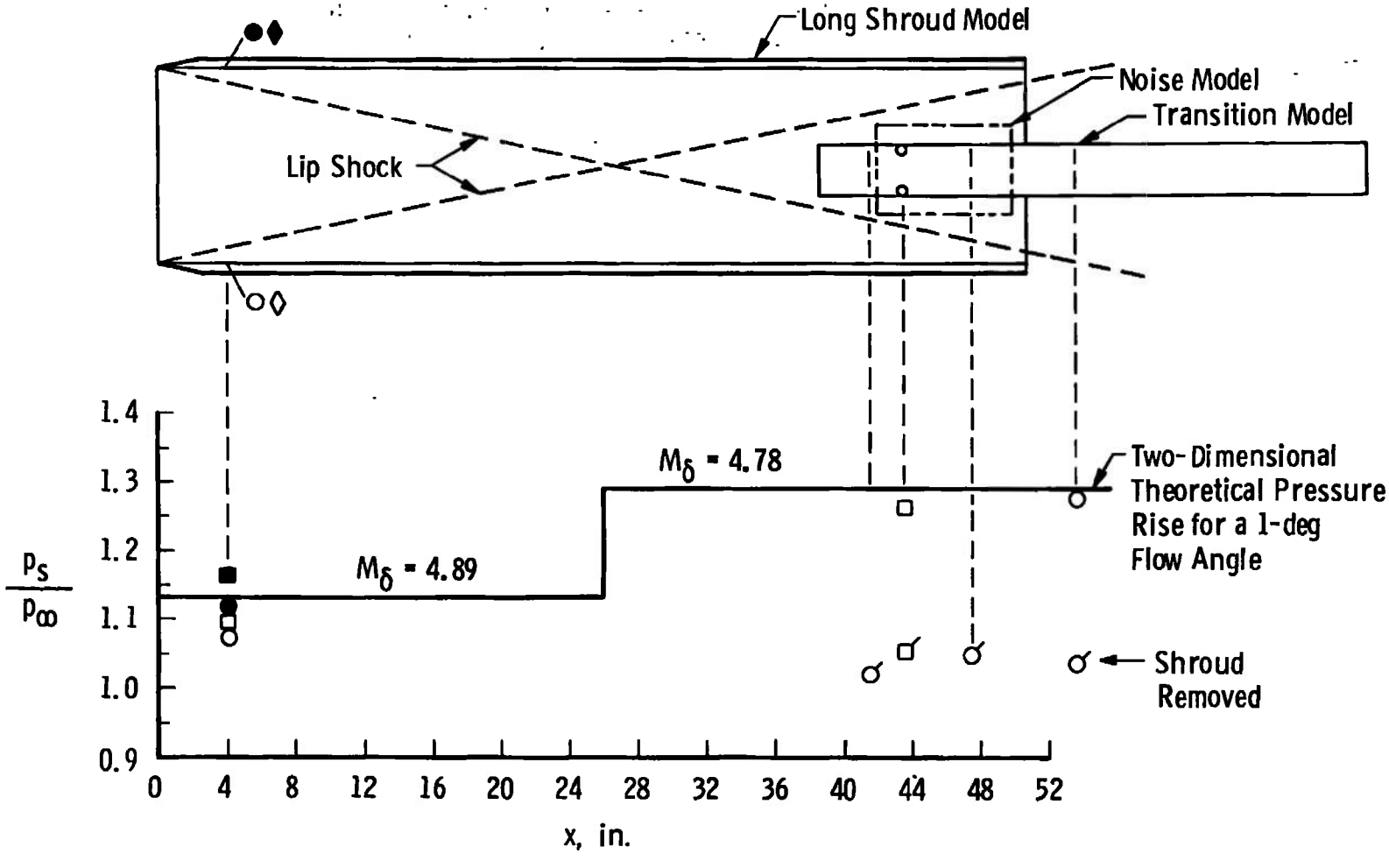

b. M_∞ = 5.0, Re/in. = 0.48 × 10^6

Fig. III-6 Concluded

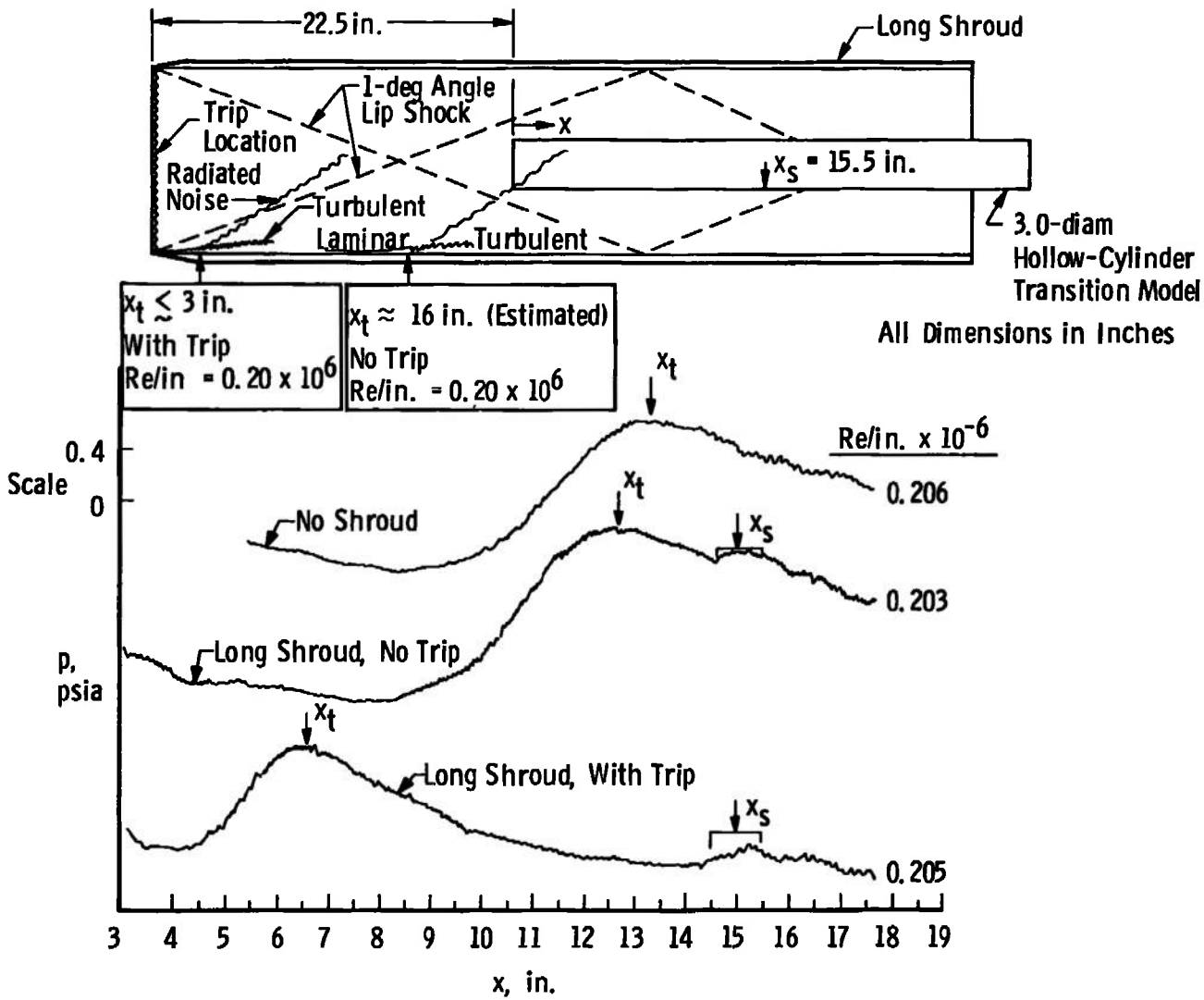

Fig. III-7 Surface Pitot Probe Pressure Traces for 3.0-in.-diam Model M_∞ = 3.0, Long Shroud Configuration

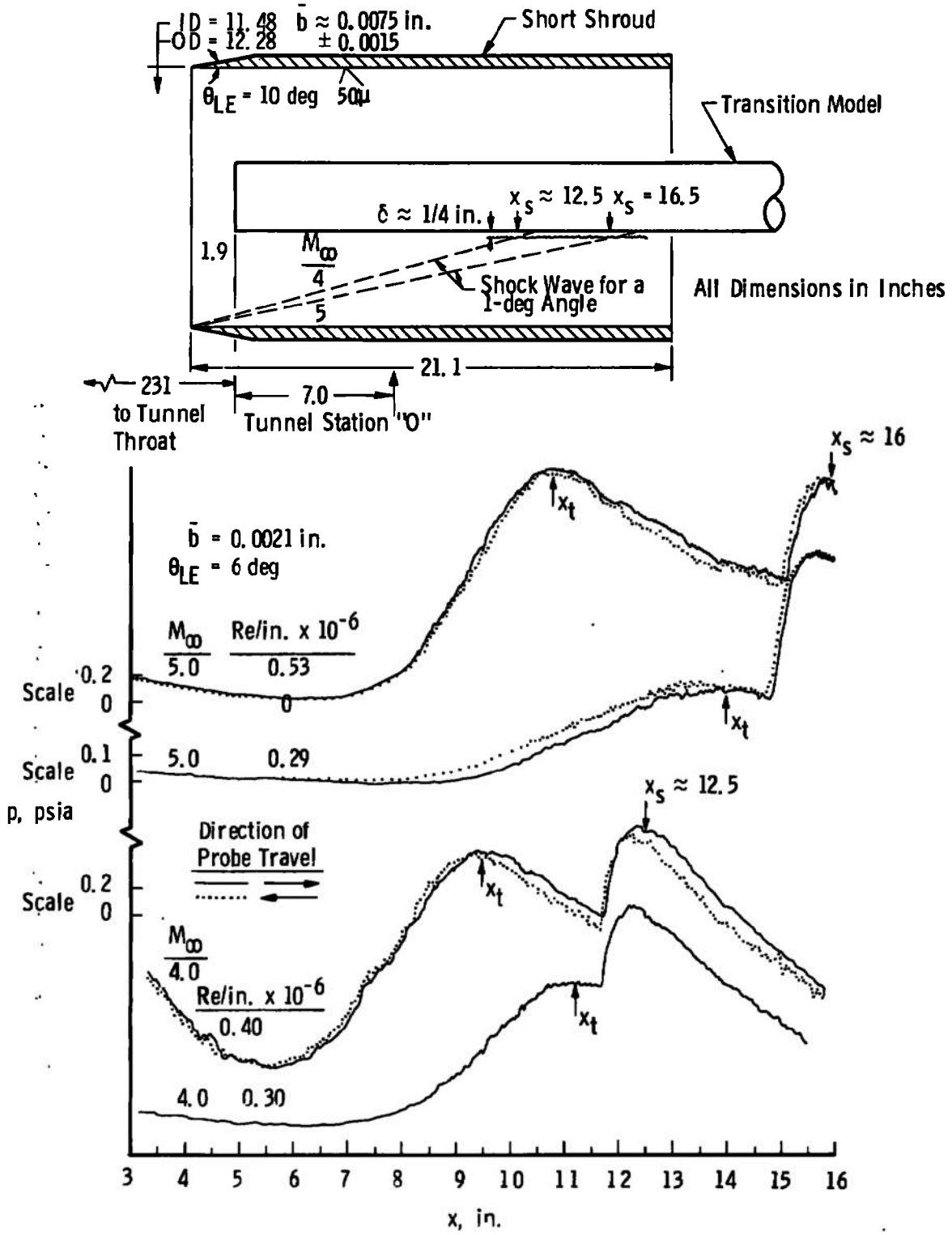

Fig. III-8 Surface Pitot Probe Pressure Traces on 3.0-in.-diam Model Short Shroud Configuration, M_∞ = 4 and 5

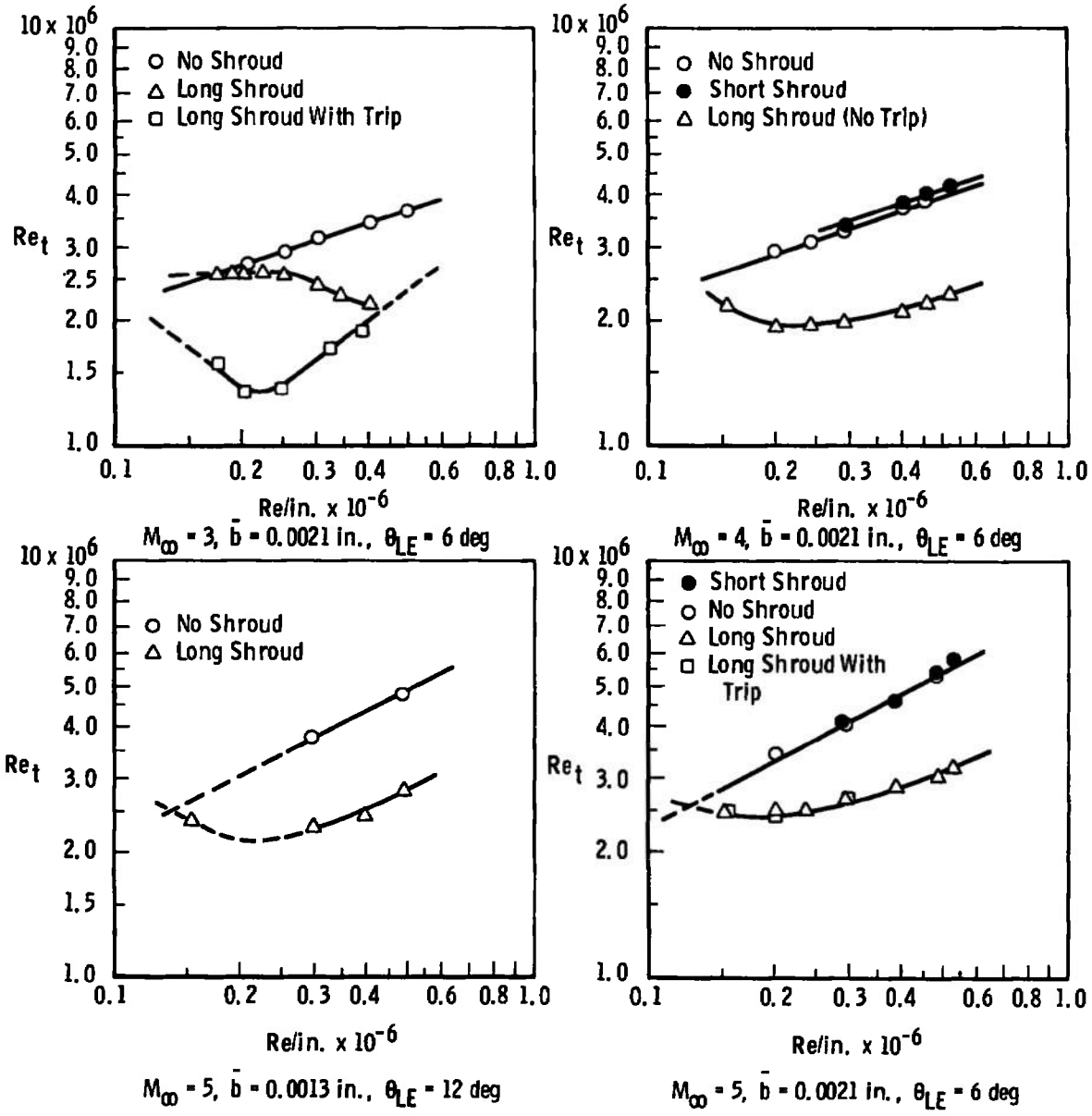

Fig. III-9 Tunnel A Transition Reynolds Data from 3.0-in.-diam Model with and without Long and Short Shroud

TABLE III-1
LONG AND SHORT SHROUD TRANSITION RESULTS

M_∞	Config.	p_o, psia	T_o, ^oR	Re/in. x 10^{-6}	x_t**, in.	Re_t x 10^{-6}	$\bar{b}$, in.	θ, deg
2.98	Long Shroud	16.6	563	0.203	12.7	2.58	0.0021	6
2.99		20.4	562	0.252	10.2	2.57		
2.99		24.7	562	0.304	8.0	2.43		
2.99		32.7	563	0.401	5.5	2.21		
2.99		28.1	562	0.345	6.6	2.28		
2.99		18.2	561	0.225	11.5	2.59		
2.98		14.2	562	0.176	14.5	2.55		
2.98		15.3	561	0.191	13.5	2.58		
4.02		28.4	566	0.202	9.5	1.92		
4.00		21.3	564	0.154	14.0	2.16		
3.99		17.7	564	0.128	*--	--		
4.02		34.0	564	0.243	8.0	1.94		
4.02		41.1	564	0.293	6.7	1.96		
4.02		56.3	564	0.403	5.2	2.09		
4.02		64.5	562	0.463	4.7	2.17		
4.02		73.4	563	0.525	4.4	2.31		
5.04		50.9	601	0.201	12.5	2.51		
5.04		82.0	638	0.296	9.0	2.66		
5.06		110.1	639	0.392	7.2	2.82		
5.06		136.5	645	0.480	6.2	2.98		
5.05		150.0	644	0.531	6.0	3.19		
5.04		66.6	641	0.238	10.5	2.50		
5.04		39.2	606	0.153	16.1	2.46		
5.04		39.1	604	0.153	15.5	2.37	0.0013	12
5.04		50.6	603	0.199	11.5	2.29		
5.04		82.0	638	0.296	8.2	2.43		
5.06		136.9	638	0.490	5.7	2.79		
5.04	Long Shroud with Trip	39.4	603	0.155	16.0	2.48	0.0021	6
5.04		50.8	601	0.200	12.0	2.40		
5.04		82.2	639	0.296	9.0	2.66		
2.98		14.3	564	0.176	9.0	1.58		
2.98		16.6	563	0.205	6.6	1.35		
2.99		20.5	565	0.250	5.5	1.37		
2.99		26.1	563	0.324	5.3	1.72		
2.99		32.8	564	0.39	4.8	1.87		
3.0	Short Shroud	--	--	--	*--	--	0.0021	6
4.02		28.2	564	0.202	*--	--		
4.02		34.4	564	0.245	*--	--		
4.02		41.3	562	0.296	11.2	3.31		
4.02		56.4	565	0.401	9.5	3.81		
4.02		64.7	569	0.457	8.7	3.98		
4.02		73.5	565	0.524	8.0	4.19		
5.05		150.6	643	0.532	10.8	5.75		
5.06		136.9	643	0.484	11.1	5.37		
5.06		109.9	643	0.389	11.7	4.55		
5.05		82.4	645	0.292	14.0	4.09		

*Shroud Lip Shock Wave Interference

**x_t Measured on 3.0-in.-diam Hollow-Cylinder Transition Model

APPENDIX IV
TRANSITION REYNOLDS NUMBER RESULTS FROM THE AEDC-VKF TUNNEL D

4.1 AEDC-VKF TUNNEL D

The AEDC-VKF Tunnel D is shown in Fig. IV-1. Additional information on the tunnel can be found in Section II.

4.2 TRANSITION REYNOLDS NUMBERS

The basic transition Reynolds number data obtained on the 3.0-in.-diam hollow-cylinder model in Tunnel D for $M_\infty = 3$ are plotted in Figs. IV-2 and IV-3 for several leading-edge geometries and two sizes of surface pitot probe tips. The location of transition was determined from continuous surface pitot pressure traces recorded on a X-Y plotter and was defined as the peak location in the pitot pressure trace (see Section III and Appendix I). These data show that there was no discernible effect on transition due to probe tip size and also no effect of the leading-edge internal bevel angle. The transition Reynolds number data obtained by Potter and Whitfield (Ref. 17) in Tunnel D using the same model are presented in Fig. IV-3 for $M_\infty = 3$, 4, and 5. Good agreement is seen to exist between the present results and the results of Ref. 17 at $M_\infty = 3$, $\bar{b} = 0.003$ in. The zero bluntness transition Reynolds number from Tunnel D used in the transition correlation presented in Section V were taken from Fig. IV-3. Transition Reynolds number results obtained in this investigation in Tunnel D are tabulated in Table IV-1.

The effectiveness of the serrated fiber glass boundary-layer trip that was used in the Tunnel A long shroud experiments (Section IV and Appendix III) was determined from tests in Tunnel D. These results are shown in Fig. IV-4 for $M_\infty = 3$.

It is of interest to note that when the boundary-layer trip was located on the inner wall of the 3.0-in.-diam model near the leading edge the turbulent boundary layer with its inherent radiated noise that was presumably present on the inner wall did not affect the boundary-layer transition on the model outer surface, as shown by the Re_t data in Fig. IV-2.

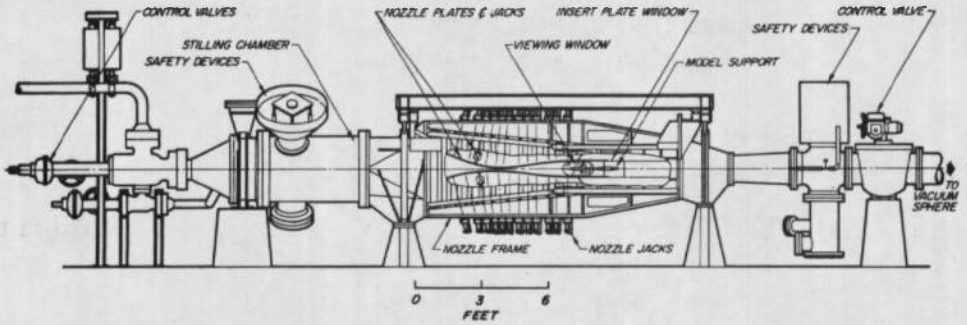

Assembly

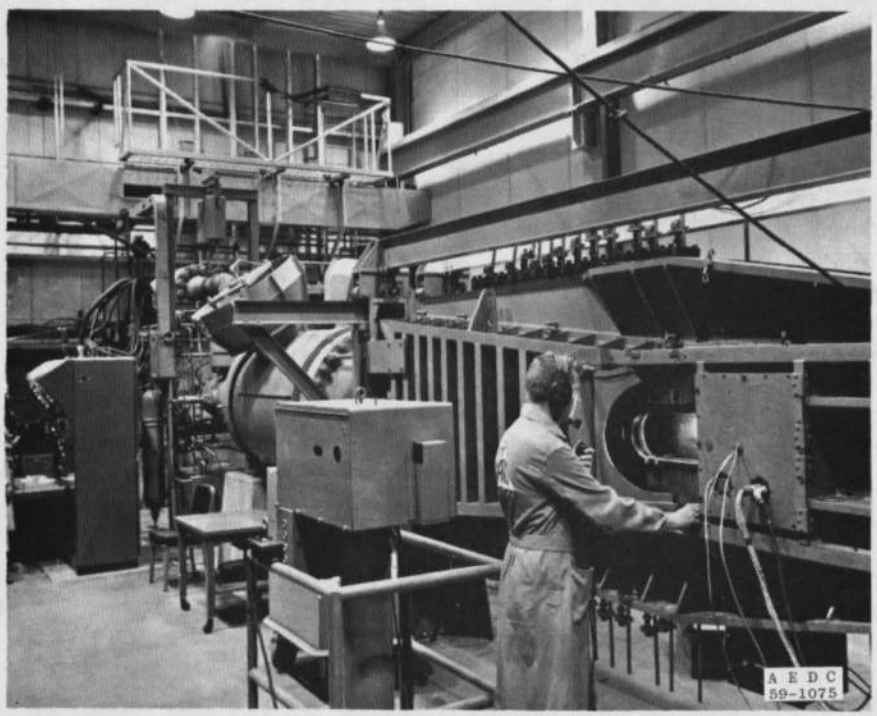

Nozzle and Test Section

Fig. IV-1 AEDC-VKF Tunnel D (12-by 12-in. Test Section)

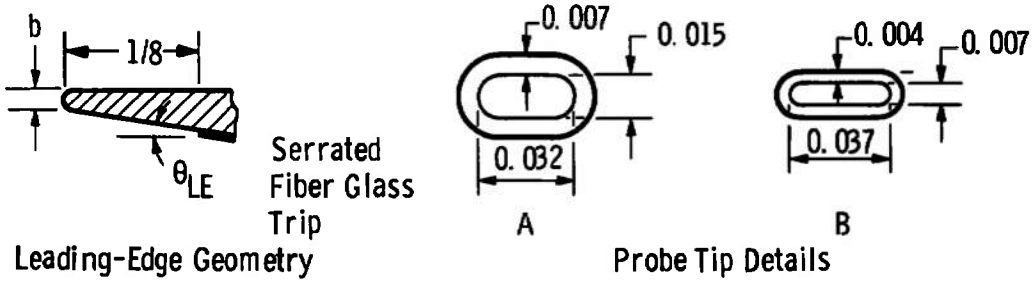

	$\bar{b}$, in.	θ_{LE}, deg	Remarks
○	0.0021	6	Probe A
◌́	0.0021	6	Probe B
△	0.0023	12	Probe A
□	0.0036	6	Probe A
■	0.0036	6	Probe A*

* - Boundary-Layer Trip on Internal Bevel Angle

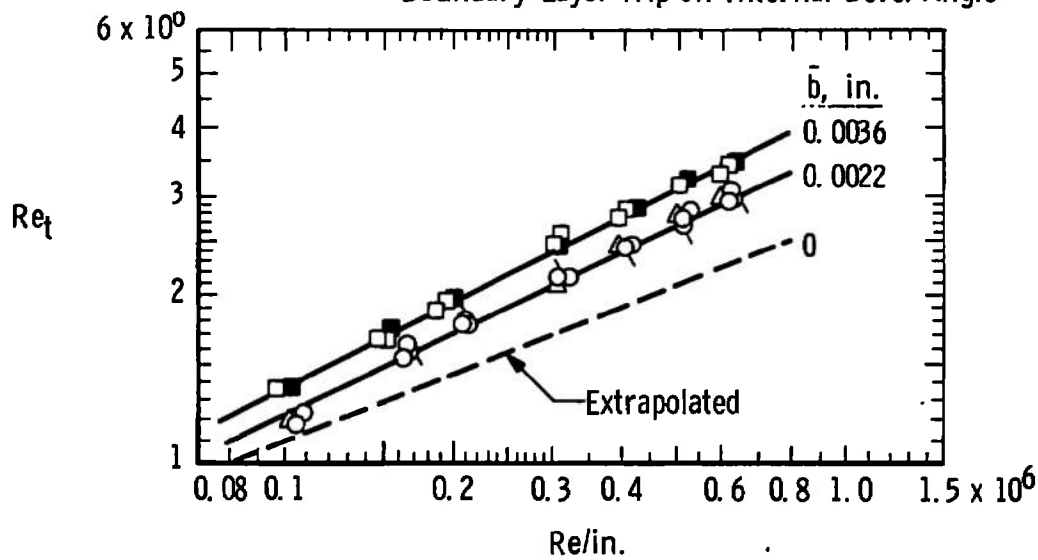

Fig. IV-2 Basic Transition Reynolds Number Data from the AEDC-VKF Tunnel D for M_∞ = 3.0 with Variable $\bar{b}$, θ_{LE}, and Re/in.

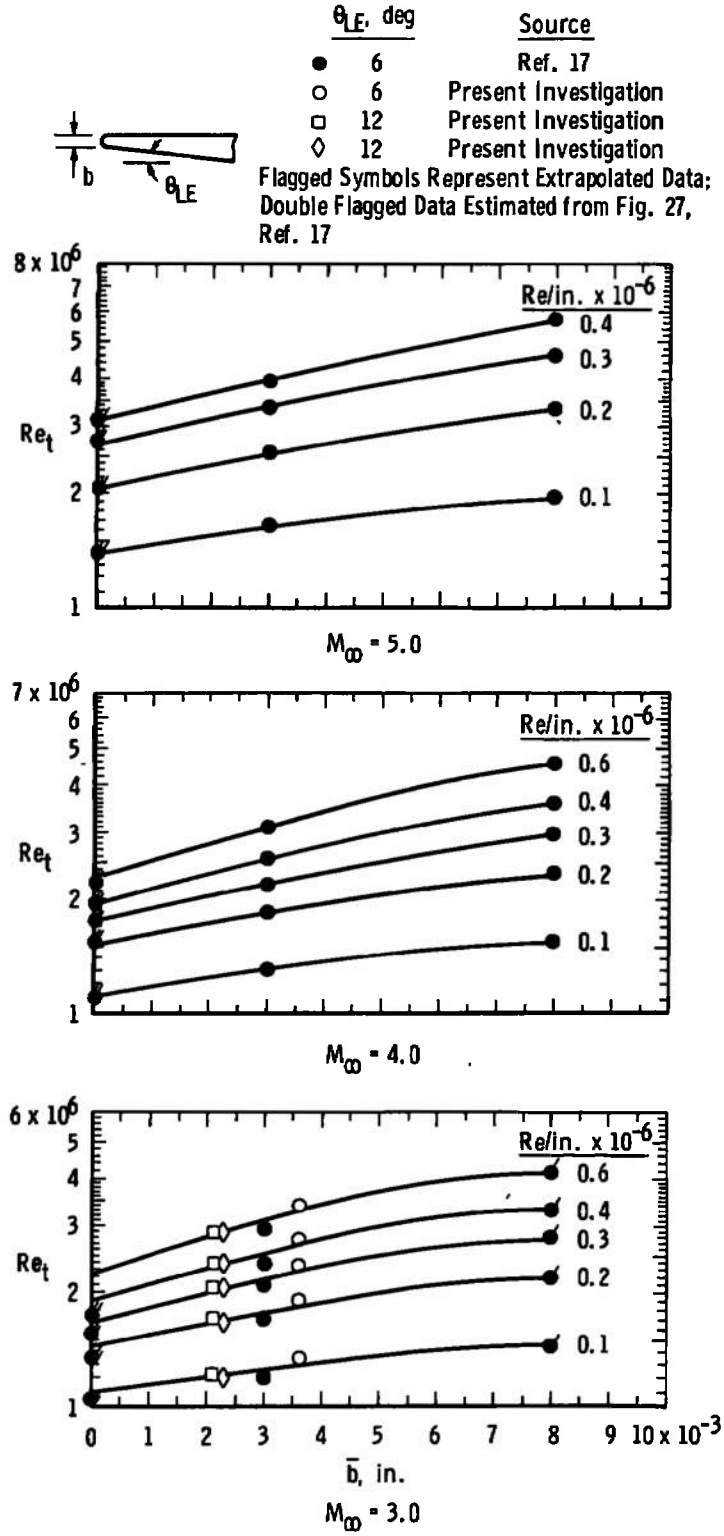

Fig. IV-3 Basic Transition Reynolds Number Data from the AEDC-VKF Tunnel D for M_∞ = 3, 4, and 5 with Variable $\bar{b}$, θ_{LE}, and Re/in.

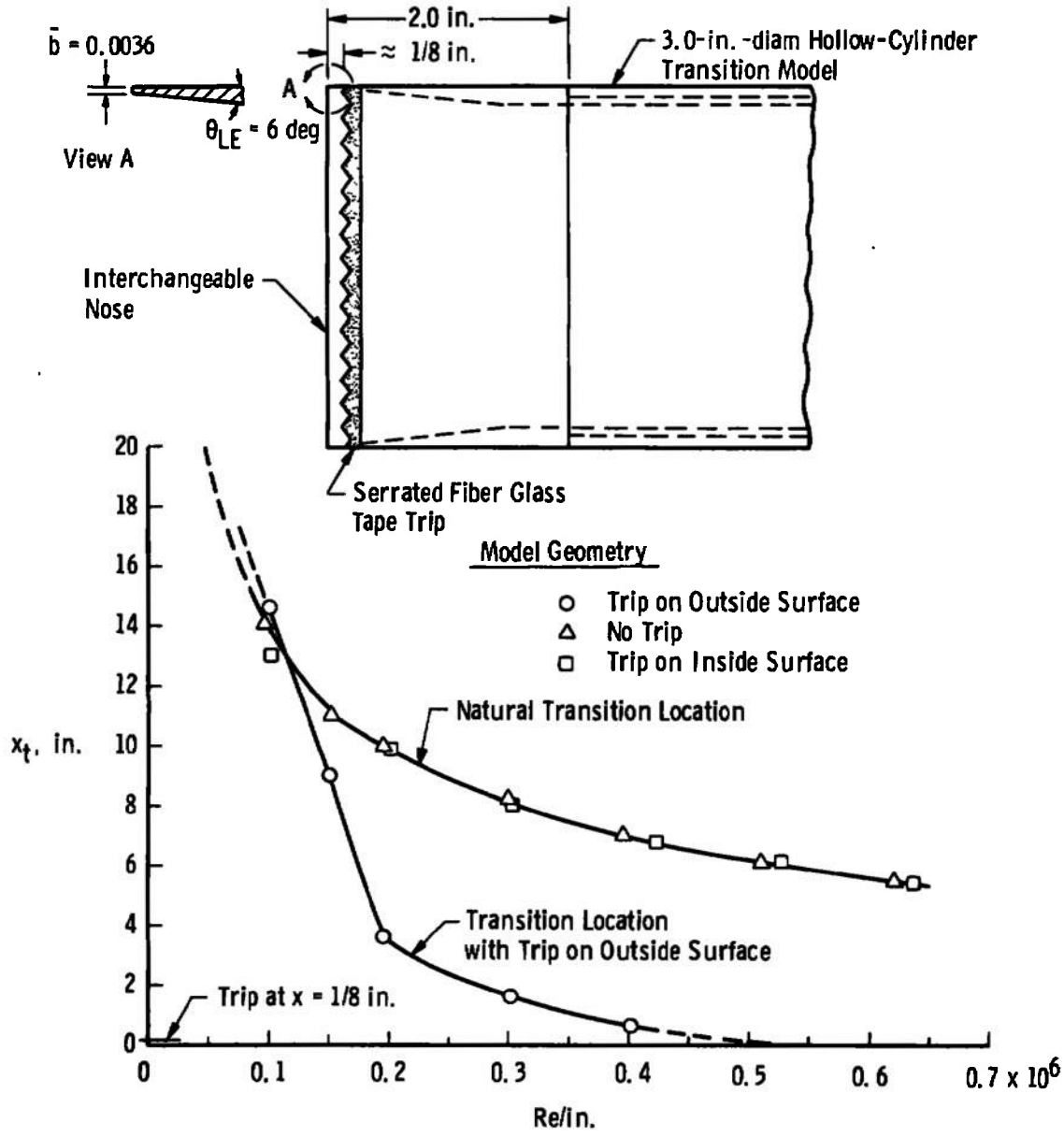

Fig. IV-4 Effectiveness of Serrated Fiber Glass Tape Boundary-Layer Trip at $M_\infty = 3.0$

TABLE IV-1
AEDC-VKF TUNNEL D TRANSITION REYNOLDS NUMBER DATA, 3.0-IN.-DIAM HOLLOW CYLINDER

M_∞	p_o, psia	T_o, °R	Re/in. x 10^{-6}	x_t, in.	Re_t x 10^{-6}	$\bar{b}$, in.	θ_{LE}, deg	Remarks
2.98	7.3	536	0.097	14.0	1.36	0.0036	6	Probe A
2.99	11.3	539	0.148	11.3	1.67			(0.015 x
2.99	14.4	540	0.188	10.0	1.88			0.032 in.)
3.00	23.8	539	0.311	8.3	2.58			
3.00	30.7	537	0.402	7.0	2.81			
3.00	37.8	533	0.501	6.3	3.16			
3.00	44.5	528	0.598	5.5	3.29			
2.98	7.3	532	0.097	14.0	1.36			
2.99	11.4	535	0.151	11.0	1.66			
3.00	14.9	537	0.195	10.0	1.95			
3.00	22.8	536	0.300	8.25	2.47			
3.00	29.9	534	0.394	7.0	2.76			
3.00	37.8	526	0.511	6.1	3.12			
3.00	44.9	518	0.620	5.5	3.41			
2.98	7.6	529	0.102	11.7	1.19	0.023	12	Probe A
3.00	23.0	533	0.305	6.8	2.07			
3.00	29.9	534	0.396	6.1	2.41			
3.00	37.9	530	0.507	5.4	2.74			
3.00	44.9	527	0.605	4.9	2.96			
2.98	7.5	523	0.103	13.2	1.36	0.036	6	**
2.99	11.5	527	0.155	11.2	1.74			Probe A
2.99	15.0	529	0.201	9.8	1.97			
3.00	22.8	529	0.305	8.0	2.44			
3.00	31.1	523	0.423	6.8	2.87			
3.00	37.9	516	0.526	6.1	3.21			
3.00	45.0	510	0.636	5.4	3.44			
2.98	7.6	523	0.105	11.2	1.18	0.0021	6	Probe A
2.98	11.6	517	0.162	9.4	1.52			
2.99	15.1	512	0.213	8.3	1.77			
3.00	22.9	511	0.323	6.6	2.13			
3.00	30.0	515	0.419	5.9	2.47			
3.00	38.0	515	0.530	5.3	2.81			
3.00	44.9	514	0.626	4.9	3.07			
2.98	7.7	513	0.109	11.2	1.22			
2.98	11.6	511	0.165	9.8	1.62			
2.99	15.1	519	0.209	8.5	1.78			
3.00	23.0	527	0.309	7.0	2.16			
3.00	30.0	528	0.403	6.0	2.42			
3.00	38.0	526	0.513	5.3	2.72			
3.00	45.0	520	0.620	4.7	2.91			
2.98	11.7	511	0.165	9.6	1.58	0.0021	6	Probe B
2.99	15.1	517	0.211	8.5	1.79			(0.007 x
3.00	23.0	529	0.308	7.0	2.16			0.0037 in.)
3.00	30.0	529	0.401	6.0	2.41			
3.00	38.1	526	0.514	5.2	2.67			
3.00	45.2	515	0.630	4.7	2.96			
3.0	--	≈530	0.1	--	1.10	0	--	Extrapolated
			0.2		1.43			Values of Re_t
			0.3		1.70			from Fig. IV-3
			0.4		1.90			
			0.5		2.09			
			0.6		2.24			
4.0		≈540	0.1		1.12			Extrapolated
			0.2		1.51			Values of Re_t
			0.3		1.76			from Fig. IV-3
			0.4		1.96			
			0.5		2.15			
			0.6		2.31			
5.0			0.1		1.40			
			0.2		2.06			
			0.3		2.65			
			0.4		3.10			

**Boundary-Layer Trip Located on Inside Bevel Angle 1/8-in. from Hollow-Cylinder Leading Edge.

APPENDIX V
DISPLACEMENT THICKNESS CORRELATION AND TURBULENT SKIN-FRICTION COEFFICIENTS

5.1 DISPLACEMENT THICKNESS CORRELATION

When the experimental tunnel wall boundary-layer displacement thickness (δ^*) values used in the transition correlation (Section V) were not available from the literature, Fig. V-1 was used to obtain an approximate δ^* value. The correlation presented in Fig. V-1 was developed by Maxwell and Jacocks in Ref. 22 by arranging the equations of Tucker (Ref. 37) in a dimensionless form:

$$\overline{\delta^*} = \frac{\delta^*}{K(X_E)^{6/7}}$$

and

$$K = 0.0131\left(\frac{\mu_o}{\rho_o a_o}\right)^{1/7}$$

where a_o Speed of sound at stagnation conditions, ft/sec

X_E Longitudinal distance from tunnel throat to nozzle aerodynamic exit plane, ft

δ^* Boundary-layer displacement thickness, ft

μ_o Coefficient of viscosity at stagnation conditions lb-sec/ft^2

ρ_o Density at stagnation conditions, lb-sec^2/ft^4

5.2 TURBULENT SKIN-FRICTION COEFFICIENT

Theoretical skin-friction coefficients determined from Ref. 21 for an adiabatic, zero pressure gradient, compressible fluid are presented in Fig. V-2. Experimental skin-friction coefficients obtained in this investigation from the AEDC-PWT-16S tunnel along with experimental values from other sources are also presented. Good agreement between the experimental and theoretical values existed.

			Facility	Test Section Size	Reference	ℓ_r, in.
	!	□	AEDC-VKF (A)	40- by 40-in.	22	---
	!	△	AEDC-PWT (SMT)	12- by 12-in.	22	---
	!	○	AEDC-VKF (D)	12- by 12-in.	33	56
	*	▽	AEDC-PWT-16S	16- by 16-ft	Present Investigation	839
	*	■	AEDC-VKF (A)	40- by 40-in.	Present Investigation	208
	*	×	JPL-20-in. SWT	18- by 20-in.	34	66 to 118
Cooled Walls	*	+	JPL-21-in. HWT	≈20- by 21-in.	34	159
	*	◇	AEDC-VKF (E)	12- by 12-in.	Unpublished VKF Data (Tunnel Side Wall)	64
	*	◇	AEDC-VKF (B)	50-in. Diameter	35	244

! $\overline{\delta^*}$ Computed at Aerodynamic Exit Plane (X_E)

* $\overline{\delta^*}$ Computed at Rake Location (X_R) = ℓ_r

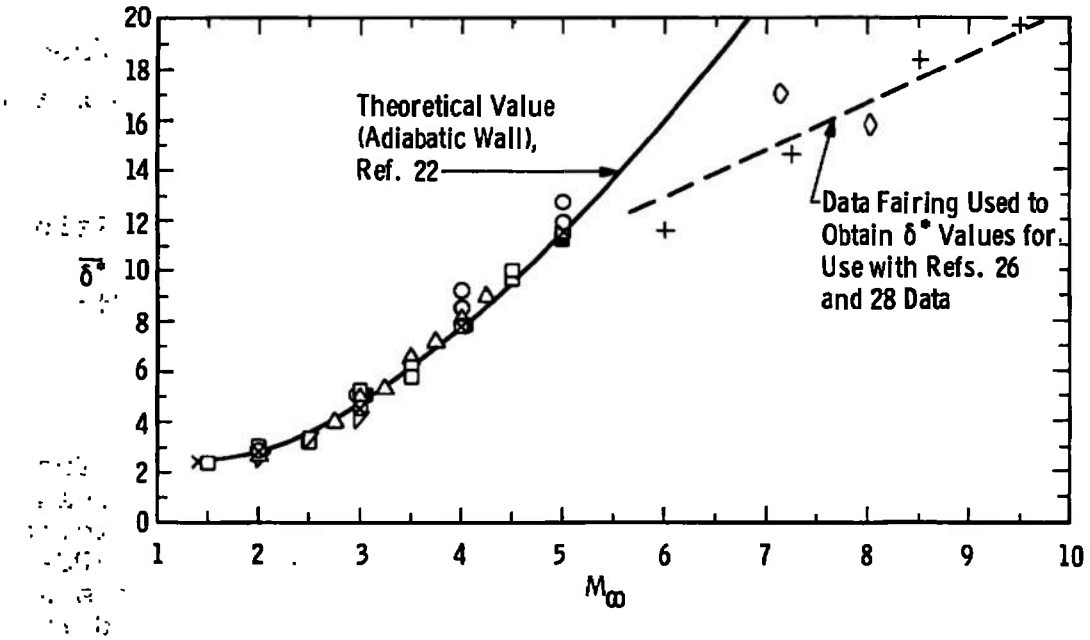

Fig. V-1 Flexible Plate Displacement Thickness Correlation for M_∞ = 1.0 to 10

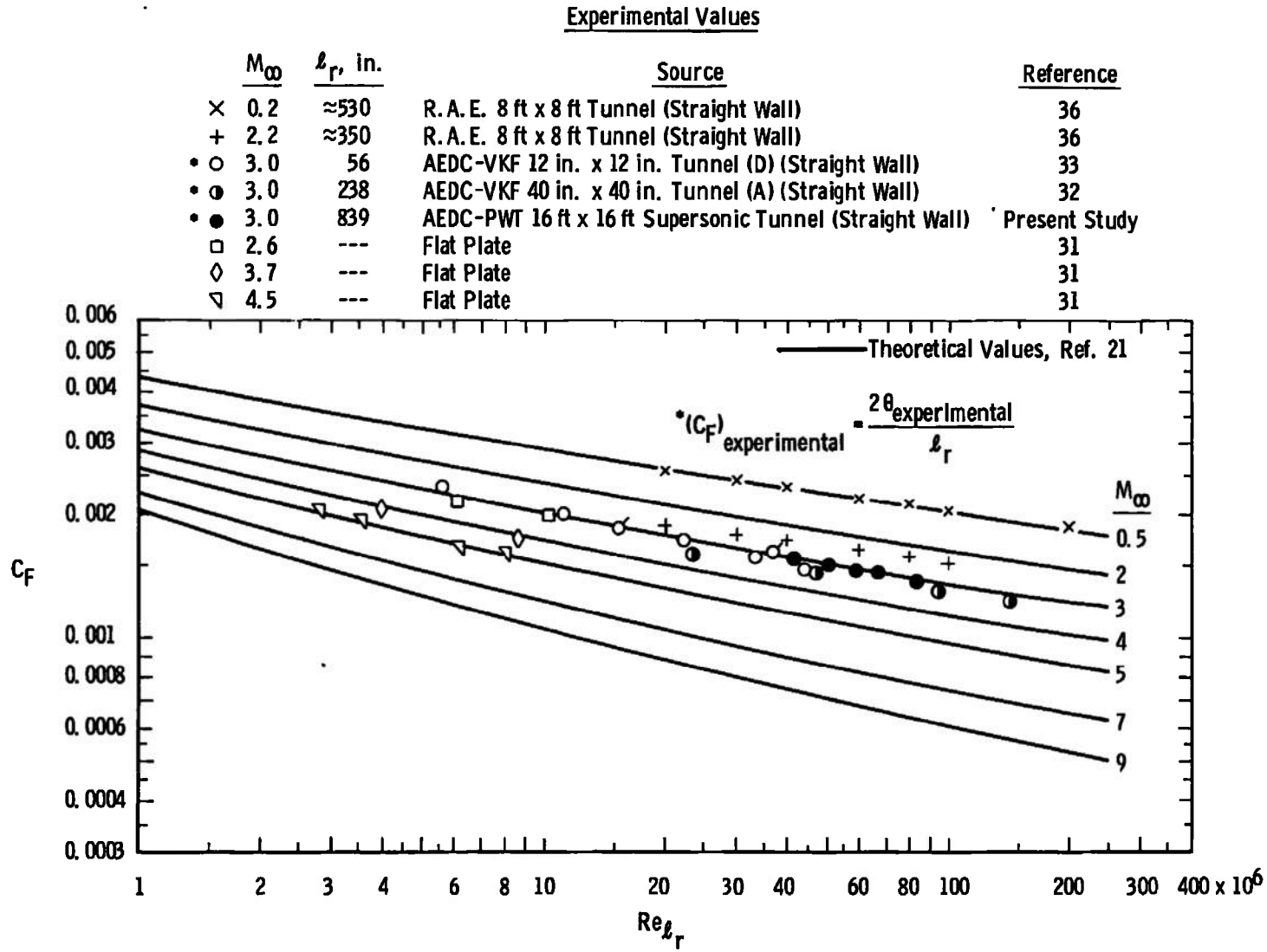

Fig. V-2 Adiabatic, Mean Turbulent Skin-Friction Coefficients as a Function of Mach Number and Length Reynolds Number

Security Classification

DOCUMENT CONTROL DATA - R & D

(Security classification of title, body of abstract and indexing annotation must be entered when the overall report is classified)

1. ORIGINATING ACTIVITY (Corporate author)	2a. REPORT SECURITY CLASSIFICATION
Arnold Engineering Development Center ARO, Inc., Operating Contractor Arnold Air Force Station, Tennessee	UNCLASSIFIED
	2b. GROUP N/A

3. REPORT TITLE

EFFECTS OF RADIATED AERODYNAMIC NOISE ON MODEL BOUNDARY-LAYER TRANSITION IN SUPERSONIC AND HYPERSONIC WIND TUNNELS

4. DESCRIPTIVE NOTES (Type of report and inclusive dates)

June 3, 1966 - January 23, 1967 Final Report

5. AUTHOR(S) (First name, middle initial, last name)

S. R. Pate and C. J. Schueler, ARO, Inc.

6. REPORT DATE	7a. TOTAL NO. OF PAGES	7b. NO. OF REFS
March 1968	92	37

8a. CONTRACT OR GRANT NO.	9a. ORIGINATOR'S REPORT NUMBER(S)
AF40(600)-1200 b. PROJECT NO. 8953 c. Program Element 6240533F d. Task 895303	AEDC-TR-67-236
	9b. OTHER REPORT NO(S) (Any other numbers that may be assigned this report) N/A

10. DISTRIBUTION STATEMENT

This document has been approved for public release and sale; its distribution is unlimited.

11. SUPPLEMENTARY NOTES	12. SPONSORING MILITARY ACTIVITY
Available in DDC	Arnold Engineering Development Center, Air Force Systems Command, Arnold Air Force Station, Tennessee

13. ABSTRACT

Boundary-layer transition and aerodynamic noise measurements were made on sharp leading-edge two-dimensional models in the AEDC supersonic wind tunnels (1 ft to 16 ft). These data showed, conclusively, a significant and continuous increase in transition Reynolds number and a significant decrease in radiated aerodynamic noise (generated by the tunnel wall turbulent boundary layer) with increasing tunnel size. Results obtained in the AEDC-VKF Tunnel A from a shroud configuration placed concentrically around a hollow cylinder transition model and a flat plate microphone model further demonstrated the strong adverse effects that radiated aerodynamic noise will have on transition. A correlation of transition Reynolds numbers based on transition data from nine wind tunnels ($3 \leq M_\infty \leq 8$) was developed. The correlation was dependent only on the tunnel wall, turbulent boundary layer, aerodynamic noise parameters (displacement thickness and skin friction), and the tunnel test section circumference.

DD FORM 1 NOV 65 1473

Security Classification

14 KEY WORDS	LINK A		LINK B		LINK C	
	ROLE	WT	ROLE	WT	ROLE	WT
noise effects						
boundary-layer transition						
Reynolds number effects						
cylinders						
flat plates						
supersonic flow						
hypersonic flow						
wind tunnel tests						